Agenzia Nazionale per le Nuove Tecnologie,
l'Energia e lo Sviluppo Economico Sostenibile

Ministero dello Sviluppo Economico

RICERCA DI SISTEMA ELETTRICO

Double-wall bayonet tube steam generator for LFR application. Preliminary characterization

D. Rozzia, A. Toti, M. Tarantino, L. Gramiccia, D. Vitale Di Maio,
F. Giannetti

CIRTEN - CONSORZIO INTERUNIVERSITARIO PER LA RICERCA TECNOLOGICA NUCLEARE

Report RdS/2011/50

DOUBLE-WALL BAYONET TUBE STEAM GENERATOR FOR LFR APPLICATION. PRELIMINARY CHARACTERIZATION

D. Rozzia, A. Toti, M. Tarantino (ENEA)
L. Gramiccia, D. Vitale Di Maio, F. Giannetti (CIRTEN)

Settembre 2011

Report Ricerca di Sistema Elettrico
Accordo di Programma Ministero dello Sviluppo Economico – ENEA
Area: Governo, Gestione e sviluppo del sistema elettrico nazionale
Progetto: Nuovo nucleare da fissione: collaborazioni internazionali e sviluppo competenze in materia nucleare

Responsabile Progetto: Paride Meloni, ENEA

ENEA Ricerca Sistema Elettrico	Sigla di identificazione NNFISS – LP3 - 032	Distrib. L	Pag. 1	di 104

Titolo

Double-wall bayonet tube steam generator for LFR application. Preliminary characterization

Descrittori

Tipologia del documento: **Rapporto Tecnico**

Collocazione contrattuale: Accordo di programma ENEA-MSE: tema di ricerca "Nuovo nucleare da fissione"

Argomenti trattati:

Sommario

The overall activity is aimed to verify the feasibility of the superheated steam double wall once through bayonet type steam generation. The work and the relative experimental campaigns will be focused on the single tube evaluation. It spans over three years. This report is subdivided in seven sections. The first one pointed out the objectives of the activity and a description of the ALFRED SG. Section two addresses the screening of candidate powders and summarize the models to determine numerically the conductivity of porous media. The calculations to support the design of the Tubes for Powders (TxP) facility are presented in section three. The layout of the Facility is given in section 4. In section five, the assessment of the single tube performance by mean of RELAP-5 is reported. Section six is preliminary to the future development. The turbulence promoters techniques are presented as well as the methodologies to measure the void fraction. They are considered strategic activities to support the single tube experimental testing. Conclusions and future developments are presented in section seven

Note

Autori:

D. Rozzia, A. Toti, M. Tarantino (ENEA)

L. Gramiccia, D. Vitale Di Maio, F. Giannetti (CIRTEN)

Copia n. **In carico a:**

2			**NOME**			
			FIRMA			
1			**NOME**			
			FIRMA			
0	**EMISSIONE**	13/09/2014	**NOME**	M. Tarantino	I. Di Piazza	P. Meloni
			FIRMA			
REV.	**DESCRIZIONE**	**DATA**		**REDAZIONE**	**CONVALIDA**	**APPROVAZIONE**

(This page has been intentionally left blank)

Abstract

One of the most promising Generation IV concepts is the Lead cooled Fast Reactor (LFR). The use of lead as primary coolant appears motivated by several reasons (low moderation, thermal properties, etc…), nevertheless, it still has several limitations that require further investigations. The actual configuration of LFR pointed out in the frame of ELSY project deals with the compact pool type reactor in which the steam generators (SG) are located inside the reactor tank. In this scenario, the steam generator design plays an important role because one of the most impacting incidents is the Steam Generator Tube Rupture (SGTR) that may propagate to the near-bough tubes. The SG proposed in ELSY is the flat spirals type. The new European project LEADER is aimed to solve the open points individuated in ELSY. In this framework, a new configuration of SG has been proposed: the super-heated steam double wall once through bayonet type. This conceptual design was studied since 60' for Sodium Reactor application. An example of facility that operates with this concept is CIRCE (ENEA Brasimone), nevertheless the application is limited to heat exchange during the Decay Heat Removal function.

The single tube vertical unit consists of three concentric tubes. Starting from the smallest one, the water crosses in down-flow the tube and heats-up. At the end of this tube, the water enters the second concentric tube in up-flow and immediately it starts to boil because of the heat exchange with the liquid lead that flows in counter-current at the tube outer surface. The tube design allows the achievement of super-heated steam. The liquid lead is not in direct contact with the second tube. The third concentric tube that creates an annulus separates it from the steam-water tubes. The study of this configuration is motivated by safety improvement. In fact, it allows the double physical separation between lead and water sides by mean of an intermediate gap. Thus, the probability of vessel pressurization by water-lead contact results reduced. Furthermore, by mean of gap pressurization (with Helium), a leakage check system should be introduced in order to prevent incident scenarios. On the other hands, the monitor-ability of the pressurized gap has to be demonstrated and the thermal efficiency has to be improved.

The overall activity is aimed to verify the feasibility of the superheated steam double wall once through bayonet type steam generation. The work and the relative experimental campaigns will be focused on the single tube evaluation. It spans over three years. The main phases of the experimental campaigns are:

- *Individuate a candidate material as gap filler in order to increase the thermal efficiency.*
- *Investigate the turbulence promoters techniques.*
- *Verify the single tube performance in representative operating conditions.*

This report is subdivided in seven sections. The first one pointed out the objectives of the activity and a description of the ALFRED SG. Section two addresses the screening of candidate powders and summarizes the models applied in the literature to determine numerically the conductivity of porous media. The pre-test calculations related to support the design of the Tubes for Powders (TxP) facility are presented in section three. The detailed description of the Facility is given in

section 4. In section five, the assessment of the single tube performance by mean of RELAP-5 is reported. Section six is preliminary to the future development. The turbulence promoters techniques are presented as well as the methodologies to measure the void fraction. They are considered strategic activities to support the single tube experimental testing; at the present stage they have to be considered as bibliographic research. Conclusions and future developments are presented in section seven.

Acknowledgments

The authors express gratitude to Mr Gino Venturi. He allows the construction of the TxP Facilty realizing the first pictures of the detailed design.

We acknowledge Alessandro Del Nevo that coordinates the development of the RELAP-5 input deck for the assessment of the single tube thermal performance.

CONTENTS

Abbreviations

Ag	Silver
Al	Aluminum
ALFRED	Advanced Lead Fast Reactor European Demonstrator
Ar	Argon
CIRCE	CIRColazione Eutettico
Cu	Copper
CR	Centro di Ricerca
DIMNP	Dipartimento di Ingegneria Meccanica, Nucleare e della Produzione
DP	Diamond Powder
ELSY	European Lead cooled SYstem
ENEA	Agenzia nazionale per le nuove tecnologie, l'energia, e lo sviluppo economico sostenibile
FR	Fast Reactor
GEN-IV	GENeration four
GFR	Gas-cooled Fast Reactor
GIF	Generation four International Forum
He	Helium
HR	Heating Rod
ID	Inner Diameter
IIR	Intermediate Interim Report
LEADER	Lead-cooled European Advanced DEmonstration Reactor
LFR	Lead cooled Fast Reactor
Mo	Molybdenum
MSR	Molten Salt Reactor
NPP	Nuclear Power Plant
OD	Outer Diameter
P	Powder (contained in the gap)
Pb	Lead
PT	Powder Tube
SCWR	Super-Critical-Water-cooled Reactor
SFR	Sodium cooled Fast Reactor
SG	Steam Generator
SGTR	Steam Generator Tube Rupture
TxP	Tubes for Powders facility
UNIPI	UNiversità degli studi di PIsa
VHTR	Very High Temperature Reactor
W	Tungsten
WT	Water Tube

List of figures

List of tables

1 Introduction

Generation IV initiative was launched by U.S. Department of Energy's Office of Nuclear Energy in 2000, with the aim to develop innovative nuclear systems (NPPs and fuel cycles), likely to reach technical maturity by 2030 [1] [2] [3]. The Lead cooled Fast Reactor operates in the fast-neutron spectrum and uses a closed fuel cycle for efficient conversion of fertile uranium. The use of lead as primary coolant is motivated by the good nuclear properties (low moderation rate that allows it to be used in fast reactors), as well as by several additional advantages. It does not give rise to fast chemical interaction with air and water, it has low vapor pressure and high boiling point (2200 K), it is relatively cheap and it has good thermal properties. Nevertheless, lead has several limitations. Lead implies corrosion and erosion problems with the structural material. To partially mitigate them is mandatory to work at relatively low temperatures (400°C-480°C in ELSY) compared to the other Generation IV reactors. Moreover problems of Lead solidification may occur due to the relatively high melting point (at 327°C).

The investigation of feasibility of the lead technology represents one of the on-going European activities. The European LFR project ELSY [4] [5] (European Lead-cooled SYstem), aimed to demonstrate that it is possible to design a competitive and safe fast critical reactor using simple engineering technical features. The ELSY reference design is a 600 MWe pool-type reactor cooled by pure lead. The ELSY project already solved some of the key technological and design issues, some of them still remain open and need further investigations. The new European project LEADER [6] (Lead-cooled European Advanced DEmonstration Reactor) starts from the results achieved in the ELSY program with a deep analysis of the hard points of the reactor configuration. The main goal of this new project is to achieve a conceptual design of a Lead Fast Reactor industrial size plant and of a scaled demonstrator of the LFR technology named ALFRED.

In this framework, a new configuration of SG has been proposed: the double wall once through bayonet superheated SG. This conceptual design was studied since ‘60 for Sodium Reactor application. An example of facility that operates with this concept is CIRCE (ENEA Brasimone, *Fig. 1*), nevertheless the application is limited to the heat exchange function only.

1.1 The ALFRED Steam Generator

ALFRED[6][7] reactor includes eight once through double wall bayonet type SGs. The layout of the primary system is reported in *Fig. 2*; the figure highlights the SG dislocation. The single SG unit is depicted in *Fig. 3*: Each SG has 508 tubes the main data are summarized in *Tab. 1.* The single vertical unit proposed for ALFRED’s SG consists of (in similarity with the CIRCE HX) three concentric tubes (*Fig. 4*). Starting from the inner tube, the water flows downward and then enters the second concentric tube in up-flow where it starts to boil because of the heat exchange with the liquid lead that flows in counter-current on the tube outer surface. The tube design allows the achievement of super-heated steam. The liquid lead is not in direct contact with the second tube. The third concentric tube separates it from the steam-water tubes. The study of this configuration is motivated by safety improvement. In fact, it allows the double physical separation between lead and water sides by mean of an intermediate gap. Furthermore, by mean of gap pressurization (with Helium), a leakage check system should be introduced in order to prevent incident scenarios.
The preliminary calculations pointed out the needing of two main features:

- An insulating layer is required in order to avoid the heat exchange (causing steam condensation) between the superheated steam that leaves the second tube and the feedwater that enters the first one. ANSALDO Nucleare proposes the use of insulating paint inserted into a slave tube.
- The achievement of superheated steam at the temperatures indicated in *Tab. 1* requires the selection of an appropriate material to be placed within the gap between the second and the third tube. The candidate materials are high conductivity powders.

The selection and characterization of appropriate powders is the main goal of the present activity. The demonstration of the gap monitor-ability is one of the objectives of the experimental campaigns that will be carried out in the next three years at ENEA CR Brasimone together with the evaluation of the single tube thermal performance.

1.2 Objective of the activity

The overall activity is aimed to verify the feasibility of the double wall once through bayonet tube. This work and the relative experimental campaigns focuses on the single tube evaluation. The main purposes of the experimental campaigns are:

- Individuate a candidate material as filler for the pressurized gap between the lead and water sides in order to increase the SG thermal efficiency.
- Demonstrate the pressure monitor-ability of the pressurized gap.
- Investigate the feasibility of candidate turbulence promoter for the water-steam side. (At the present stage the design does not include turbulence promoters. Nevertheless, this item will be the subject of further assessment).
- Verify the single tube performance in representative operating conditions.

The present report is concentrated on the annular gap: several metallic/non-metallic powders will be investigated as filling materials with the aim to experimentally determinate their thermal conductivities. The Tube for Powders (TxP) facility is designed to test high conductivity powders. The TxP design has been terminated and the construction of the Facility is ongoing under. The first experimental campaign is planned in October 2011.

1.3 Structure of the report

This report is subdivided in seven sections. This first one point out the objectives of the activity and a description of the ALFRED SG. Section two addresses the screening of candidate powders and summarizes the models applied in the literature to determine numerically the conductivity of porous media. The pre-test calculations related to support the design of the Tubes for Powders (TxP) facility are presented in section three. The detailed description of the Facility is given in section four. In section five, the assessment of the single tube performance by mean of RELAP-5 is reported. Section six is preliminary to the future development. The turbulence promoters techniques are presented as well as the methodologies to measure the void fraction. They are considered strategic activities to support the single tube experimental testing; at the present stage they have to be considered as bibliographic research. Conclusions and future developments are presented in section seven.

<table>
<tr><th colspan="4">Steam Generator general properties</th></tr>
<tr><th>Description</th><th>Quantity</th><th>Description</th><th>Quantity</th></tr>
<tr><td>Removed Power [MW]</td><td>37.5</td><td>Number of tubes</td><td>508</td></tr>
<tr><td>Feed-water flow rate [kg/s]</td><td>24.1</td><td>Water pressure [bar]</td><td>180</td></tr>
<tr><td>Bundle geometry</td><td>triangular</td><td>Pitch / tube diameter</td><td>1.42</td></tr>
<tr><td>Feed-water temperature [°C]</td><td>335</td><td>Steam outlet temperature [°C]</td><td>450</td></tr>
<tr><td>Lead inlet temperature [°C]</td><td>480</td><td>Lead outlet temperature [°C]</td><td>400</td></tr>
<tr><th colspan="4">Bayonet tube geometry</th></tr>
<tr><th>Description</th><th>Quantity</th><th>Description</th><th>Quantity</th></tr>
<tr><td>Slave tube outer diameter [mm]</td><td>9.52</td><td>Slave tube thickness [mm]</td><td>1.07</td></tr>
<tr><td>Inner tube outer diameter [mm]</td><td>19.05</td><td>Inner tube thickness [mm]</td><td>1.88</td></tr>
<tr><td>Second tube outer diameter [mm]</td><td>25.40</td><td>Second tube thickness[mm]</td><td>1.88</td></tr>
<tr><td>Third tube outer diameter [mm]</td><td>35.52</td><td>Third tube thickness [mm]</td><td>2.11</td></tr>
<tr><td>Powder annular gap width [mm]</td><td>1.07</td><td>Length of heat exchange [mm]</td><td>6000</td></tr>
<tr><td>Argon plenum height [mm]</td><td>1000</td><td>He plenum height [mm]</td><td>800</td></tr>
<tr><td>Steam plenum height [mm]</td><td>800</td><td>T91 plates thickness [mm]</td><td>250</td></tr>
</table>

Tab. 1 - ALFRED SG main data (from the conceptual design).

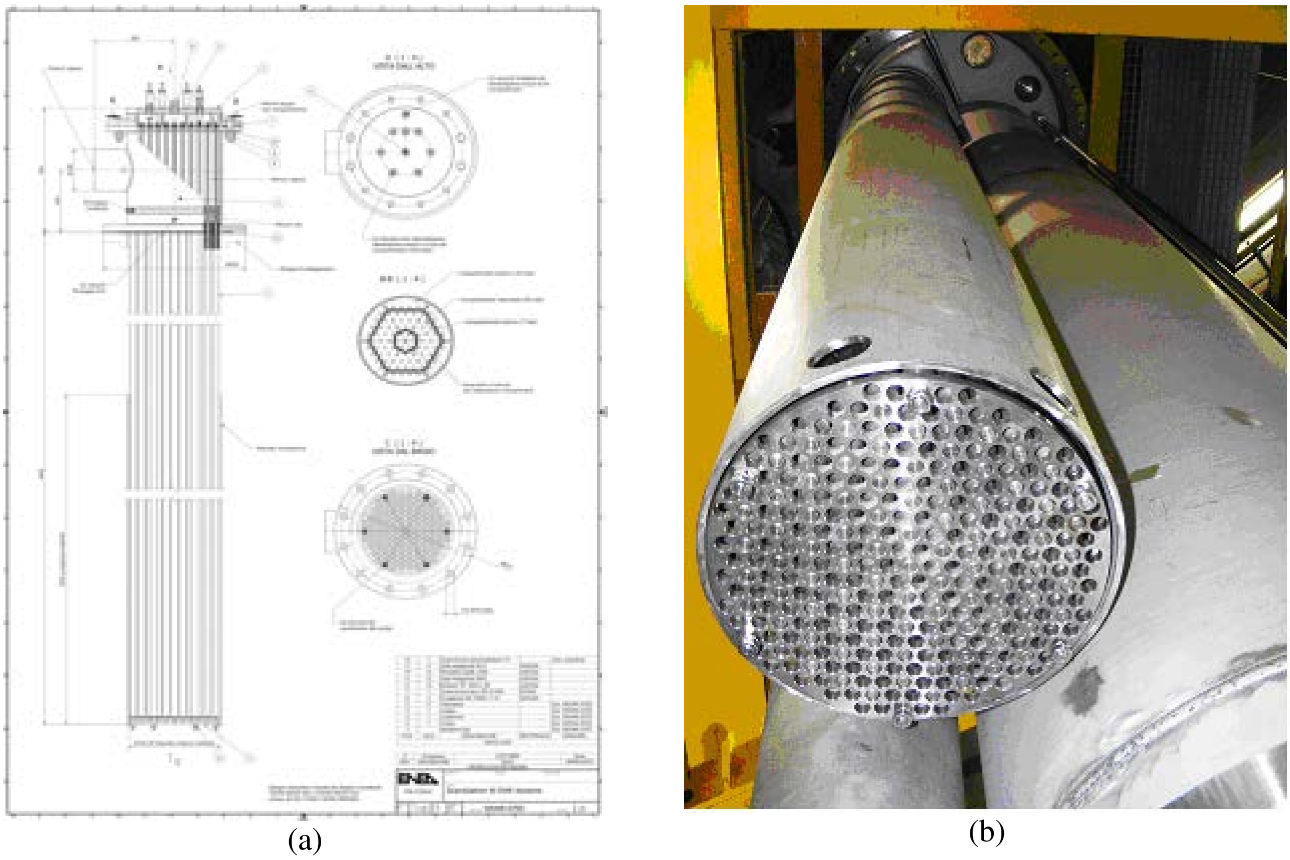

(a) (b)

Fig. 1 – Double wall once through bayonet Heat Exchanger of CIRCE.

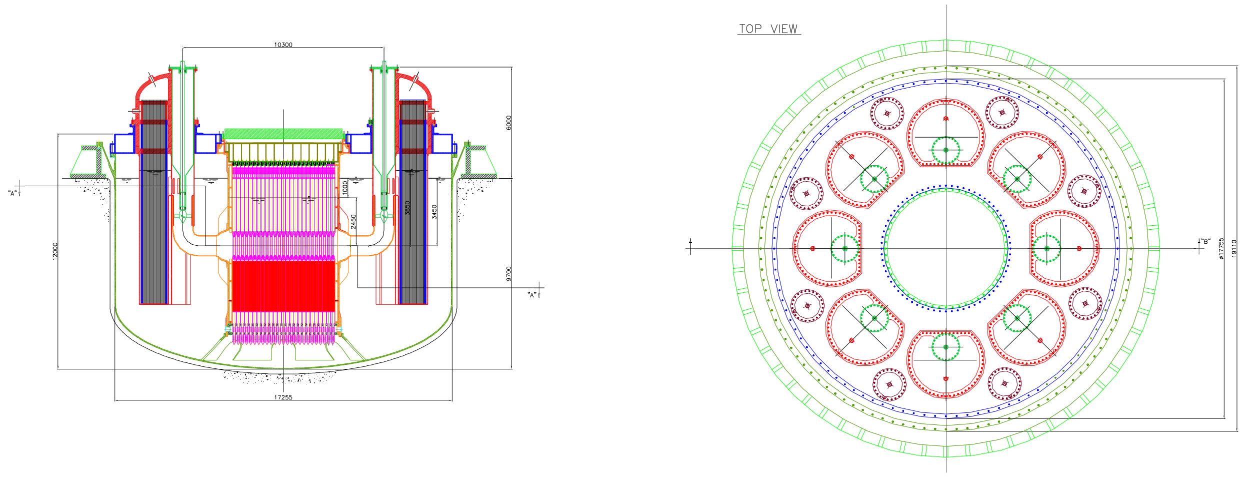

Fig. 2 – ALFRED primary system configuration.

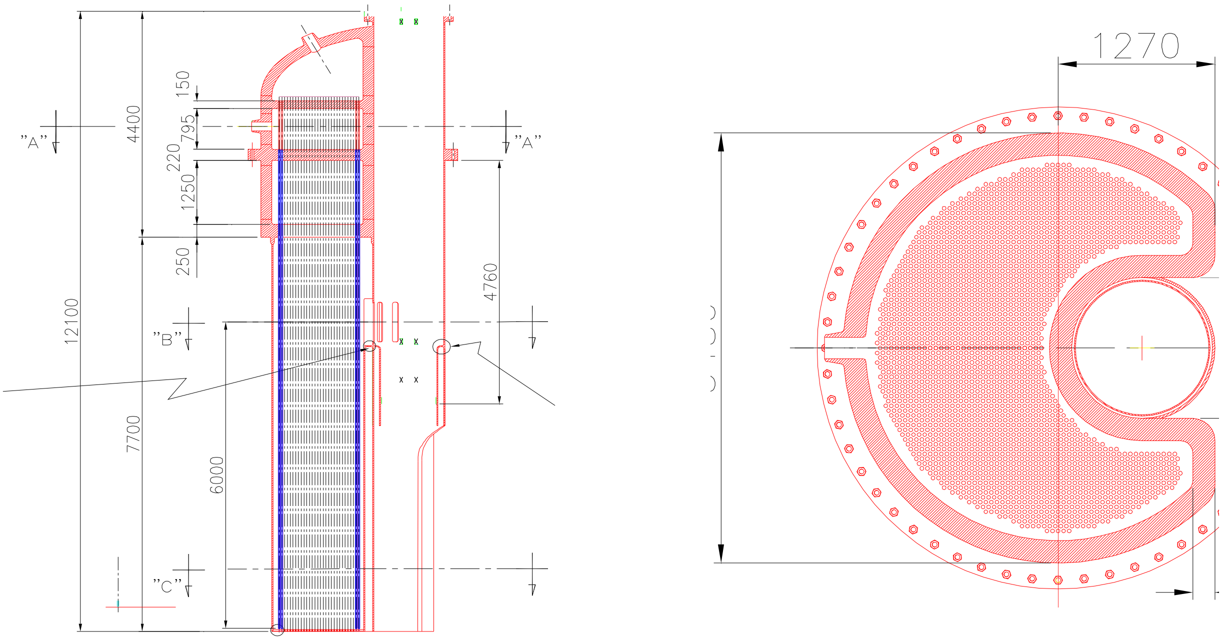

Fig. 3 – ALFRED SG conceptual design.

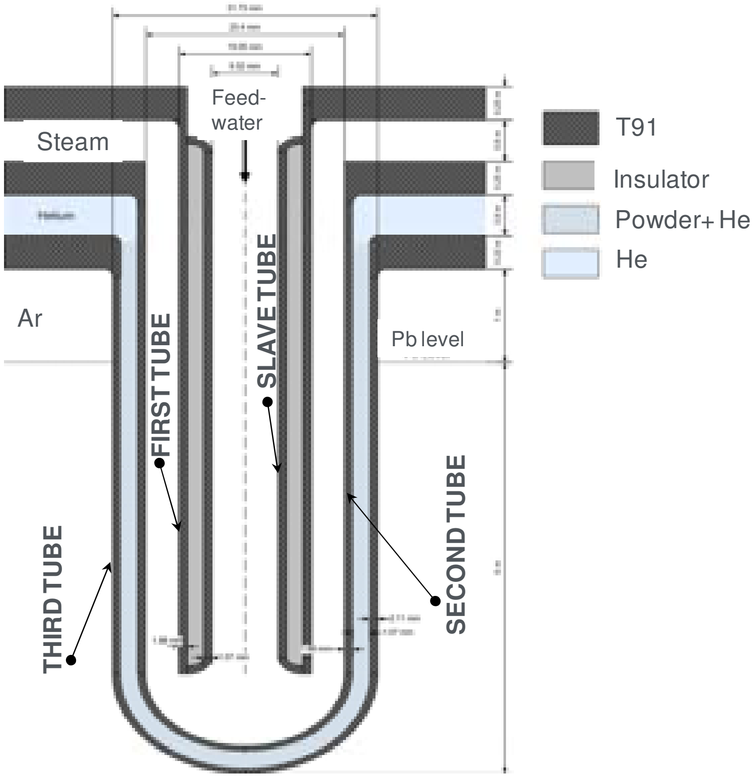

Fig. 4 – ALFRED SG Bayonet Tube scheme.

2 Screening of Powders and Conductivity Correlations

Porous medium deals with materials consisting of a solid matrix with an interconnected void. It is assumed that the solid matrix is either rigid (the usual situation) or it undergoes small deformation. The interconnectedness of the void (the pores) allows the flow of one or more fluids through the material. In the simplest situation ("single-phase flow"), a single fluid saturates the void. In "two-phase flow" a liquid and a gas share the void space [8].

2.1 Screening of candidate powders: criteria definition

Nine criteria have been developed in order to make a screening among the candidate powders and to individuate the powders to be tested. The summary of the results obtained is included in *Tab. 7*.

In the first analysis the synthetic diamond was selected as the most promising solution. The design of the facility was executed taking into account of the difficulties that rise up when measuring a temperature drop of a very high conductivity material (diamond is more than 1200 W/mK) in a relatively short gap. The diamond was then abandoned at the end of the design phase due to the prohibitive cost. Nevertheless, the TxP Facility allows to test high conductivity powders as Copper (400W/mK) or Brass (130W/mK) as well as medium conductivity powders i.e. stainless steel AISI-1010 (60 W/mK). These three materials have been selected for the first experimental campaign.

Criterion 1 Thermal conductivity:
One of the most important features required by the filling material is the high value of the thermal conductivity. In order to enhance the heat transfer coefficient, the conductivity limit is set to 50 W/(mK) (of the pure 99.5% dense material). The investigations are reported in *Tab. 2*.

Criterion 2 Melting point:
The operative conditions expected in ALFRED SG are 400°C - 480°C for the primary coolant. In order to maintain heat removal function in any operating condition, it is required that the powder's melting temperature is sufficiently above these values. An inferior limit for this parameter can be fixed to 900 °C. The investigations are reported in *Tab. 2*.

Criterion 3 Solid phase transitions temperatures:
In the expected operating conditions, allotropic phase transformations of the candidate materials have to be checked. In particular, it should be verified that phase transformations do not induce specific volume variations, or thermal conductivity deterioration, or the formation of anisotropies directions within the material. The investigations are reported in *Tab. 3*.

Criterion 4 Chemical reaction with Lead
If fast chemical reactions occur, a considerable amount of energy may be generated in the event of rupture of the tube connected to the Lead. Therefore, no exothermic chemical reactions with molten lead are allowed. No investigations are conducted; it is assumed that this criterion is satisfied for each material.

Criterion 5 Chemical reactions with water, steam and oxygen:

Analogous considerations of criterion 4 can be made for potential fast chemical reactions with water or steam at high temperature (300 °C) and pressure (180 bar). The investigations are reported in *Tab. 4*. Large oxidation at high temperature has to be avoided.

Criterion 6 Thermo-mechanical integral-time effects in operating conditions:

An important issue is the maintenance the homogeneous compaction state of the powder. Vibrations and tube differential thermal expansions induce sliding of the SG tubes that can produce a different compaction grade in the gap. The effects may range from the heterogeneity of the heat transfer coefficient, with a deviation from the expected thermal behavior of the component, up to the creation of localized constrains that do not allow the tube thermal deformation during power excursions. In addition, diffusion and transport phenomena may play a role in the creation of different region of thermal conductivity oriented in the thermal gradient direction.

This criterion partially belongs to the objectives of the experiment.

Criterion 7 Chemical integral-time effects in operating conditions:

The chemical interaction (essentially corrosion), between the filler material and the SG tubes is not allowed. The thin layer of the reaction products would represents an additional thermal resistance that involves the deterioration of the SG thermal performance. Furthermore, the mechanical properties of the steel tubes may be affected.

A potential risk to be considered is the Galvanic Corrosion, an electro-chemical process in which one metal corrodes preferentially another one when both metals are in electrical contact. Metals can be arranged in a Galvanic Series, representing their potential for electrolytic corrosion. A metal higher in this scale will corrode preferentially the metals ranked below. The greater is the distance between the metals in the Galvanic Series, the higher is the current that will flow between them causing galvanic attack. For example, when Aluminum, Copper or Magnesium are in contact with steel (carbon steel or stainless steel), galvanic corrosion can occur. Instead, carbon and graphite are very ineffective to initiate severe corrosion of stainless steels. On the other hands, steels can be doped with materials that inhibit corrosion. An investigation of this phenomenon is out of the aim of this activity.

Tab. 7 reports potential susceptibility to initiate corrosion for those materials ranked above stainless steel.

Criterion 8 Radiation damage

The effect of the radiation damage on thermal conductivity and on mechanical behavior of powder is more or less unknown. Nevertheless, materials that experience massive nuclear reactions with neutrons have to be avoided. It is assumed that materials with consistent neutron capture microscopic cross section (σa) that give rise to activation are excluded. The investigations are reported in *Tab. 5*.

Criterion 9 cost

Costs are analyzed in *Tab. 6*.

2.2 Conductivity of porous media

The porosity φ of a porous medium is defined as the fraction of the total volume of the medium that is occupied by void space. Thus, (1 - φ) is the fraction that is occupied by solid. For an isotropic medium the "surface porosity" (that is, the fraction of void area to total area of a typical cross section), will normally be equal to φ. Assuming the solid fraction Ψ = (1 - φ) their relations with densities are expressed by:

$$\varphi = (\rho_s - \rho_m)/ (\rho_s - \rho_f) \qquad \text{Eq. 1}$$

$$(1\text{-}\varphi)= \Psi = (\rho_m - \rho_f)/ (\rho_s - \rho_f) \qquad \text{Eq. 2}$$

List of symbols

s, f, m	refers to solid, fluid and overall volume respectively,
φ	is the porosity [/],
ρ	is density [kg/m^3],
c	is specific heat of the solid [J/(kg*K)],
c_p	is the specific heat at constant pressure of the fluid [J/(kg*K)],
k	is the thermal conductivity [W/(m*K)],
v	average fluid velocity [m/s]
q'''	is the heat production per unit volume [W/m^3].
Ψ	is the solid fraction [/],
T	is the temperature [°C]

2.2.1 Heat transfer through a porous medium

Heat transport through porous media is of great interest in chemical, mechanical, geological, environmental and petroleum applications [9]. Packed beds are widely used in various industrial equipment including heat exchangers, dryers, absorbers, distillation and extraction columns, chemical reactors, calcinators, and incinerators. Porous media applications arise also in the design of cry-coolers, heat pipes, enhanced oil recovery, and geothermal and petroleum applications (involving porous rocks and soil). Recent applications of porous media arise in microelectronics for electronic packaging (device encapsulation) as thermal interface materials (TIM) for efficient disposal of the generated heat.

A distinction is made between an average taken with respect to a volume element *Vm* of the medium (incorporating both solid and fluid material) and one taken with respect to a volume element *Vf* consisting of fluid only [8]. For example, we denote the average of the fluid velocity over *Vm* by **v** = (*u, v, w*), this is called seepage velocity. Taking an average of the fluid velocity over a volume *Vf* we get the intrinsic average velocity **V**, which is related to **v** by the Dupuit-Forchheimer relationship.

$$\boldsymbol{v} = \varphi\, V \qquad \text{Eq. 3}$$

Conservation of mass is expressed by the continuity equation:

$$\varphi\, \partial\rho_f/\partial t + \nabla *(\rho_f\ \boldsymbol{v}) = 0 \qquad \text{Eq. 4}$$

Hypothesis: the medium is isotropic and where radiative effects, viscous dissipation, the work done by pressure changes and gravity effects are negligible [8].

$T_s = T_f = T$, where T_s and T_f are the temperatures of the solid and fluid phases, respectively. Here we also assume that heat conduction in the solid and fluid phases takes place in parallel so that there is no net heat transfer from one phase to the other. Taking averages over an elemental volume of the medium, for the solid phase:

$$(1 - \varphi)\,(\rho c)_s\,\partial T_s/\partial t = (1 - \varphi)\nabla *(k_s \nabla T_s) + (1 - \varphi)\, q_s''' \qquad \text{Eq. 5}$$

{Variation into a unit volume due to solid} = {flux at the external surface due to solid} + {volumetric source term due to solid}

For the fluid phase:

$$\varphi\,(\rho c_p)_f \partial T_f/\partial t + (\rho c_p)_f\, \boldsymbol{v} *\nabla T_f = \varphi\nabla *(k_f \nabla T_f) + \varphi\, q_f''' \qquad \text{Eq. 6}$$

{Variation due to fluid} + {convective term, due to seepage velocity} = {flux at the external surface due to fluid} + {volumetric source due to fluid}

Setting $Ts = Tf = T$ and adding Eqs. 5 and 6 we have:

$$(\rho c)_m\, \partial T/\partial t + (\rho c)_f\, \boldsymbol{v} * \nabla T = \nabla *(k_m \nabla T) + q_m''' \qquad \text{Eq. 7}$$

$$(\rho c)_m = (1 - \varphi)\,(\rho c)_s + \varphi\,(\rho c_p)_f \qquad \text{Eq. 8}$$

$$k_m = (1 - \varphi)\, k_s + \varphi\, k_f \qquad \text{Eq. 9}$$

$$q_m''' = (1 - \varphi)\, q_s''' + \varphi\, q_f''' \qquad \text{Eq. 10}$$

The general, more complex, heat transfer equation accounts for the terms summarized in the hypothesis and is well described in Ref. [8]. With respect to the aim of this activity, only thermal conductivity will be discussed with detail in the following.

2.2.2 Assessment of thermal conductivity of a porous medium

In general, the structure of a porous medium is very complex, consisting of different grain (pore) sizes and geometries. A detailed prediction of the effective thermal conductivity of heterogeneous media requires knowledge of the shape, size, location (distribution) and conductivity of each particle in the system together with interaction between particles [8].

If the heat conduction in the solid and fluid phases occurs in parallel, then Eq. 9 gives the overall conductivity k_A. On the other hand, if the structure and orientation of the porous medium is such that the heat conduction takes place in series, with all of the heat flux passing through both solid and fluid, then the overall conductivity k_H is given by:

$$1/k_H = (1 - \varphi)/\, k_s + \varphi/\, k_f \qquad \text{Eq. 11}$$

We always have $k_H \le k_A$, with equality if and only if $ks = k\,f$. Therefore, k_A and k_H will provide upper and lower bounds, respectively, on the actual overall conductivity k_m.
For practical purposes, a rough and ready estimate for k_m is provided by k_G, the weighted geometric mean of k_s and k_f, defined by [8]:

$$k_G = k_s^{(1 - \varphi)} * k_f^{\varphi} \qquad \text{Eq. 12}$$

This provides a good estimate so long as k_s and k_f are not too different from each other.

For a sufficiently dilute dispersion (suspension) of spheres, Maxwell (1865) obtained the following expression for the stagnant thermal conductivity of a packed-sphere bed [9]:

$$k_m / k_f = [2\,\varphi + (k_s / k_f)\,(3 - 2\,\varphi)] \,/\, [(3 - \varphi) + (k_s / k_f)\,\varphi] \qquad \text{Eq. 13}$$

Assuming $\lambda = (k_s / k_f)$

$$k_m / k_f = [\lambda + 2 - 2\,\Psi\,(1 - \lambda)] \,/\, [\lambda + 2 + \Psi\,(1 - \lambda)] \qquad \text{Eq. 14}$$

Maxwell's equation is valid for $\Psi \rightarrow 0$, since it was derived on the assumption that the solid spheres are sufficiently apart that they do not mutually interact. Nevertheless, it provides a lower bound for the stagnant thermal conductivity of a packed-sphere bed.

Lord Rayleigh (1892) extended Maxwell's model to higher order in the particle concentration Ψ, by taking into account the concentration of induced octupole moments. The case of a cubic array of uniform size spheres (simple cubic packing) was considered, and the effect on the potential in the neighborhood of a sphere by 248 of its closest neighbors (lying within the first 15 shells around a central sphere) was investigated. Rayleigh solved the Laplace equation for the potential inside and about a sphere invoking the principle of superposition to take into account the effect of surrounding spheres on the field in the neighborhood of the central sphere. The following expression is obtained for the effective thermal conductivity of the packed bed [9]:

$$k_m / k_f = \{[(\lambda + 2)/(1 - \lambda)] - 2\,\Psi - 0.525\,[(3 - 3\lambda)/[(4 + 3\lambda)]\,\Psi^{10/3}\} \,/\, \{[(\lambda + 2)/(1 - \lambda)] + \Psi - 0.525\,[(3 - 3\lambda)/[(4 + 3\lambda)]\,\Psi^{10/3}\} \qquad \text{Eq. 15}$$

This expression approaches Maxwell's result by neglecting higher order terms in Ψ. At $\Psi = 0.5236$, the spherical particles in the cubic lattice are in point contact, and for $\lambda \rightarrow +\infty$ the effective conductivity should approach ∞ at $\Psi = 0.5236$. These qualitative conditions are not satisfied by Rayleigh's expression.

Meredith and Tobias (1960) modified Rayleigh's result, providing an analytical expression that agrees more satisfactorily with the data in the critical range near $\Psi = 0.5236$. This expression is as follows[9]:

$$k_m / k_f = \{[(\lambda + 2)/(1 - \lambda)] - 2\,\Psi + 0.409\,[(6 + 3\lambda)/[(4 + 3\lambda)]\,\Psi^{7/3} - 2.133\,[(3 - 3\,\Psi)/[(4 + 3\,\Psi)]\,\Psi^{10/3}\} / \ldots$$

$$\ldots / \{[(\lambda + 2)/(1 - \lambda)] + \Psi + 0.409\,[(6 + 3\lambda)/[(4 + 3\lambda)]\,\Psi^{7/3} - 2.133\,[(3 - 3\,\Psi)/[(4 + 3\,\Psi)]\,\Psi^{10/3}\} \qquad \text{Eq. 16}$$

As $\lambda \rightarrow +\infty$, the data are in satisfactory agreement with the modified expression, except for $\Psi = 0.5161$ where the data considerably exceed the theory

Woodside (1961) considered a unit cube containing one-eighth of a sphere of radius R. The general case is considered in that the uniform spherical particles are not in contact. The final expression for the effective medium conductivity is shown to be [9]:

$$k_m / k_f = 1 - (6\,\Psi/\pi)^{1/3}\,\{1 - [(a^2 - 1)/a]*\ln[(a + 1)/(a - 1)]\} \qquad \text{Eq. 17}$$

$$a = \{1 + 4/[\pi\,(\lambda - 1)\,(6\,\Psi/\pi)^{2/3}]\}^{1/2} \qquad \text{Eq. 18}$$

In deriving the above equation, it was assumed that

- the gas spaces are small enough that heat transfer by convection may be neglected,
- the isotherms are planes perpendicular to the direction of heat flow.

The second assumption is valid only when $k_s / k_f = 1$. The errors will be greater the larger the value of k_s / k_f . As with Rayleigh's model, it is limited to $\Psi = 0.5236$. It appears that the accuracy of the model has not been sufficiently tested against measurements.

Zehner and Schlunder (1970) arrived at an analytical expression for the effective stagnant thermal conductivity of a packed bed. They considered for the unit cell one-eighth of a cylinder (inner cylinder of unit radius and outer cylinder of radius R). Fluid is filled between the inner and outer cylinders while the inner cylinder consists of both the solid and the fluid phases with its interface A_{fs} described by [10]:

$$r^2 + z^2 /[B - (B - 1)\, z]^2 = 1 \qquad \text{Eq. 19}$$

Where the quantity labeled as B is the shape factor characterizing the geometrical effect of the solid particle. For B → *0,* the boundary becomes the z-axis with no solid volume; for B = 1 the solid becomes a sphere, and for B →+ ∞ the solid occupies the entire inner cylinder.
The effective thermal conductivity of a packed bed is expressed by:

$$k_m/ k_f = 1 - (1 - \varphi)^{1/2} + [2\, (1 - \varphi)^{1/2}) / (1 - \xi B)] * \{[(1 - \xi)\, B/ (1 - \xi B)^2] * \ln (1/ \xi B) - (B + 1)/2 - \dots$$

$$\dots - (B-1)/ (1 - \xi B)\} \qquad \text{Eq. 20}$$

$$B = C[(1 - \varphi)/ \varphi]^m \qquad \text{Eq. 21}$$

$$\xi = 1 / \lambda = 1 / (k_s / k_f) = k_f / k_s \qquad \text{Eq. 22}$$

With m =10/9. The constant C depends on the shape of the particle. Zehner and Schlunder suggest that C =1.25, 1.40 and 2.5 for spheres, broken (irregular particles) and cylinders respectively.
Krupiczka approximated a packed bed as a bundle of long cylinders and numerically solved a set of two heat conduction equations in two dimensions with perfect contact at the solid–fluid interface. He then extended the results to a spherical lattice and proposed a correlation for the dimensionless effective thermal conductivity [10]:

$$k_m/ k_f = [\lambda]^{\,(0.208 - 0.757 * \log \varphi - 0.057 * \log \lambda)} \qquad \text{Eq. 23}$$

Hsu *et al* developed a lumped-parameter model for the effective stagnant thermal conductivity of some two-dimensional and three-dimensional spatially periodic media. The geometries under investigation include arrays of touching and non-touching in-line squares and cylinders (two-dimensional), as well as touching and non-touching in-line cubes (three-dimensional). The dimensionless effective stagnant thermal conductivity, $k_e^{\,+} = k_m/ k_f$, for three-dimensional cubes with thermal resistance is expressed as[10]:

$$k_m/ k_f = 1 - \gamma_a^2 - 2\, \gamma_a \gamma_c + 2\, \gamma_a^2 \gamma_c + \gamma_a^2 \gamma_c^2 /(1/\lambda) + (\gamma_a^2 - \gamma_a^2 \gamma_c^2) / (1 - \gamma_a + \gamma_a/\lambda) + \dots$$

$$\dots + 2(\gamma_a \gamma_c - \gamma_a^2 \gamma_c^2) / (1 - \gamma_a \gamma_c + \gamma_a \gamma_c /\lambda) \qquad \text{Eq. 24}$$

The porosity, φ, is related to the geometrical parameters (γ_a and γ_c) by:

$$\Psi = 1 - \varphi = (1 - 3\gamma_c^2)\, \gamma_a^3 + 3\, \gamma_a^2 \gamma_c^2 \qquad \text{Eq. 25}$$

A comparison of the results based on Eq. 24 with existing experimental data shows that they are in excellent agreement with the experimental data if the contact resistance parameter $\gamma_c = 0.13$ is chosen at a porosity of 0.36. However, no comparison with experimental data at different porosities was given.

More refined models available for conductivity determination are reported in Ref. [10].

2.2.3 Conclusive remarks

The correlations presented in this section will be applied for the calculation of the conductivity of selected powders in section 3. The aim is to support the design of the TxP Facility and in particular to provide prediction of a possible realistic range of the powder conductivity.

It should be pointed out that each correlation calculates the conductivity of the powder based on a more or less complicated function that depends from three parameters:

1. The conductivity of the solid material (99.5% dense),
2. The conductivity of the fluid dispersed in the powders,
3. The porosity,
4. Hsu and Zehner correlations account for particle shape also but will be not analyzed at this step.

The weakness points of the correlations can be summarized as follow:

1. Some of them are ideal correlations (i. e. parallel, series), and some others apply in specific range of porosity,
2. Each correlation investigated assumes spherical particles and does not account for the particle shape influence,
3. The influence of the particles diameter is not considered.

Criterion 1 Melting point Criterion 2 Thermal conductivity			
Material	**Melting point (°C)**	**Thermal conductivity (at 100°C) [W/mK]**	**Notes**
Al	660	240	Refs. [11], [13]
Ag	961	422	
Cr	1860	88	
Cu	1084	391	
Fe	1536	72	
Mg	650	154	
Mo	2620	135	
Ni	1453	83	
Si	1410	112	
W	3400	166	
AISI1010	1510	61	
Brass (30%Zn)	930	133	
Boron-Nitride	2700	160	
Diamond£	3400	1250	

Tab. 2 – Criteria 1 and 2 conductivity and melting point.

Criterion 3 Solid phase transitions temperatures		
Material	**Allotropic or diagram phases**	**Notes**
Al	• Face-centered cubic no allotropic phase transformations	Refs. [14], [15], [16]
Ag	• Face-centered cubic, no allotropic phase transformations	Refs. [14], [15], [17]
Cr	• Body-centered cubic, no allotropic phase transformations	Refs. [14], [15], [18]
Cu	• Face-centered cubic, no allotropic phase transformations	Refs. [14], [15], [19]
Fe	• Body-centered cubic α-iron, or ferrite, T < 912°C • Face-centered cubic Γ-iron 912 < T < 1394 °C • Body-centered cubic δ-iron T > 1538 °C	Refs. [14], [15], [20]
Mg	• Hexagonal, no allotropic phase transformations	Refs. [14], [15], [21]
Mo	• Body centered cubic, no allotropic phase transformations	Refs. [14], [15], [22]
Ni	• Face-centered cubic, no allotropic phase transformations	Refs. [14], [15], [23]
Si	• Diamond cubic, no allotropic phase transformations	Refs. [14], [15], [24]
W	• no allotropic phase transformations	Refs. [14], [15], [25]
AISI1010	• stable perlite + ferrite until 1000 °C	Ref. [26]
Brass (<30%Zn)	• Alloys containing up to about 35% zinc are single-phase dendritic α and are renowned for their ductility. • Between 35 and 37.5% zinc, α and β' exist. The phase β' transforms to β at 454 °C. • Between 37.5 and 42% zinc, the body-centered cubic β' phase appears and the hardness increases. The phase β' transforms to β at 460 °C. • Above 42% β and γ' exist. The phase γ' transform to γ at 468 °C. The presence of γ causes embrittlement.	Ref. [27]
BN	• Not addressed	--.
Diamond	• Stable	Ref. [13]

Tab. 3 – Criterion 3, Solid phase transitions temperatures.

Criterion 5 Chemical reactions with water, steam and oxygen		
Material	**Description**	**Notes**
Al	• Al powder heated in steam produces hydrogen and Al oxide. $2Al + 3H_2O \rightarrow Al_2O_3 + H_2$ + 3,520 kcal / kg of Al • Al will burn in oxygen if it is powdered, $3Al + O_2 \rightarrow Al_2O_3$ + 393.3 kcal / mol	Refs. [16], [28], [29]
Ag	• No evidence of hazardous reactions with steam • No evidence of hazardous reactions with Oxygen	Refs. [17]
Cr	• No evidence of hazardous reactions with steam • No evidence of hazardous reactions with Oxygen	Refs. [18]
Cu	• No evidence of hazardous reactions with steam • No evidence of hazardous reactions with Oxygen	Refs. [19]
Fe	• Fast reaction with steam over 200°C $2Fe + 3H_2O \rightarrow Fe_2O_3 + H_2$ • No evidence of hazardous reactions with Oxygen	Refs. [20]
Mg	• Mg burns in steam with its typical white flame to produce white oxide and hydrogen. $Mg + H_2O \rightarrow MgO + H_2$ • Mg burns in oxygen with an intense white flame to give white solid oxide.$2Mg + O_2 \rightarrow 2MgO$	Refs. [21], [28]
Mo	• No evidence of hazardous reactions with steam under 1100°C • No evidence of hazardous reactions with Oxygen	Refs. [22], [31],[32]
Ni	• Reaction with steam only at high temperature • Powder Ni can burst with Oxygen	Refs. [23], [33]
Si	• Si powdered will react with steam at red heat to produce silicon dioxide and hydrogen. $Si + 2H_2O \rightarrow SiO_2 + 2H_2$ • Si will burn in oxygen if heated strongly enough. Silicon dioxide is produced. $Si + O_2 \rightarrow SiO_2$	Refs. [24], [28]
W	• No evidence of hazardous reactions with steam • Powder W can burst with Oxygen	Refs. [25], [34]
AISI1010	• No evidence of hazardous reactions with steam • No evidence of hazardous reactions with Oxygen	Ref. [26]
Brass (<30%Zn)	• No evidence of hazardous reactions with steam • No evidence of hazardous reactions with Oxygen.	Ref. [27]
Boron Nitride	• Not addressed	--.
Diamond	• No evidence of hazardous reactions with steam • No evidence of hazardous reactions with Oxygen	Ref. [13]

Tab. 4 – Criterion 5, Chemical reactions with water, steam and oxygen.

Criterion 8 Radiation damage		
Material	**Description**	**Notes**
Al	• Isotope Al^{27} content in nature is > 99.5% • σa = 0.23 [10^{-28} m^2]	Refs. [16], [35]
Ag	• Isotopes Ag^{107} (52%) and Ag^{109} • n + Ag^{107} → Ag^{108}→ (β 418 y) → Pd^{108} σa = 64.00 [10^{-28} m^2]	Refs. [17], [35]
Cr	• Isotopes Cr^{52} (84%), Cr^{53} (10%) and Cr^{54} (2%) • σa = 3.10 [10^{-28} m^2]	Refs. [18], [35]
Cu	• Isotopes Cu^{63} (70%) Cu^{65} (30%) • σa = 3.80 [10^{-28} m^2]	Refs. [19], [35]
Fe	• Isotopes Fe^{54} (6%), Fe^{56} (92%), Fe^{57} (2%) • σa = 2.55 [10^{-28} m^2]	Refs. [20], [35]
Mg	• Isotopes Mg^{24} (80%) Mg^{25} (10%) Mg^{26} (11%) • σa = 0.063 [10^{-28} m^2]	Refs. [21], [35]
Mo	• Isotopes Mo^{98} (24%), other five stable isotopes • σa = 2.65 [10^{-28} m^2]	Refs. [22], [35]
Ni	• Isotopes Ni^{58} (68%) Ni^{60} (26%) Ni^{61} (1%) Ni^{62} (4%) Ni^{64} (1%) • σa = 4.43 [10^{-28} m^2]	Refs. [23], [35]
Si	• Isotopes Si^{28} (92%), Si^{29} (5%), Si^{30} (3%) • σa = 0.16 [10^{-28} m^2]	Refs. [24], [35]
W	• Isotopes W^{184} (31%), other five isotopes • σa = 18.50 [10^{-28} m^2]	Refs. [25], [35]
AISI1010	• σa = 2.55 [10^{-28} m^2]	Ref. [35]
Brass (<30%Zn)	• not addressed	--
Boron Nitride	• B^{10} (20%), B^{11} (80%) • B^{10} +n → Li^7 + α σa = 759 [10^{-28} m^2]	Ref. [35]
Diamond	• σa = 2.55 [10^{-28} m^2]	Ref. [35] Appendix E

Tab. 5 – Criterion 8, Radiation damage.

Criterion 9 Cost			
Material	**Average price (qualitative)**	**Material**	**Average price (qualitative)**
Al	24500 US$/ton	Ni	26500 US$/ton
Ag	1200000 US$/ton	Si	2000 US$/ton
Cr	10000 US$/ton	W	40000 US$/ton
Cu	9600 US$/ton	AISI1010	600 US$/ton
Fe	200 US$/ton	Brass (<30%Zn)	To be added the precise price of the powder
Mg	3000 US$/ton	Boron Nitride	NA
Mo	38000 US$/ton	Diamond	12500 €/kg

Tab. 6 – Criterion 9, Cost.

Material	Criterion (1)	Criterion (2)	Criterion (3)	Criterion (4)	Criterion (5)	Criterion (6)	Criterion (7)	Criterion (8)	Criterion (9)
Al	S	NS	S	S	NS	PT	PS	U	S
Ag	S	S	S	S	S	PT	PS	NS	NS
Cr	S	S	S	S	S	PT	S	U	S
Cu	S	S	S	S	S	PT	PS	U	S
Fe	S	S	S	S	S	PT	S	U	S
Mg	S	NS	S	S	NS	PT	PS	U	S
Mo	S	S	S	S	S	PT	S	U	S
Ni	S	S	S	S	NS	PT	S	U	S
Si	S	S	S	S	NS	PT	NA	U	S
W	S	S	S	S	NS	PT	NA	U	S
AISI1010	NS	S	S	S	S	PT	PS	U	S
Brass (30%Zn)	S	S	S[$]	S	S	PT	PS	U	S
Boron Nitride	S	S	NA	NA	NA	PT	NA	NS	NA
Diamond	S	S	S	S	S	PT	S	U	NS

S → Satisfied
NS → Not Satisfied
[$] Zn content as to be maintained under 30%
PS → Potentially Susceptible

U → Unknown
PT → Partially Tested in the experiment
NA → Not addressed

Tab. 7 – Criteria for the screening and ranking of the candidate powders materials.

3 Design of the Tubes for Powders Facility

3.1 TxP conceptual design

The main objectives of the Tubes for Powders (TxP) Facility are connected to the evaluation of the thermal performance of several candidate powders for the application to the ALFRED SG[51][52]. In particular it is focused on:

- Determine the thermal conductivity of the powders into a representative annular gap.
- Determine the influence of the powder compaction grade on the conductivity.
- Investigate the influence of the filling gas (Helium) pressure.
- Investigate the impact of selected thermal cycle.

The TxP facility consists of three concentric tubes; a conceptual scheme is reported in *Fig. 5*. The tube labeled as IT contains a heating rod HR that generates 25 kW (maximum). The free volume between the HR and the first tube (HP zone) is filled with high conductivity powders. In the first design diamond powder was selected for the HP zone. The intent of this zone (15 mm in width), was to obtain fruitful data on this material if the gap temperature drop resulted negligible. When the diamond solution was abandoned this objective was maintained in order to analyze high conductivity powders as copper. The gap between the IT and the PT tubes is designed to test several powders specimens, it is about 6 mm in width. In the outer tube, WT, a water flow removes the generated thermal power.

The design includes 48 + 1 + 1 thermocouples located in three azimuthal and four axial directions. Twelve are inserted at HR outer surface, 24 are located in IT (12 in the inner, 12 in the outer surfaces). The remaining 12 thermocouples are positioned in the inner surface of WT. The main data are given in *Tab. 8*. One thermocouple is contained in the heating rod, at its center. One additional axially removable thermocouple will be inserted in HP. Its goal is to measure with great resolution the axial temperatures profile.

For the system described in, *Fig. 5* and *Tab. 8*, the heat conduction equation is:

$$q' = 2\pi \cdot \frac{T_1 - T_{water}}{\sum R_{th}} = \frac{T_1 - T_{water}}{\frac{1}{k_{DP}}\ln\frac{r_2}{r_1} + \frac{1}{k_{IT}}\ln\frac{r_3}{r_2} + \frac{1}{k_{Powder}}\ln\frac{r_4}{r_3} + \frac{1}{k_{PT}}\ln\frac{r_5}{r_4} + \frac{1}{hr_5}} \qquad \textit{Eq. 26}$$

where:

q’	is the linear power [W/m],
r_i	is referred to the *i* radius reported in columns 4 and 5 of *Tab. 8*,
k_i	is referred to the thermal conductivity [W/mK], with i according to *Tab. 8*,
T	Temperature [K]
h	is the heat transfer coefficient

In this configuration the quantity q’ is imposed as constant by the heating rod located in the inner tube, which has in charge for the heat generation.

The thermal resistances of the tubes are calculated assuming a conductivity of 16 W/mK (AISI 304 L). The heat transfer coefficient of the water is calculated assuming an inlet temperature of 14 °C and a mass flow of 0.4 kg/s (0.2 m/s); it is derived from Reynolds number by mean of Dittus Boelter correlation (*Tab. 8*).

The structure is instrumented with 48 + 2 thermocouples. The 24 thermocouples located at the gap borders (see *Fig. 5*), allow to the measure of the temperature difference between the tubes – walls that embed the powders under testing. The thermal conductivity of the powder is calculated by:

$$k_{Powder} = \frac{q' \ln \frac{r_4}{r_3}}{2\pi \left(T_3 - T_4\right)} \qquad \textit{Eq. 27}$$

The conductivity of the high conductivity powder (synthetic diamond in the first design) surrounding the heating rod, k_{HP} can be evaluated in the same manner since T_1 and T_2 are measured by mean of further 24 thermocouples (see *Fig. 5*). T (r_i, z, φ) refers to the thermocouple T located at radius r_i according with *Tab. 8*, elevation z = 0, 1, 2 3 (starting from the bottom), and azimuthal position φ = 0, 1, 2 (corresponding to 0°, 120°, -120°). The thermocouple T_0 is placed inside the heating rod at its center.

3.2 TxP design – Assessment of thermal performances

3.2.1 TxP requirements

The design calculations are aimed to evaluate the thermal conductivity of candidate powders, and the related temperatures reached during the experiment. In particular is required that:

- The maximum temperature, T max has to be limited to 550°C in order to preserve the heating rod integrity;
- Large temperature gradients should be avoided in the steel tubes in order to minimize differential deformations;
- A representative value of the temperature drop across the gap has to be obtained to minimize the effect of measurement accuracy (+/-1°C). The temperature drop should be larger than 20°C. Alternatively, the HP zone will be used to get the measure.

3.2.2 Representative correlations for the assessment of powder conductivity

In order to check the criteria reported in 3.2.1, the TxP performances must be investigated taking into account of the powder conductivity. The purpose of the following analysis is to restrict to a given representative range the conductivities on the basis of selected correlations.

The conductivity of the solid materials have been reported in *Tab. 9* [11][13]. They have been taken as reference to calculate the conductivity of the corresponding powders on the basis of the correlations discussed in section 2.2.2.
In *Tab. 10*, a summary of the investigated correlations is given. It should be pointed out that each correlation calculates the conductivity of the powder based on a more or less complicated function that depends by three parameters:

1. The conductivity of the solid material (99.5% dense),
2. The conductivity of the fluid dispersed in the powders:
    a. Assumed as Helium with constant conductivity of 0.2 W/mK

3. The porosity:
    b. Investigated in the range [0.1-0.9]

The weakness points of the correlations can be summarized as follow:

1. Some of them are ideal correlations (i. e. parallel, series), and some others apply in specific range of porosity,
2. Each correlation assumes spherical particles and does not account for the particle shape influence,
3. The influence of the particles diameter is not considered.

The calculations have been implemented by mean of excel working sheets that automatically produce the conductivity tables at each value of the porosity (to be introduced as input). A sample of the working sheets out-put is reported in *Tab. 11* in the hypothesis of porosity equal to 0.3 using the case 1 correlation (defined in *Tab. 10*). The complete summary of the results is included in Ref. [12].

The conductivity of diamond powder as function of porosity (using the seven different correlations) is given in *Fig. 6*. The same analysis is repeated in the case of copper (*Fig. 7*) and brass (*Fig. 8*).

Parallel and series bound the results (*Fig. 6, Fig. 7* and *Fig. 8)*, these approximation are idealized cases. Cases 3 and 4 underestimate the conductivity because they are recommended at high porosity. Case 6 highlights a representative trend between 0.3 and 0.5. Finally, case 5 is excluded from the analysis since it gives no physical results for porosities under 0.4 (negative results).

The remaining two correlations are selected as representative range that embed the effective conductivity.

- Case 1 represents the weighted geometric mean of k_s (solid) and k_f (fluid). It is as usual recommended when k_s and k_f are similar. Nevertheless, it is assumed as upper bound because the investigated models apply to large porosities ranges (>0.5).
- Case 2 represents the Kuprikza model. It is assumed as lower bound.

3.2.3 Preliminary thermal assessment of the HP zone

This section is aimed to verify the thermal performance of the HP zone filled with different powders. Diamond, Copper, Brass and AISI 10-10 will be presented in the following.

The following conservative assumptions are applied:

- The power of the heating rod is considered at the maximum operating value (25 kW),
- The minimum powder porosity at which the temperature limit should not be over-passed is 0.30. If this hypothesis is not satisfied the operating power should be reduced.
- The conductivity of the powder is calculated at 300°C.
- The filling gas considered is Helium with constant conductivity (0.2 [W/(mK)], 1 bar).
- The conductivity of the powder contained in the gap, P-PT is fixed conservatively equal to 2.5 [W/(mK)].

Tab. 12 summarizes the hypothesis assumed for the calculations. The results are depicted from *Fig. 9* to *Fig. 12*. The maximum power can be operated only if HP zone is filled with diamond (the corresponding limit of porosity is 0.30). Copper, Brass and AISI-1010 powders require a power reduction respectively to 20, 15 and 13 kW (the porosity limit is in the range 0.32 -0.40).

3.2.4 Thermal assessment of the TxP Facility

On the basis of the preliminary analyses reported in section 3.2.3, four different configurations have been investigated assuming different powders contained in the HP zone. The hypothesis are summarized in *Tab. 13*:

- The power of the heating rod is established according to section 3.2.3,
- HP zone: assessed with four different powders: diamond, copper, brass and AISI-1010 at 0.3 porosity treated with correlations labeled as case 1 and case 2. Helium is assumed as fluid. Each investigation represents a possible configuration.
- Powder zone: each configuration defined above is exploited against diamond, copper, brass and AISI-1010 in the porosity range 0.1-0.5. The conductivity of the powder is calculated at 100°C. Helium is assumed as filling fluid (0.2 [W/(mK)], 1 bar).

The calculations are focused to the verification of the requirements reported in 3.2.1. The final configuration has not been still selected. It will be defined after the execution of preliminary tests: the powders will be heated into a furnace up to 500°C in order to analyze their chemical-mechanical behavior to high temperature.

3.2.4.1 Configuration with diamond powder

This investigation deals with the hypothesis introduced in *Tab. 13*. The power is set to 25kW.

In *Fig. 13* the temperature drop in the HP zone is depicted. Constant temperature drop is designed. If the measurements obtained in the powder zone are not suitable for conductivity assessment (temperature drop under 20°C) of the diamond, HP zone is suitable to calculate the conductivity of 0.3 porosity diamond (at least 30°C are experienced).

The assessment of the thermal performance is presented in *Fig. 14*. Diamond powder is considered in the powder zone. The temperature limit is respected at whatever porosity of the diamond contained in the powder zone. The temperature drop within the powder zone is surely suitable for conductivity measurement above 0.40 porosity. In the range of porosities 0.30-0.40 HP zone may be required to get useful measures.
Copper, Brass and AISI-1010 are assessed from *Fig. 15* to *Fig. 17*. The porosity of the powders should be limited to 0.45 (Brass) and 0.4 (AISI-1010) to preserve the HR integrity. The temperature drop in the powder zone is always suitable for conductivity determination (above 0.30 porosity), with the exception copper. In order to investigate copper a the configuration of the HP with copper may be necessary.

3.2.4.2 Configuration with copper powder

This investigation deals with the hypothesis introduced in *Tab. 13*. The power is set to 20kW.

The results are depicted from *Fig. 18* to *Fig. 21*. The temperature drop in the HP zone is suitable for conductivity assessment to calculate the conductivity of 0.3 porosity copper (at least 45°C are experienced, *Fig. 18*). The copper conductivity may require the use of the HP zone to be evaluated (*Fig. 19*). Brass and AISI-1010 can be investigated with no limitation of porosity (in the range 0.30-0.50).

3.2.4.3 Configuration with brass powder

This investigation deals with the hypothesis introduced in *Tab. 13*. The power is set to 15kW.

The results are depicted from *Fig. 22* to *Fig. 25*. The HP is not required to get fruitful data on brass conductivity. It is not recommended to test powders with higher conductivity than brass (see *Fig. 23*).

3.2.4.4 Configuration with AISI-1010 powder

This investigation deals with the hypothesis introduced in *Tab. 13*. The power is set to 13kW.

The results are depicted from *Fig. 26* to *Fig. 29*. The HP is not required to get fruitful data on AISI-1010 conductivity. It is not recommended to test powders with higher conductivity than AISI-1010 (see *Fig. 27* and *Fig. 28*).

3.3 TxP design - Preliminary thermo-mechanical verification of steel tubes

The calculations hereafter reported are considered conservative because were performed at 25kW considering diamond as most promising solution. Diamond was then abandoned and the power was reduced (at maximum TxP will be operated at 20kW in the copper configuration). The following assumptions were applied:

- The IT is considered as a thick cylinder (sIT/<rIT> = 15.2%)
- No load are considered applied to the steel tubes
- No constrains are applied to the tube boundaries
- Only radial temperature variation is applied
- The hypothesis at which temperatures are calculated are summarized in *Tab. 13.*

A scheme of the geometry is reported in *Fig. 30*. The tube material is AISI 304 L [36]; its main properties are summarized in *Tab. 14* and *Fig. 31*, *Fig. 32*. PT can be considered as a thin cylinder. At maximum power, when subjected to the water flow (characterized in *Tab. 22*), PT experiences a temperature drop of 10 °C with a maximum temperature of 65°C.

Under the thick cylinder hypothesis the radial displacement, w (according with the direction indicated in *Fig. 30*) is expressed by:

$$\partial^2 w \partial r^2 + (1/r)\, \partial w/\partial r - w/r^2 = 0 \qquad \text{Eq. 28}$$

The solution of this equation is in the form:

$$w\,(r) = Ar + B/r \qquad \text{Eq. 29}$$

Displacements and deformations are connected as follow:

$$\varepsilon_r = \partial w/\partial r = (1/E)\,[\sigma_r - \nu(\sigma_\theta + \sigma_a)] + \alpha\,\Delta T(r) \qquad \text{Eq. 30}$$

$$\varepsilon_\theta = w/r = (1/E)\,[\sigma_\theta - \nu(\sigma_r + \sigma_a)] + \alpha\,\Delta T(r) \qquad \text{Eq. 31}$$

Assuming b and a respectively the outer and the inner radius of the cylinder, the boundary conditions are: $\sigma_r\,(r = a) = \sigma_r\,(r = b) = 0$. Radial temperature is expressed as [37]:

$$T = T(r) = T_e + \frac{T_i - T_e}{\ln\left(b/a\right)} \ln\left(\frac{b}{r}\right)$$

Eq. 32

The solutions of the previous equations are

$$\sigma_r = \frac{\alpha E (T_i - T_e)}{2(1-\nu)\ln\left(b/a\right)} \left[-\ln\left(b/r\right) - \frac{a^2}{b^2 - a^2}\left(1 - \frac{b^2}{r^2}\right)\ln\left(b/a\right) \right]$$

$$\sigma_t = \frac{\alpha E (T_i - T_e)}{2(1-\nu)\ln\left(b/a\right)} \left[1 - \ln\left(b/r\right) - \frac{a^2}{b^2 - a^2}\left(1 + \frac{b^2}{r^2}\right)\ln\left(b/a\right) \right]$$

Eq. 33

Equilibrium in axial direction gives:

$$\int_a^b 2\pi r \cdot \sigma_a \cdot dr = \int_a^b 2\pi r \left\{ \frac{\alpha E}{(1-\nu)} \left[\frac{2\nu}{b^2 - a^2} \cdot \int_a^b (\Delta T) r dr - (\Delta T) \right] + E\varepsilon_0 \right\} dr = 0$$

Eq. 34

That allows the calculation of axial stress using Eq. 32.

$$E\varepsilon_0 = \frac{2\alpha E}{b^2 - a^2} \int_a^b (\Delta T) r dr$$

Eq. 35

$$\sigma_a = -\frac{\alpha E}{(1-\nu)} \left[\frac{2}{b^2 - a^2} \int_a^b (\Delta T) r dr - (\Delta T) \right]$$

Eq. 36

Von Mises criterion is then applied:

$$\sigma_y = \sqrt{\frac{1}{2}\left[(\sigma_r - \sigma_\theta)^2 + (\sigma_r - \sigma_z)^2 + (\sigma_\theta - \sigma_z)^2\right]}$$

Eq. 37

3.3.1 Diamond powder

The verifications are executed assuming the maximum temperatures reported in *Tab. 15*. They correspond with the hypothesis of porosity equal to 0.5 of the diamond contained within the gap. For sake of completeness, the temperatures corresponding to all the porosities investigated are also attached.

The stresses have been calculated by mean of Eqs. 33 and 36. The effect of temperature on Young modulus and linear expansion coefficient is also considered (by linear extrapolation from the data of *Tab. 14*).

The results are reported in *Fig. 33, Fig. 34* and *Tab. 16*. The equivalent stress is calculated at the inner radius (on the basis of Eq. 37), that corresponds to the most affected point. Then, it is compared with the sigma 0.2% evaluated at the temperature experienced in the same point. The results are reported in *Tab. 21*.

Diamond powder results satisfactorily verified, the minimum safety coefficient (defined as the ration sigma02% / equivalent sigma) is 1.14.

3.3.2 Copper powder

The verifications are executed assuming the maximum temperatures reported in *Tab. 17*. They correspond with the hypothesis of porosity equal to 0.5 of the copper contained within the gap. For sake of completeness, the temperatures corresponding to all the porosities investigated are also attached.
The stresses have been calculated by mean of Eqs. 33 and 36. The effect of temperature on Young modulus and linear expansion coefficient is also considered.

The results are reported in *Fig. 35, Fig. 36* and *Tab. 18*. The equivalent stress is calculated at the inner radius (on the basis of Eq. 37), that corresponds to the most affected point. Then, it is compared with the sigma 0.2% evaluated at the temperature experienced at the same point. The results are reported in *Tab. 21*.

Copper powder result verified, the minimum safety coefficient (defined as the ration sigma02% / equivalent sigma) is 1.04.

3.3.3 Brass powder

The verifications are executed assuming the maximum temperatures reported in *Tab. 19*. They correspond with the hypothesis of porosity equal to 0.5 of the brass contained within the gap. For sake of completeness, the temperatures corresponding to all the porosities investigated are also attached.
The stresses have been calculated by mean of Eqs. 33 and 36. The effect of temperature on Young modulus and linear expansion coefficient is also considered.

The results are reported in *Fig. 37, Fig. 38* and *Tab. 20*. The equivalent stress is calculated at the inner radius (on the basis of Eq. 37), that corresponds to the most affected point. Then, it is compared with the sigma 0.2% evaluated at the temperature experienced in the same point. The results are reported in *Tab. 21*.

Brass powder results verified only for case 1. If case 2 is considered, the equivalent stress over-pass the sigma0.2%. Therefore, the stresses have to be reduced by decreasing the Brass powder porosity or decreasing the power achieved in the heating rod.

3.3.4 Thermo-mechanical verification of PT

The stresses achieved in PT has been calculated using Eq. 33 and 36. The results are reported in *Tab. 22*. The equivalent and the sigma 0.2 stresses result:

$$\sigma_{eq} = 22.3\ N/mm^2 << \sigma_{0.2} = 155.5\ N/mm^2 \qquad \text{Eq. 38}$$

3.4 TxP design – detailed mechanical verification: status of the activity

This section is still under development. It should include the detailed results achieved by the ANSYS nodalization of the TxP Facility.

Geometrical Parameters								
Tube label	**Material**	**Unit**	**Inner radius**		**Outer radius**		**Thickness**	**length**
HR	AISI304L	mm	r0	14.50	r_1	16.00	1.50	1200 active
IT	AISI304L	mm	r_2	31.34	r_3	36.34	5.00	1500
PT	AISI304L	mm	r_4	42.45	r_5	44.45	2.00	1400
WT	AISI304L	mm	r_6	51.13	r_7	57.15	6.02	1400

Other Parameters			
Water Temp. inlet	14 °C	**Reynolds**	3523
Water Temp. outlet	30 °C	**Nusselt (by mean of Dittus Boelter)**	30
Water average Temp.	22 °C	**Helium pressure**	4 bar
Water mass flow	0.4 kg/s	**Service water pressure**	6 bar
Water average velocity	0.2 m/s	**HR Power**	25 kW

Tab. 8 – TxP main data.

Material label	**Melting Point [°C]**	**Thermal conductivity [W/mK]**				
		At 100°C	***At 200°C***	***At 300°C***	***At 400°C***	***At 600°C***
Al	660	240	238	234	228	215
Ag	961	422	417	409	401	386
Cr	1860	88	85	82	77	69
Cu	1084	391	389	384	378	366
Fe	1536	72	63	56	50	39
Mg	650	154	152	150	148	145
Mo	2620	135	131	127	123	116
Ni	1453	83	74	67	64	69
Si	1410	112	82	66	54	38
W	3400	166	153	141	134	125
AISI1010	1510	61	55	50	45	36
Brass (30%Zn)	930	133	143	146	147	148
Boron-Nitride	2700	160	--	--	--	--
Diamond[£]	3400	1250	1090	930	770	450
Air	Filling gas	0.029	0.037	0.043	0.049	0.060
Ar	Filling gas	0.020	0.025	0.029	0.032	0.036
He	Filling gas	0.174	0.207	0.232	0.275	0.309

[£] 1350 W/mK At 20 °C

Tab. 9 – Conductivity of candidate solid materials and filling gases at different temperatures.

Id.	Descript.	Correlation	Notes
Case 1	--	$k_G = k_s^{1-\varphi} k_f^{\varphi}$	Ref. [8]
Case 2	Kupriczka model	$k_e^{+} = \frac{k_e}{k_f} = (\beta)^{0.280-0.757\log\varphi-0.057\log\beta}$	Ref. [10]
Case 3	Maxwell model	$\frac{k_e}{k_f} = \frac{2\varphi + (k_s/k_f)(3-2\varphi)}{3-\varphi+(k_s/k_f)\varphi}$	Ref. [9]
Case 4	Rayleigh model	$\frac{k_e}{k_f} = \frac{[(2+\lambda)/(1-\lambda)] - 2\phi - 0.525[(3-3\lambda)/(4+3\lambda)]\phi^{10/3}}{[(2+\lambda)/(1-\lambda)] + \phi - 0.525[(3-3\lambda)/(4+3\lambda)]\phi^{10/3}}$	Ref. [9] $\phi = 1-\varphi$
Case 5	Rayleigh Extended model	$\frac{k_e}{k_f} = \frac{\frac{2+\lambda}{1-\lambda} - 2\phi + 0.409\frac{6+3\lambda}{4+3\lambda}\phi^{7/3} - 2.133\frac{3-3\phi}{4+3\phi}\phi^{10/3}}{\frac{2+\lambda}{1-\lambda} + \phi + 0.409\frac{6+3\lambda}{4+3\lambda}\phi^{7/3} - 0.906\frac{3-3\lambda}{4+3\lambda}\phi^{10/3}}$	Ref. [9] $\phi = 1-\varphi$
Case 6	Zehner model	$\frac{k_e}{k_f} = 1-(1-\varphi)^{1/2} + \frac{2(1-\varphi)^{1/2}}{1-B/\beta}\left[\frac{(1-1/\beta)B}{(1-B/\beta)^2}\ln\frac{\beta}{B} - \frac{B+1}{2} - \frac{B-1}{1-B/\beta}\right]$ $B = 1.25\left(\frac{1-\varphi}{\varphi}\right)^{10/9} \qquad \beta = k_s/k_f$	Ref. [10]
Parallel	--	$k_m = (1-\varphi)k_s + \varphi k_f$	Ref. [8]
Series	--	$\frac{1}{k_H} = \frac{(1-\varphi)}{k_s} k_s + \frac{\varphi}{k_f}$	Ref. [8]

Tab. 10 – Summary of the correlations investigated to assess the conductivity of the powders.

Material label	Filler He	Thermal conductivity [W/mK], φ=0.3				
		100°c	200°C	300°C	400°C	600°C
Al	Kf 0.20 W/mK	28.61	28.44	28.10	27.60	26.49
Ag		42.46	42.11	41.54	40.97	39.90
Cr		14.17	13.83	13.49	12.91	11.95
Cu		40.26	40.11	39.75	39.31	38.44
Fe		12.32	11.22	10.33	9.54	8.02
Mg		20.97	20.78	20.59	20.39	20.10
Mo		19.12	18.72	18.32	17.92	17.20
Ni		13.60	12.55	11.71	11.34	11.95
Si		16.78	13.49	11.59	10.07	7.87
W		22.10	20.87	19.71	19.02	18.12
AISI1010		10.97	10.20	9.54	8.86	7.58
Brass (30%Zn)		18.92	19.91	20.20	20.30	20.39
Diamond£		90.81	82.51	73.83	64.69	44.42
Correlation	$k_G = k_s^{1-\varphi} k_f^{\varphi}$.					

Tab. 11 – Calculation of conductivities by mean of case 1 correlation.

<table>
<tr><th>Description</th><th>label</th><th>Material</th><th>ID [mm]</th><th>OD [mm]</th><th>Conductivity [W/mK]</th><th colspan="2">Additional notes</th></tr>
<tr><td rowspan="2">Heating rod</td><td rowspan="2">HR</td><td rowspan="2">AISI304L</td><td rowspan="2">29.0</td><td rowspan="2">32.0</td><td rowspan="2">--</td><td>Max Power [W]</td><td>25000</td></tr>
<tr><td>Active length [mm]</td><td>1200</td></tr>
<tr><td>Internal Tube</td><td>IT</td><td>AISI304L</td><td>62.7</td><td>72.7</td><td>16</td><td colspan="2"></td></tr>
<tr><td>Powder Tube</td><td>PT</td><td>AISI304L</td><td>84.9</td><td>88.9</td><td>16</td><td colspan="2"></td></tr>
<tr><td>Water Tube</td><td>WT</td><td>AISI304L</td><td>102.3</td><td>114.3</td><td>16</td><td colspan="2">Wetted by water at T_{avg} 22°C</td></tr>
<tr><td>Filling gas</td><td>--</td><td>Helium</td><td>--</td><td>--</td><td>0.2</td><td colspan="2">Considered in both IT and PT</td></tr>
<tr><th colspan="8">Assessment of HP performance</th></tr>
<tr><th>Description</th><th>label</th><th>Material</th><th>ID [mm]</th><th>OD [mm]</th><th>Porosity [/]</th><th>Correlation/s</th><th>Additional notes</th></tr>
<tr><td>HP zone</td><td>P-IT</td><td>Diamond
Copper
Brass
AISI-1010</td><td>32.0</td><td>62.7</td><td>Range: [0.1-0.5]</td><td>Case 1, 2
conductivity taken at 300 °C</td><td>--</td></tr>
<tr><td>Gap zone</td><td>P-PT</td><td>--</td><td>72.7</td><td>84.9</td><td>--</td><td>K_{Powder} = 2.5 W/mK</td><td>Conservative assumption</td></tr>
</table>

Tab. 12 – Summary of the assumptions to assess the temperature peaks of the HP zone.

<table>
<tr><th colspan="8">Reference Case 1</th></tr>
<tr><th>Description</th><th>label</th><th>Material</th><th>ID [mm]</th><th>OD [mm]</th><th>Porosity [/]</th><th>Correlation/s</th><th>Additional notes</th></tr>
<tr><td>HP zone</td><td>P-IT</td><td>Diamond,
Copper,
Brass,
AISI-1010</td><td>32.0</td><td>62.7</td><td>0.3</td><td>Case 1, conductivity taken at 300 °C
$k_G = k_s^{1-\varphi} k_f^{\varphi}.$</td><td></td></tr>
<tr><td>Gap zone</td><td>P-PT</td><td>Diamond,
Copper,
Brass,
AISI-1010</td><td>72.7</td><td>84.9</td><td>Range: [0.1-0.5]</td><td>Case 1, conductivity taken at 100 °C</td><td>Ag, Mo, W are also assessed</td></tr>
<tr><th colspan="8">Reference Case 2</th></tr>
<tr><th>Description</th><th>label</th><th>Material</th><th>ID [mm]</th><th>OD [mm]</th><th>Porosity [/]</th><th>Correlation/s</th><th>Additional notes</th></tr>
<tr><td>HP zone</td><td>P-IT</td><td>Diamond,
Copper,
Brass,
AISI-1010</td><td>32.0</td><td>62.7</td><td>0.3</td><td>Case 2, conductivity taken at 300 °C
$k_e^* = \frac{k_e}{k_f} = (\beta)^{0.280-0.757\log\varepsilon-0.057\log\beta},$</td><td></td></tr>
<tr><td>Gap zone</td><td>P-PT</td><td>Diamond,
Copper,
Brass,
AISI-1010</td><td>72.7</td><td>84.9</td><td>Range: [0.1-0.5]</td><td>Case 2 conductivity taken at 100 °C</td><td>Ag, Mo, W are also assessed</td></tr>
</table>

Tab. 13 – Summary of the assumptions for the assessment of the TxP thermal performance.

AISI 304 L technical data												
Description	**Temperature [°C]**											**Range**
	20	**100**	**150**	**200**	**250**	**300**	**350**	**400**	**450**	**500**	**550**	
Sigma 0.2 [N/mm^2]	--	145	130	118	108	100	94	89	85	81	80	80 - 145
Sigma 1.0 [N/mm^2]	--	180	160	145	135	127	121	116	112	109	108	108 - 180
Sigma rup. [N/mm^2]	--	--	--	--	--	--	--	--	--	--	--	460 - 680
a [°C^{-1}]	--	1.60E-05	--	1.65E-05	--	1.70E-05	--	1.75E-05	--	1.80E-05	--	1.6e-5 - 1.8e-5
E [N/mm^2]	200000	194000	--	186000	--	179000	--	172000	--	165000	--	165000 - 200000

Tab. 14 – Mechanical properties of AISI 304 L.

Material	**Case 1 Reference, Case 1 applied to HP**			
	Porosity	**T2 [°C]**	**T3 [°C]**	**T2-T3 [°C]**
Diamond	0.10	116	85	32
	0.15	117	85	
	0.20	118	86	
	0.25	119	87	
	0.30	121	89	
	0.35	124	92	
	0.40	129	97	
	0.50	**147**	**115**	
	Case 2 Reference, Case 2 applied to HP			
	Porosity	**T2[°C]**	**T3 [°C]**	**T2-T3[°C]**
	0.10	117	86	32
	0.15	121	90	
	0.20	129	98	
	0.25	142	110	
	0.30	160	129	
	0.35	186	154	
	0.40	218	187	
	0.50	**311**	**280**	

Tab. 15 – Temperatures of tubes as function of the powder zone porosity, Diamond powder.

Case 1			Radius [mm]	Case 2		
σ_r [N/mm^2]	σ_θ [N/mm^2]	σ_a[N/mm^2]		σ_r [N/mm^2]	σ_θ [N/mm^2]	σ_a[N/mm^2]
0.0	-73.0	-73.0	31.35	0.0	-71.4	-71.4
-0.4	-66.6	-67.1	31.55	-0.4	-65.1	-65.6
-0.8	-60.3	-61.1	31.75	-0.8	-59.0	-59.8
-1.2	-54.0	-55.2	31.95	-1.2	-52.8	-54.0
-1.5	-47.9	-49.4	32.15	-1.5	-46.8	-48.3
-1.8	-41.8	-43.5	32.35	-1.7	-40.8	-42.6
-2.0	-35.7	-37.7	32.55	-2.0	-35.0	-36.9
-2.2	-29.8	-32.0	32.75	-2.1	-29.1	-31.3
-2.3	-23.9	-26.2	32.95	-2.3	-23.4	-25.7
-2.4	-18.1	-20.5	33.15	-2.4	-17.7	-20.1
-2.5	-12.4	-14.9	33.35	-2.5	-12.1	-14.6
-2.6	-6.7	-9.2	33.55	-2.5	-6.5	-9.0
-2.6	-1.1	-3.6	33.75	-2.5	-1.0	-3.6
-2.6	4.5	1.9	33.95	-2.5	4.4	1.9
-2.5	10.0	7.5	34.15	-2.4	9.7	7.3
-2.4	15.4	13.0	34.35	-2.4	15.0	12.7
-2.3	20.7	18.4	34.55	-2.2	20.3	18.1
-2.1	26.0	23.9	34.75	-2.1	25.5	23.4
-2.0	31.3	29.3	34.95	-1.9	30.6	28.7
-1.8	36.4	34.7	35.15	-1.7	35.7	34.0
-1.5	41.6	40.0	35.35	-1.5	40.7	39.2
-1.3	46.6	45.4	35.55	-1.2	45.7	44.4
-1.0	51.7	50.7	35.75	-1.0	50.6	49.6
-0.7	56.6	55.9	35.95	-0.7	55.5	54.8
-0.4	61.5	61.2	36.15	-0.3	60.3	59.9
0.0	66.4	66.4	36.35	0.0	65.0	65.0
Diamond Powder						

Tab. 16 – Stress states in IT, Diamond powder, porosity 0.5, cases 1 and 2.

Material	Case 1 Reference, Case 1 applied to HP			
	Porosity	**T2 [°C]**	**T3 [°C]**	**T2-T3 [°C]**
Copper	0.10	118	86	32
	0.15	119	88	
	0.20	121	90	
	0.25	124	92	
	0.30	128	96	
	0.35	133	102	
	0.40	142	110	
	0.50	**172**	**140**	
	Case 2 Reference, Case 2 applied to HP			
	Porosity	**T2 [°C]**	**T3 [°C]**	**T2-T3 [°C]**
	0.10	119	88	32
	0.15	126	95	
	0.20	138	106	
	0.25	155	123	
	0.30	177	146	
	0.35	206	175	
	0.40	242	210	
	0.50	**336**	**305**	

Tab. 17 – Temperatures of tubes as function of the powder zone porosity, Copper powder.

Case 1			Radius [mm]	Case 2		
σ_r [N/mm^2]	σ_θ [N/mm^2]	σ_a[N/mm^2]		σ_r [N/mm^2]	σ_θ [N/mm^2]	σ_a[N/mm^2]
0.0	-72.8	-72.8	31.35	0.0	-71.1	-71.1
-0.4	-66.4	-66.9	31.55	-0.4	-64.9	-65.3
-0.8	-60.1	-60.9	31.75	-0.8	-58.7	-59.5
-1.2	-53.9	-55.1	31.95	-1.2	-52.6	-53.8
-1.5	-47.7	-49.2	32.15	-1.5	-46.6	-48.1
-1.8	-41.6	-43.4	32.35	-1.7	-40.7	-42.4
-2.0	-35.6	-37.6	32.55	-1.9	-34.8	-36.8
-2.2	-29.7	-31.9	32.75	-2.1	-29.0	-31.1
-2.3	-23.8	-26.2	32.95	-2.3	-23.3	-25.6
-2.4	-18.0	-20.5	33.15	-2.4	-17.6	-20.0
-2.5	-12.3	-14.8	33.35	-2.5	-12.0	-14.5
-2.6	-6.7	-9.2	33.55	-2.5	-6.5	-9.0
-2.6	-1.1	-3.6	33.75	-2.5	-1.0	-3.6
-2.5	4.5	1.9	33.95	-2.5	4.4	1.9
-2.5	9.9	7.4	34.15	-2.4	9.7	7.3
-2.4	15.3	12.9	34.35	-2.3	15.0	12.6
-2.3	20.7	18.4	34.55	-2.2	20.2	18.0
-2.1	26.0	23.8	34.75	-2.1	25.4	23.3
-2.0	31.2	29.2	34.95	-1.9	30.5	28.6
-1.8	36.3	34.6	35.15	-1.7	35.5	33.8
-1.5	41.5	39.9	35.35	-1.5	40.5	39.1
-1.3	46.5	45.2	35.55	-1.2	45.5	44.3
-1.0	51.5	50.5	35.75	-1.0	50.4	49.4
-0.7	56.5	55.8	35.95	-0.7	55.2	54.6
-0.4	61.4	61.0	36.15	-0.3	60.0	59.7
0.0	66.2	66.2	36.35	0.0	64.8	64.8
Copper Powder						

Tab. 18 – Stress states in IT, Copper powder, porosity 0.5, cases 1 and 2.

Material	**Case 1 Reference, Case 1 applied to HP**			
	Porosity	**T2 [°C]**	**T3 [°C]**	**T2-T3 [°C]**
Brass	0.10	123	91	32
	0.15	125	94	
	0.20	129	98	
	0.25	134	103	
	0.30	142	110	
	0.35	152	120	
	0.40	166	134	
	0.50	**212**	**181**	
	Case 2 Reference, Case 2 applied to HP			
	Porosity	**T2 [°C]**	**T3 [°C]**	**T2-T3 [°C]**
	0.10	124	92	32
	0.15	135	104	
	0.20	152	121	
	0.25	175	143	
	0.30	203	172	
	0.35	238	206	
	0.40	278	247	
	0.50	**378**	**346**	

Tab. 19 – Temperatures of tubes as function of the powder zone porosity, Brass powder.

Case 1			Radius [mm]	Case 2		
σ_r [N/mm^2]	σ_θ [N/mm^2]	σ_a[N/mm^2]		σ_r [N/mm^2]	σ_θ [N/mm^2]	σ_a[N/mm^2]
0.0	-72.4	-72.4	31.35	0.0	-70.6	-70.6
-0.4	-66.1	-66.5	31.55	-0.4	-64.4	-64.9
-0.8	-59.8	-60.6	31.75	-0.8	-58.3	-59.1
-1.2	-53.6	-54.8	31.95	-1.2	-52.3	-53.4
-1.5	-47.5	-49.0	32.15	-1.5	-46.3	-47.7
-1.8	-41.4	-43.2	32.35	-1.7	-40.4	-42.1
-2.0	-35.5	-37.4	32.55	-1.9	-34.6	-36.5
-2.2	-29.5	-31.7	32.75	-2.1	-28.8	-30.9
-2.3	-23.7	-26.0	32.95	-2.3	-23.1	-25.4
-2.4	-18.0	-20.4	33.15	-2.4	-17.5	-19.9
-2.5	-12.3	-14.8	33.35	-2.4	-12.0	-14.4
-2.5	-6.6	-9.2	33.55	-2.5	-6.5	-8.9
-2.6	-1.1	-3.6	33.75	-2.5	-1.0	-3.5
-2.5	4.4	1.9	33.95	-2.5	4.3	1.9
-2.5	9.9	7.4	34.15	-2.4	9.6	7.2
-2.4	15.3	12.9	34.35	-2.3	14.9	12.6
-2.3	20.6	18.3	34.55	-2.2	20.1	17.9
-2.1	25.8	23.7	34.75	-2.1	25.2	23.1
-1.9	31.0	29.1	34.95	-1.9	30.3	28.4
-1.7	36.2	34.4	35.15	-1.7	35.3	33.6
-1.5	41.3	39.7	35.35	-1.5	40.3	38.8
-1.3	46.3	45.0	35.55	-1.2	45.2	44.0
-1.0	51.3	50.3	35.75	-1.0	50.1	49.1
-0.7	56.2	55.5	35.95	-0.7	54.9	54.2
-0.4	61.1	60.7	36.15	-0.3	59.6	59.3
0.0	65.9	65.9	36.35	0.0	64.4	64.4
Brass Powder						

Tab. 20 – Stress states in IT, Brass powder, porosity 0.5, cases 1 and 2.

Material	Case	Temp. [C]	Sigma 0.2 [N/mm^2]	Sigma eq. [N/mm^2]	Cs= (Sigma0.2/ Sigmaeq)	Notes
Diamond	1	147	130.9	73.0	1.79	admissible
	2	312	81.4	71.4	1.14	admissible
Copper	1	172	123.4	72.8	1.69	admissible
	2	337	73.9	71.1	1.04	admissible
Brass	1	213	111.1	72.4	1.53	admissible
	2	378	61.6	70.6	0.87	Not admissible

Tab. 21 – Thermo-Mechanical verification of IT: Results.

PT			Radius [mm]	Temperature [°C]	Water side data
σ_r [N/mm^2]	σ_θ [N/mm^2]	σ_a[N/mm^2]			
0.0	-22.2	-22.2	42.45	84.0	**Water velocity**: 0.2 m/s **Hydraulic Diameter**: 13.4 mm **Re**: 3523 **Nu**: 30 **Tin**: 14°C **Mass flow**: 0.4 kg/s **Heat transfer coefficient:** 1430 W/m^2 K (according to Dittus Boelter)
0.0	-20.4	-20.4	42.53	83.6	
-0.1	-18.6	-18.7	42.61	83.2	
-0.1	-16.8	-16.9	42.69	82.8	
-0.1	-14.9	-15.1	42.77	82.4	
-0.2	-13.1	-13.3	42.85	82.0	
-0.2	-11.4	-11.5	42.93	81.6	
-0.2	-9.6	-9.8	43.01	81.2	
-0.2	-7.8	-8.0	43.09	80.7	
-0.2	-6.0	-6.2	43.17	80.3	
-0.2	-4.2	-4.5	43.25	79.9	
-0.2	-2.5	-2.7	43.33	79.5	
-0.3	-0.7	-1.0	43.41	79.1	
-0.3	1.0	0.8	43.49	78.7	
-0.2	2.8	2.5	43.57	78.3	
-0.2	4.5	4.3	43.65	77.9	
-0.2	6.3	6.0	43.73	77.5	
-0.2	8.0	7.8	43.81	77.2	
-0.2	9.7	9.5	43.89	76.8	
-0.2	11.4	11.2	43.97	76.4	
-0.2	13.1	13.0	44.05	76.0	
-0.1	14.8	14.7	44.13	75.6	
-0.1	16.5	16.4	44.21	75.2	
-0.1	18.2	18.1	44.29	74.8	
0.0	19.9	19.9	44.37	74.4	
0.0	21.6	21.6	44.45	74.0	

Tab. 22 – Stress states in PT.

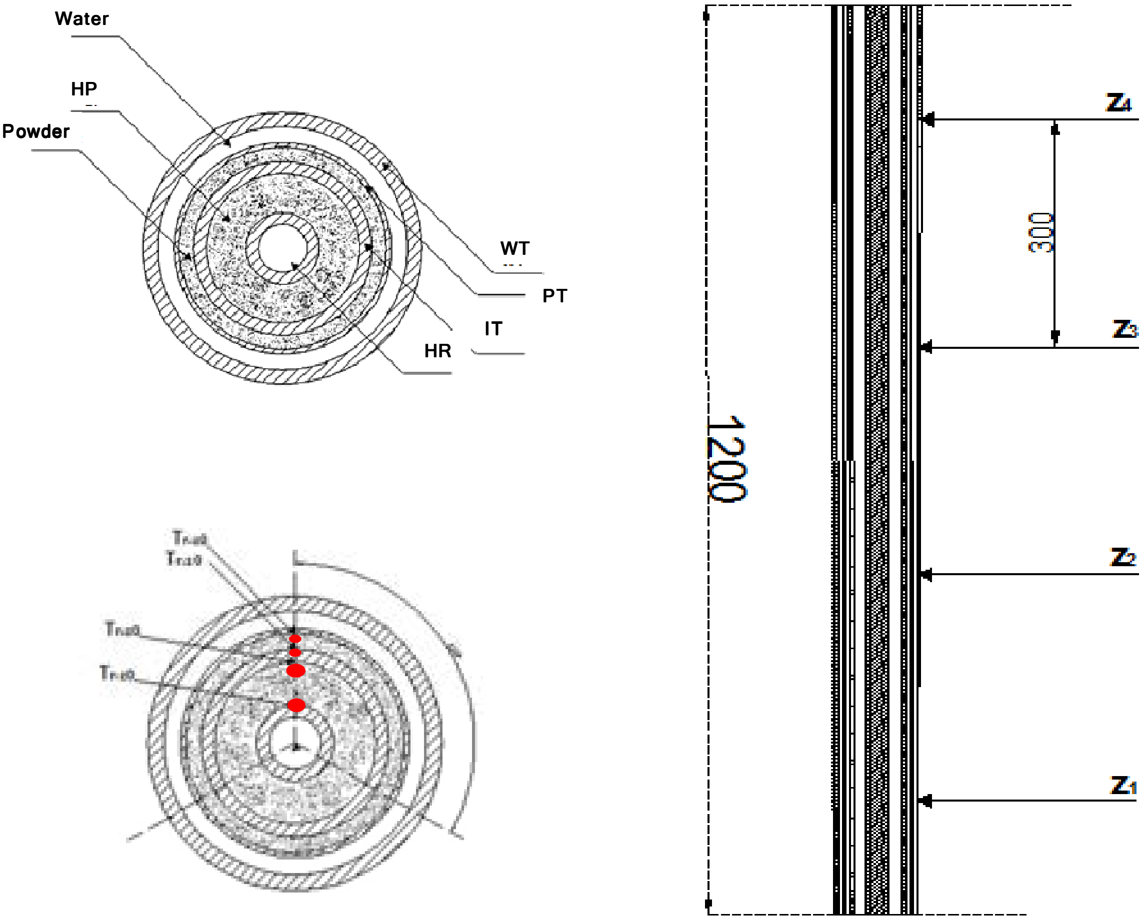

Fig. 5 – TxP instrumentation scheme.

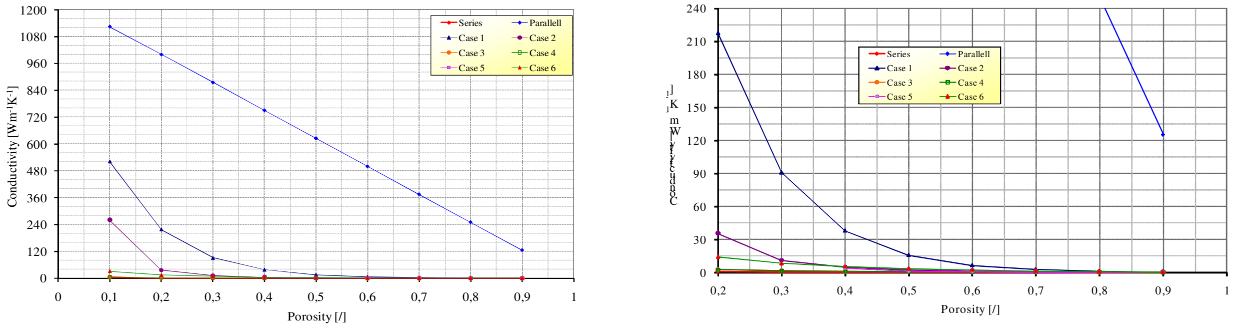

a)…overall porosities

b)…porosity over 0.2

Fig. 6 – Assessment of Diamond conductivity: models comparison as function of porosity.

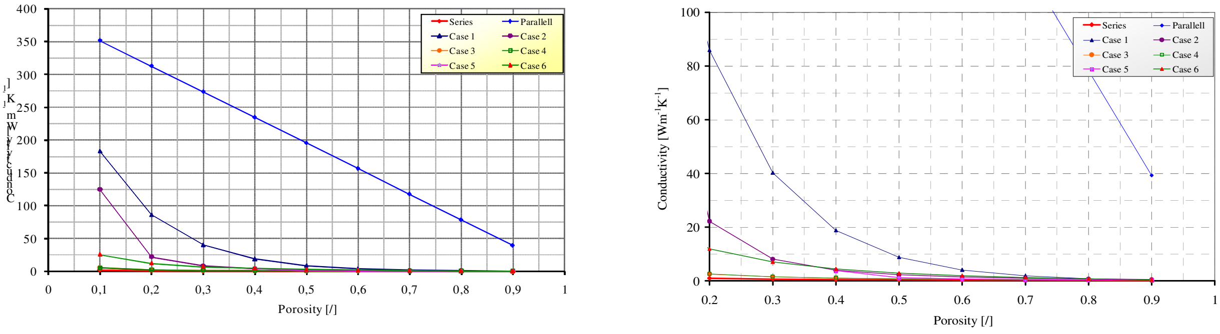

a)…overall porosities

b)…porosity over 0.2

Fig. 7 – Assessment of Copper conductivity: models comparison as function of porosity.

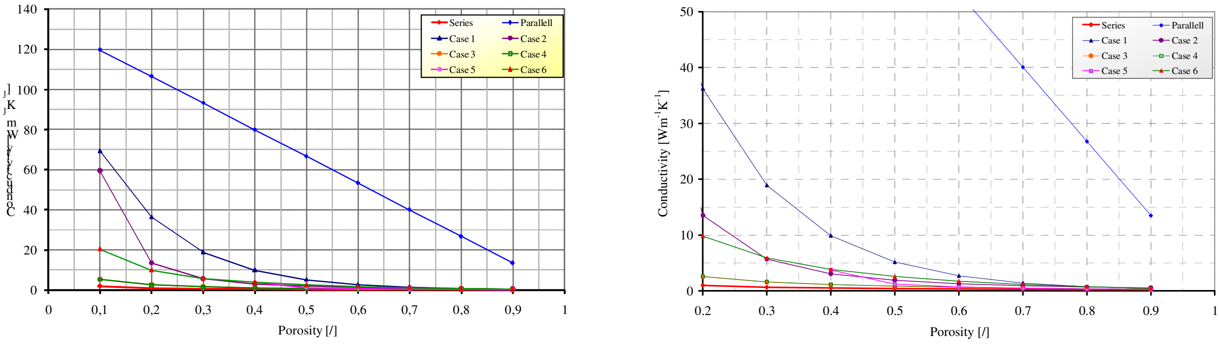

a)…overall porosities

b)…porosity over 0.2

Fig. 8 – Assessment of Brass conductivity: models comparison as function of porosity.

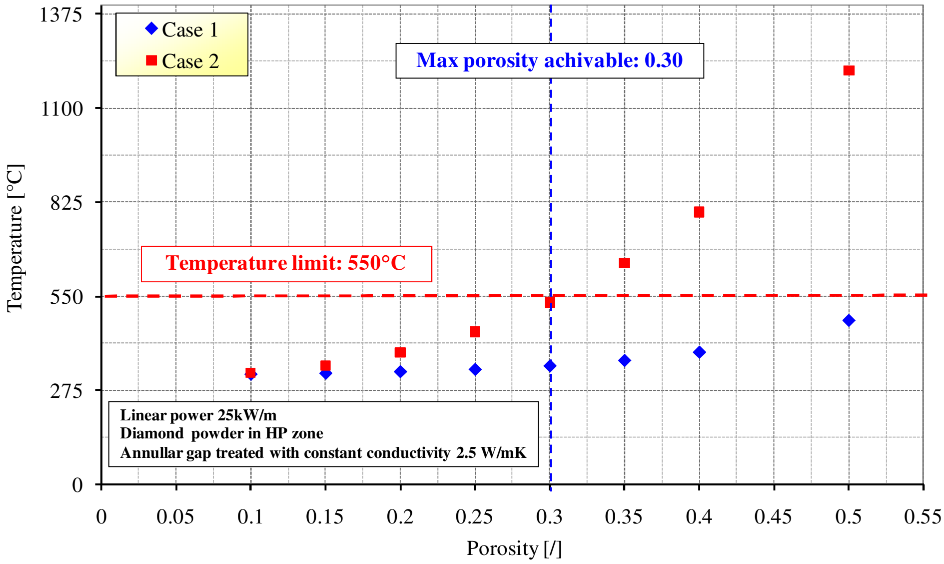

Fig. 9 – Diamond powder: design limits of HP zone, assessment of the maximum temperature assuming 2.5 W/mK as gap conductivity and max. linear power: comparison between the selected reference models (case 1 and case2), as function of porosity.

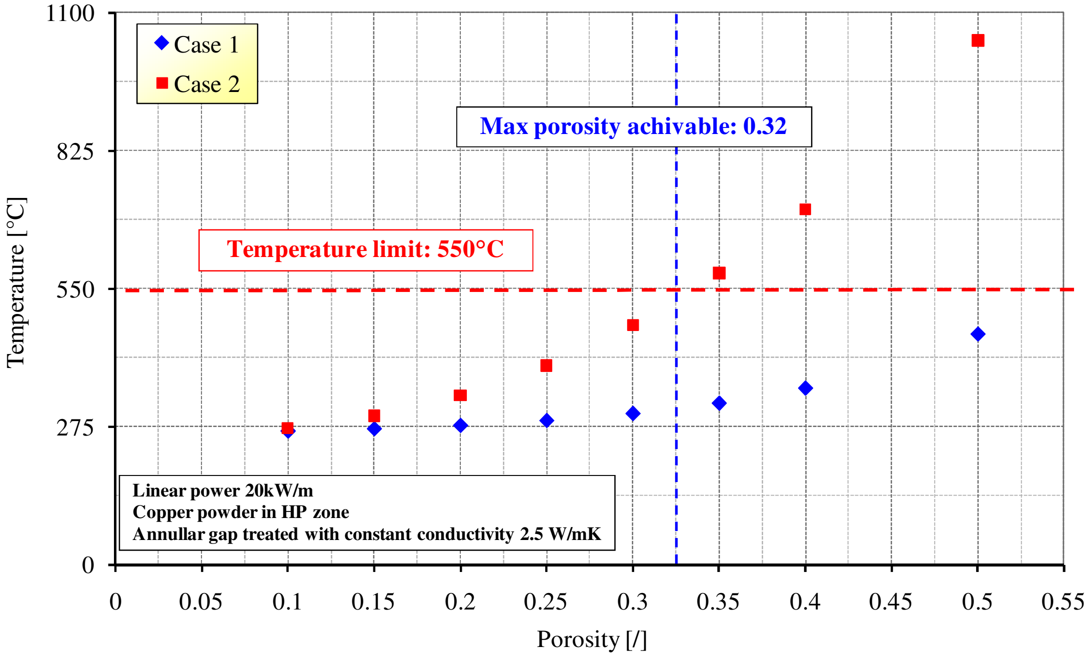

Fig. 10 – Copper powder: design limits of HP zone, assessment of the maximum temperature assuming 2.5 W/mK as gap conductivity and max. linear power: comparison between the selected reference models (case 1 and case2), as function of porosity.

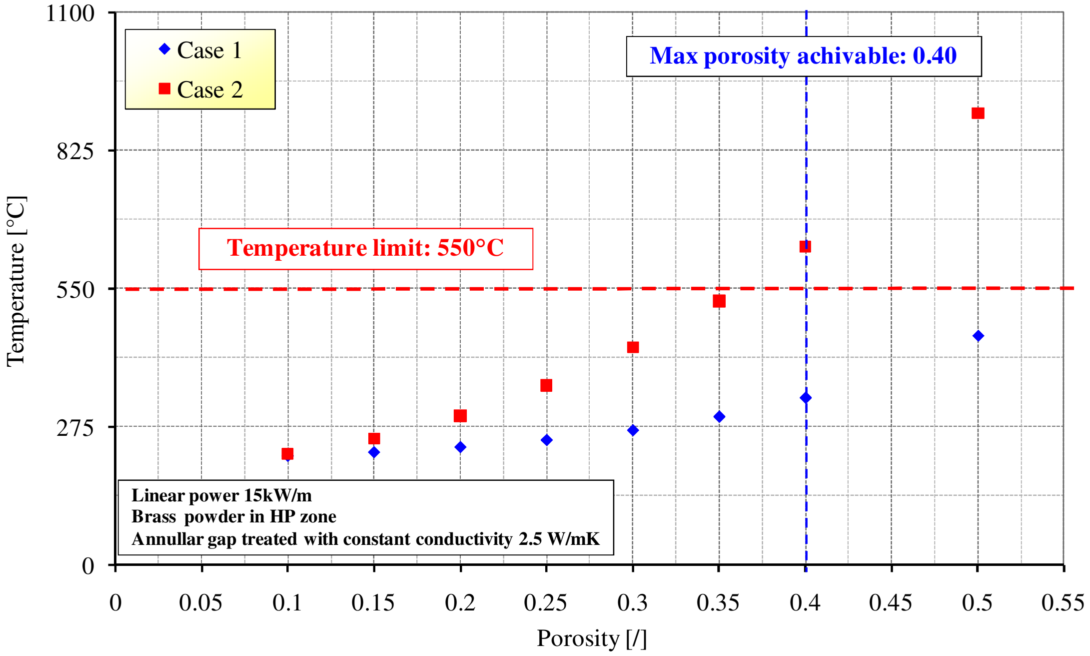

Fig. 11 – Brass powder: design limits of HP zone, assessment of the maximum temperature assuming 2.5 W/mK as gap conductivity and max. linear power: comparison between the selected reference models (case 1 and case2), as function of porosity.

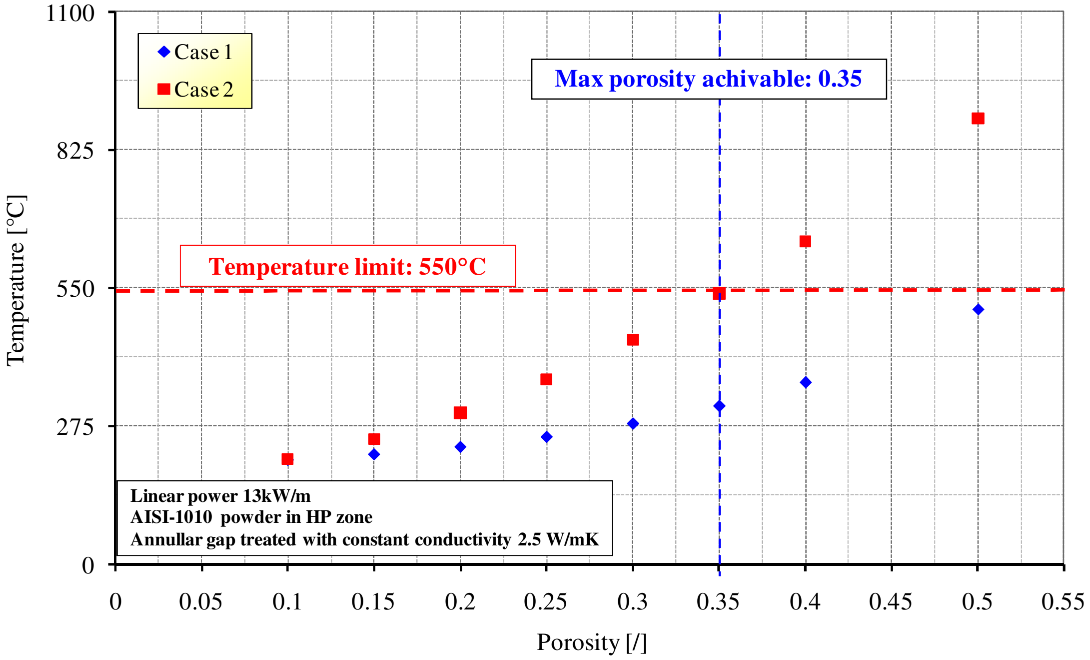

Fig. 12 – AISI-1010 powder: design limits of HP zone, assessment of the maximum temperature assuming 2.5 W/mK as gap conductivity and max. linear power: comparison between the selected reference models (case 1 and case2), as function of porosity.

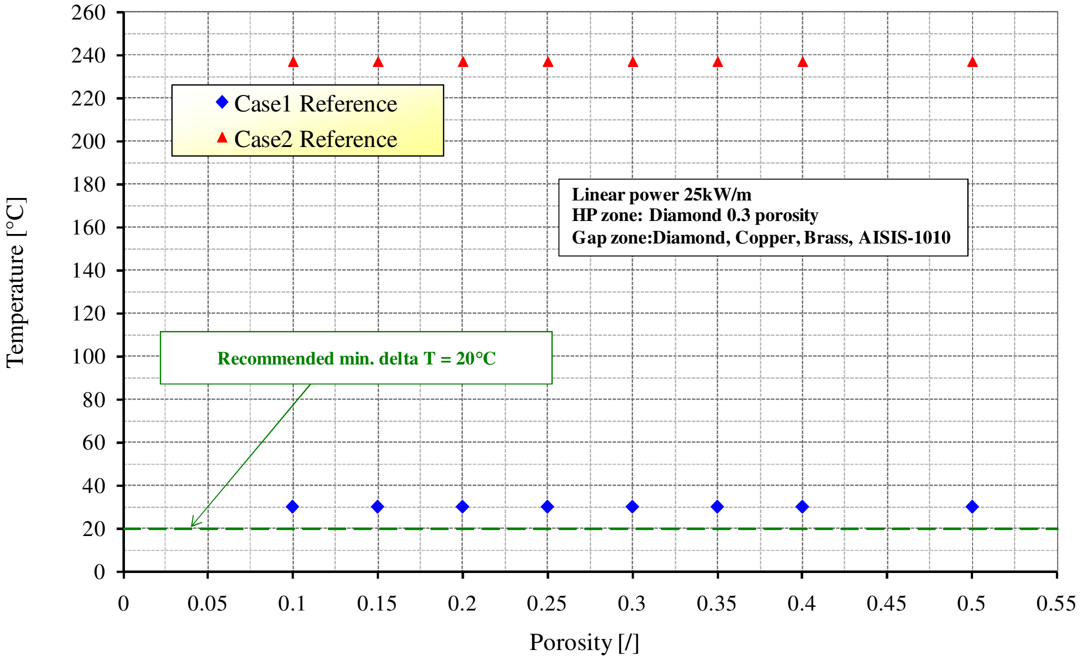

Fig. 13 – Assessment of TxP Thermal performance: configuration diamond, temperature drop in the HP zone.

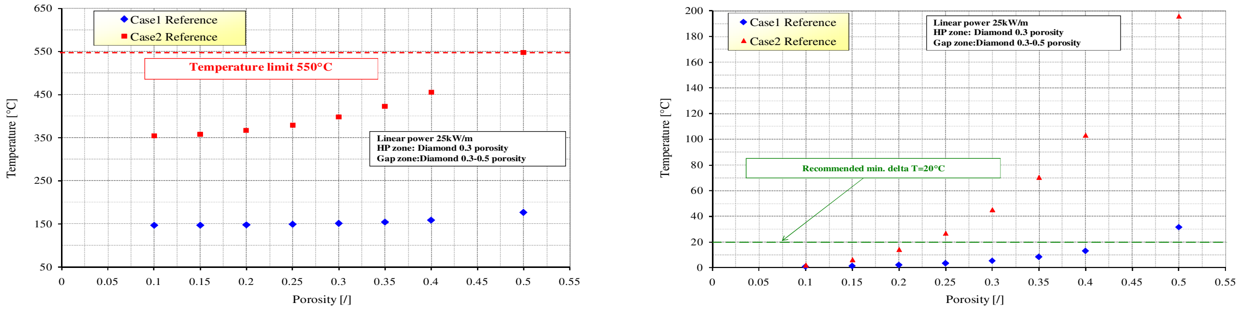

a)…Max Temperature. *b)…Temperature drop in the powder zone*

Fig. 14 – Assessment of TxP performance: config. diamond (HP zone) diamond (powder zone).

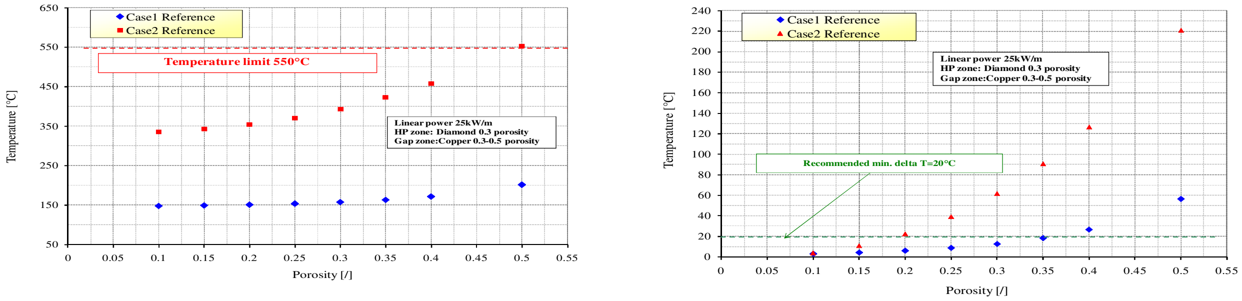

a)…Max Temperature. *b)…Temperature drop in the powder zone*

Fig. 15 – Assessment of TxP performance: configuration diamond (HP zone) copper (powder zone).

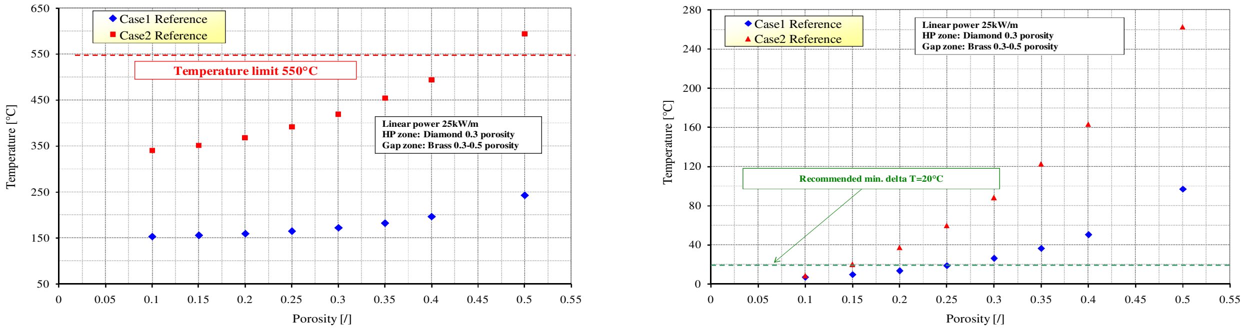

a)…Max Temperature. *b)…Temperature drop in the powder zone*

Fig. 16 – Assessment of TxP performance: configuration diamond (HP zone) brass (powder zone).

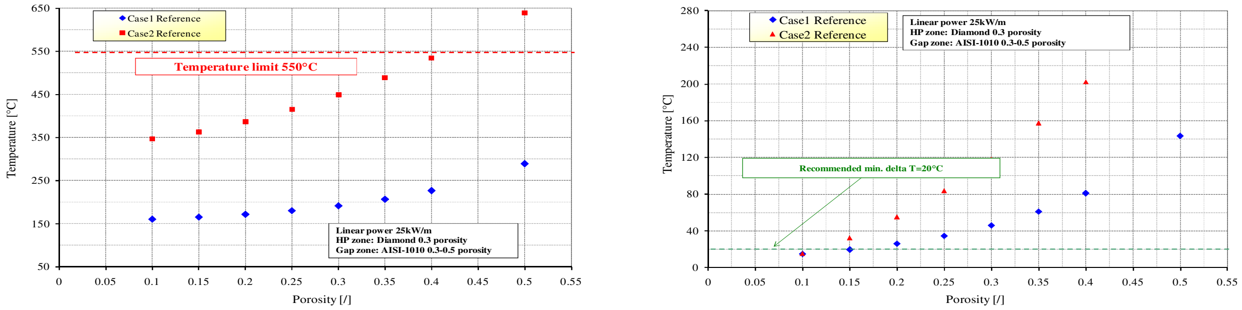

a)…Max Temperature. *b)…Temperature drop in the powder zone*

Fig. 17 – Assessment of TxP performance: diamond (HP zone) AISI-1010 (powder zone).

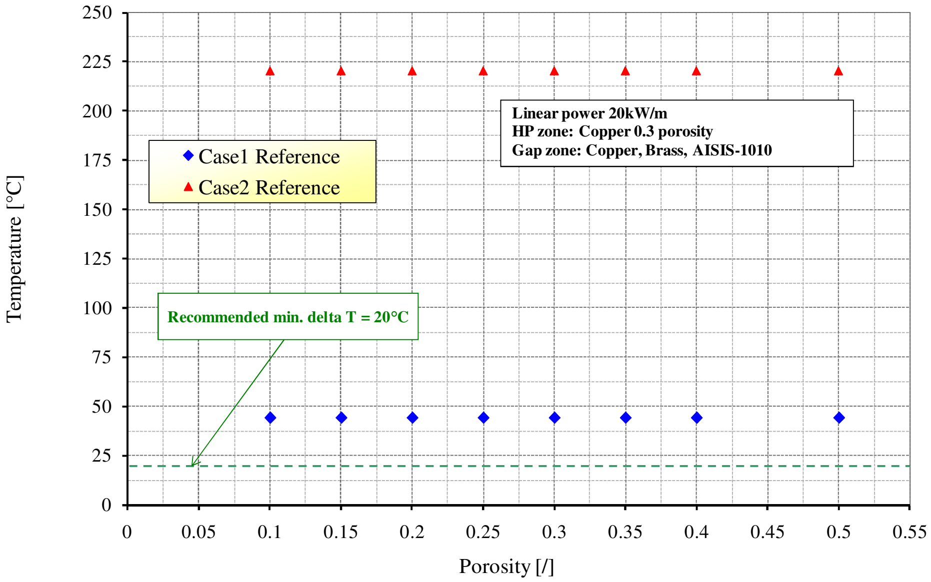

Fig. 18 – Assessment of TxP performance: configuration copper temperature drop in the HP zone.

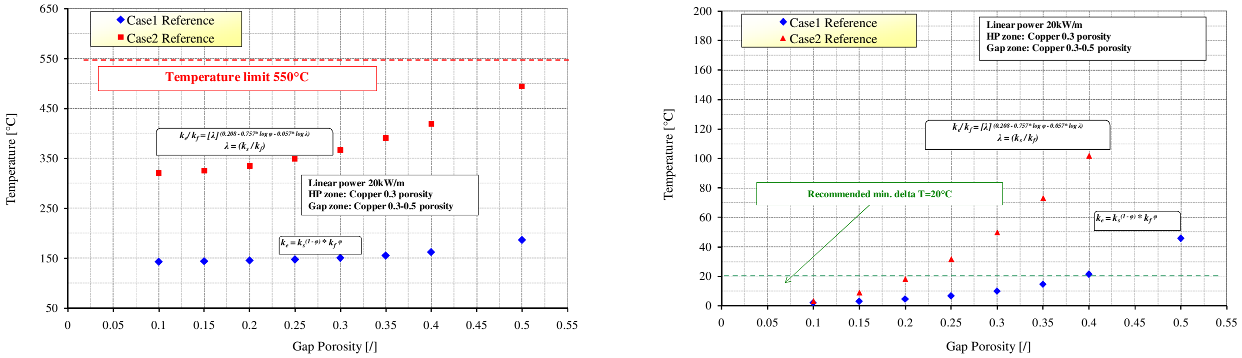

a)…Max Temperature. *b)…Temperature drop in the powder zone*

Fig. 19 – Assessment of TxP performance: configuration copper (HP zone) copper (powder zone).

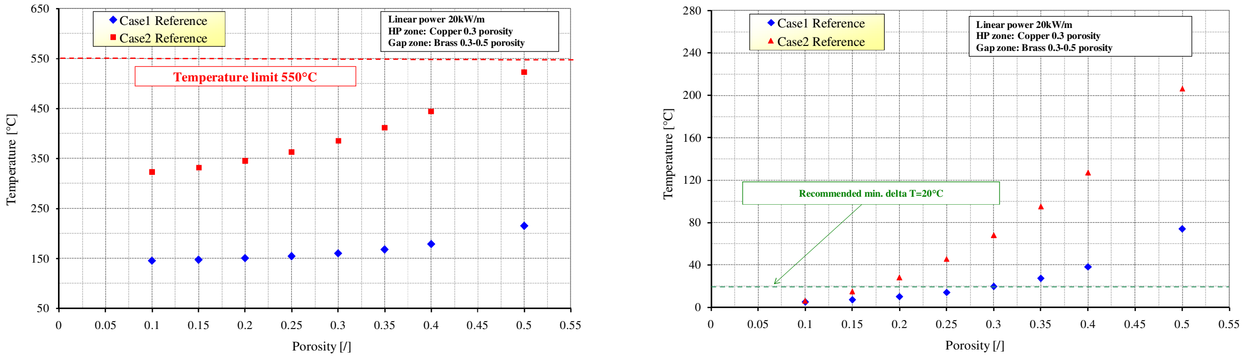

a)…Max Temperature. *b)…Temperature drop in the powder zone*

Fig. 20 – Assessment of TxP performance: configuration copper (HP zone) brass (powder zone).

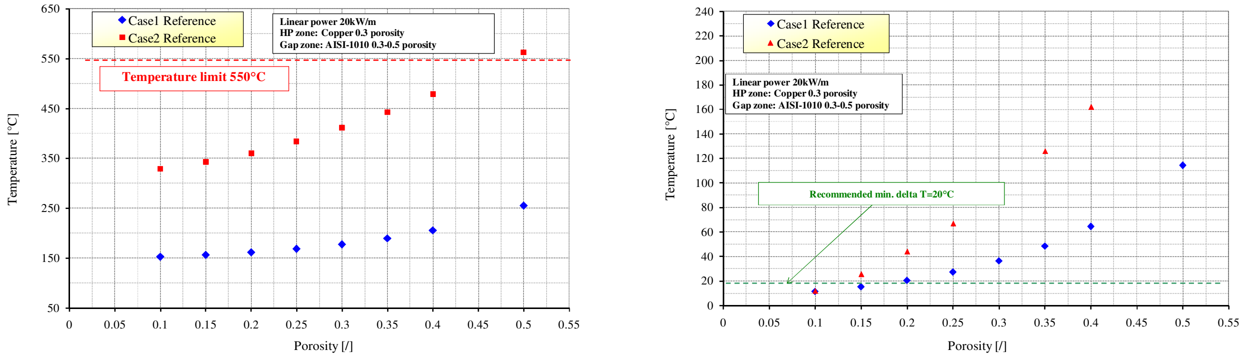

a)…Max Temperature. *b)…Temperature drop in the powder zone*

Fig. 21 – Assessment of TxP performance: configuration copper (HP zone) AISI-1010 (powder zone).

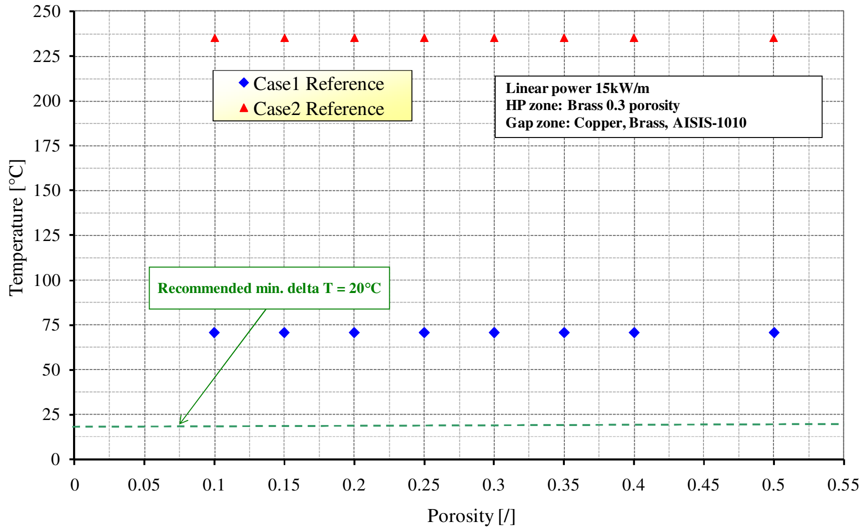

Fig. 22 – Assessment of TxP performance: configuration brass temperature drop in the HP zone.

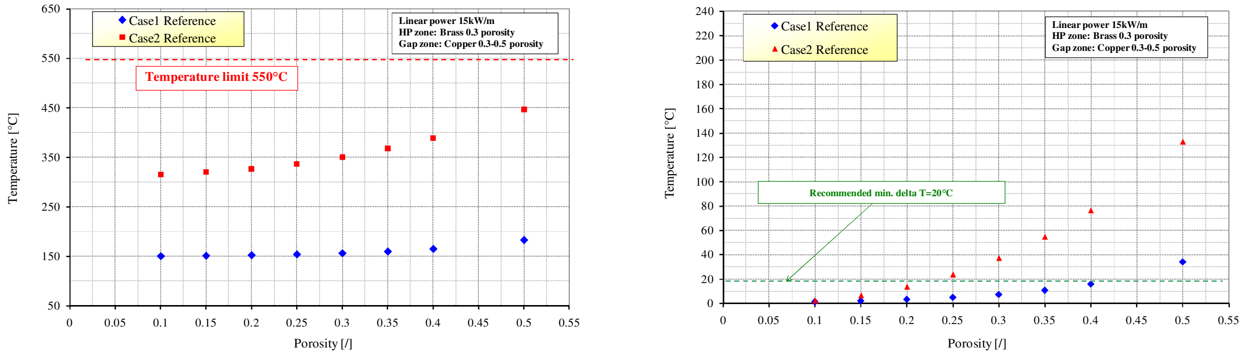

a)…Max Temperature. *b)…Temperature drop in the powder zone*

Fig. 23 – Assessment of TxP performance: configuration brass (HP zone) copper (powder zone).

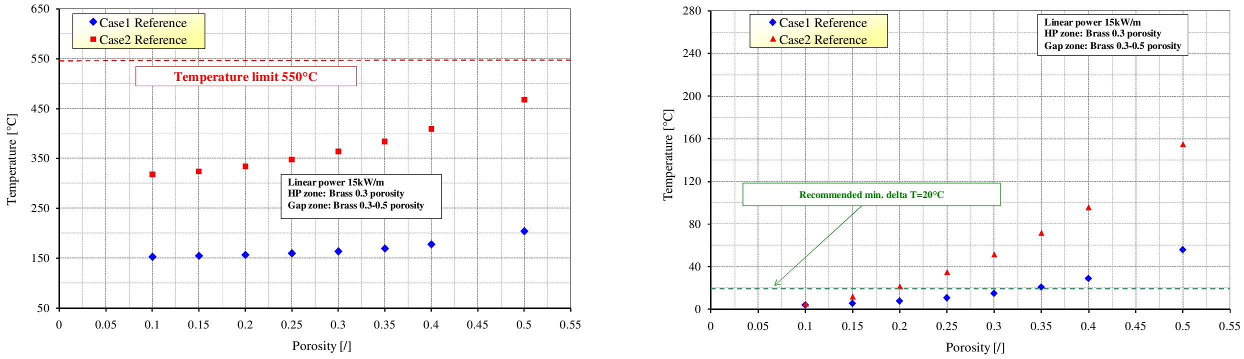

a)…Max Temperature. *b)…Temperature drop in the powder zone*

Fig. 24 – Assessment of TxP performance: configuration brass (HP zone) brass (powder zone).

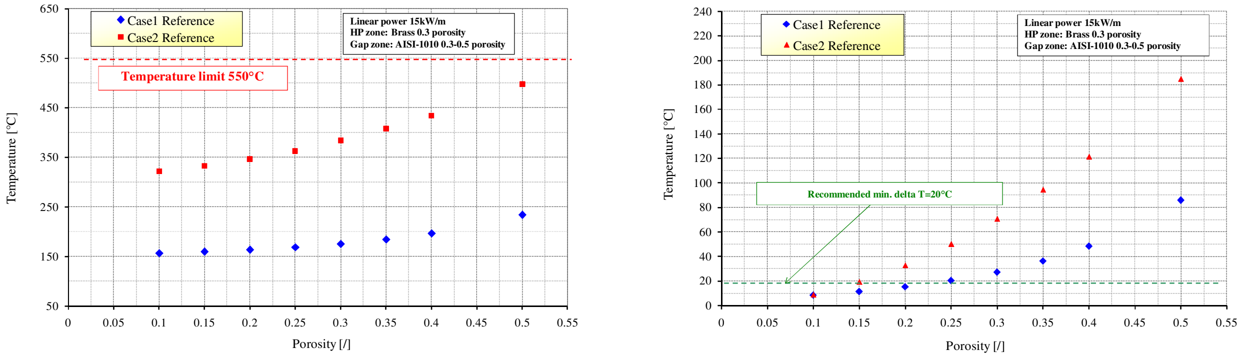

a)…Max Temperature. *b)…Temperature drop in the powder zone*

Fig. 25 – Assessment of TxP performance: configuration brass (HP zone) AISI-1010 (powder zone).

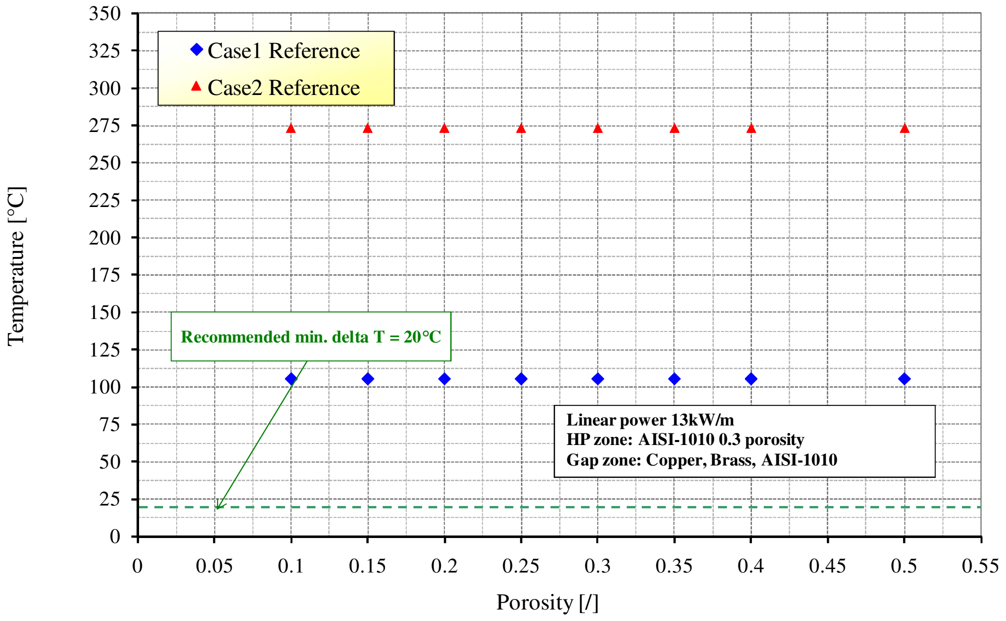

Fig. 26 – Assessment of TxP performance: config. AISI-1010 temperature drop in the HP zone.

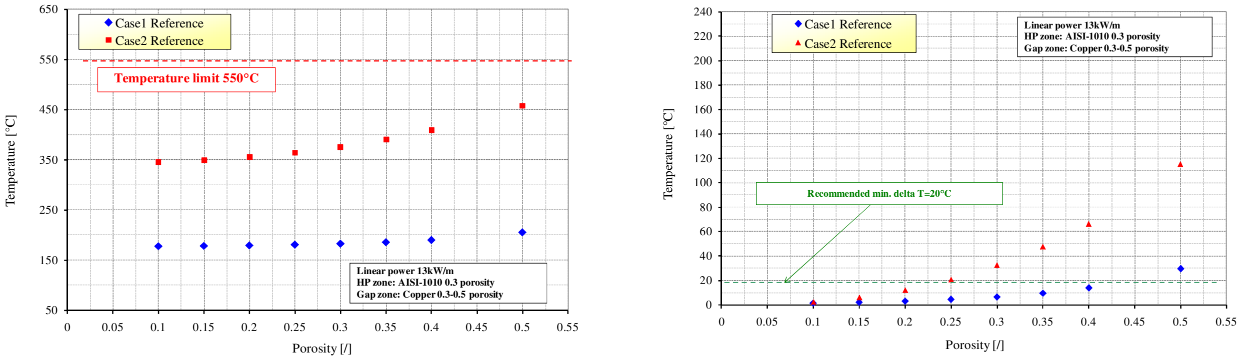

a)…Max Temperature. *b)…Temperature drop in the powder zone*

Fig. 27 – Assessment of TxP performance: config. AISI-1010 (HP zone) copper (powder zone).

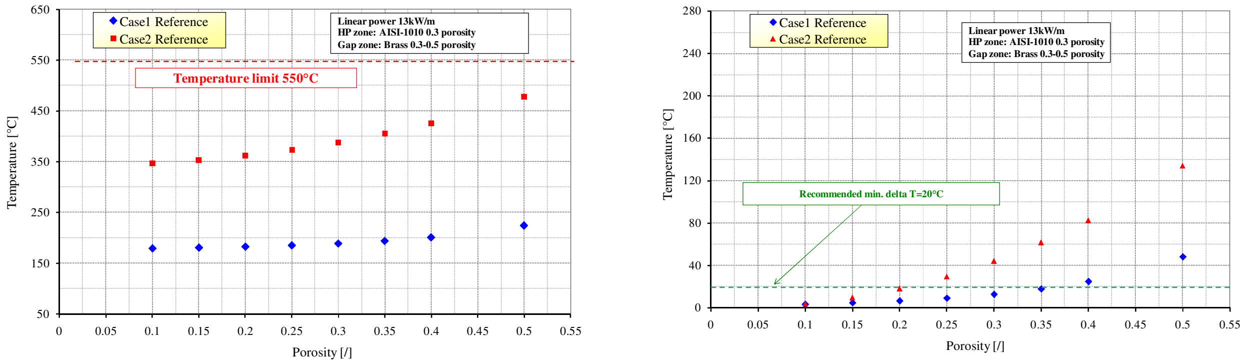

a)…Max Temperature. *b)…Temperature drop in the powder zone*

Fig. 28 – Assessment of TxP performance: config. AISI-1010 (HP zone) brass (powder zone).

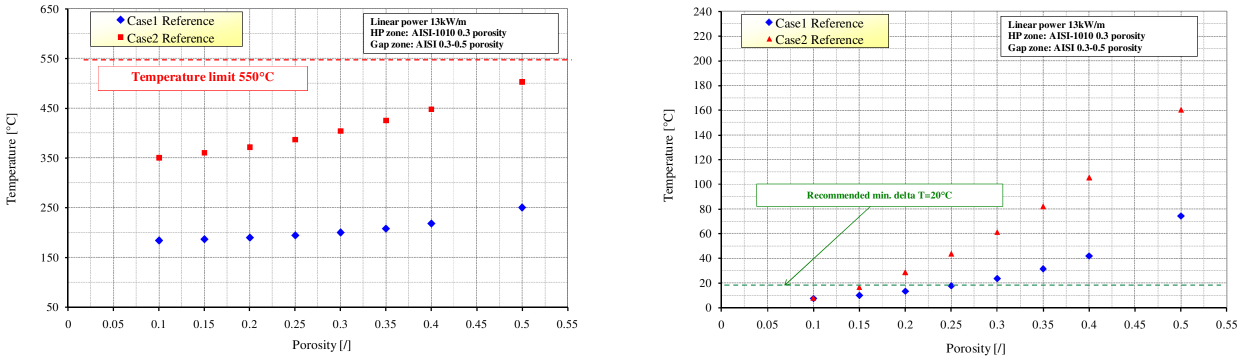

a)…Max Temperature. *b)…Temperature drop in the powder zone*

Fig. 29 – Assessment of TxP performance: config. AISI-1010 (HP zone) AISI-1010 (powder zone).

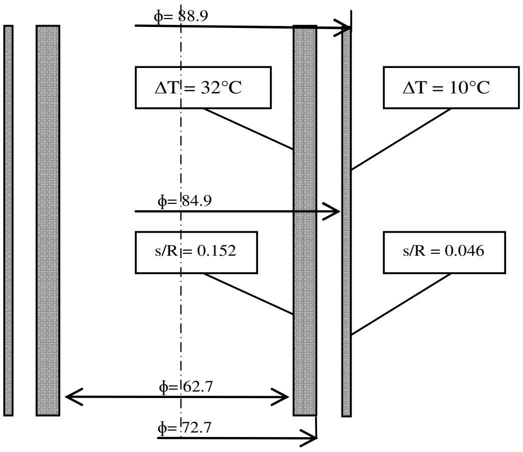

Fig. 30 – Conceptual schematization adopted for the preliminary thermo-mechanical analysis.

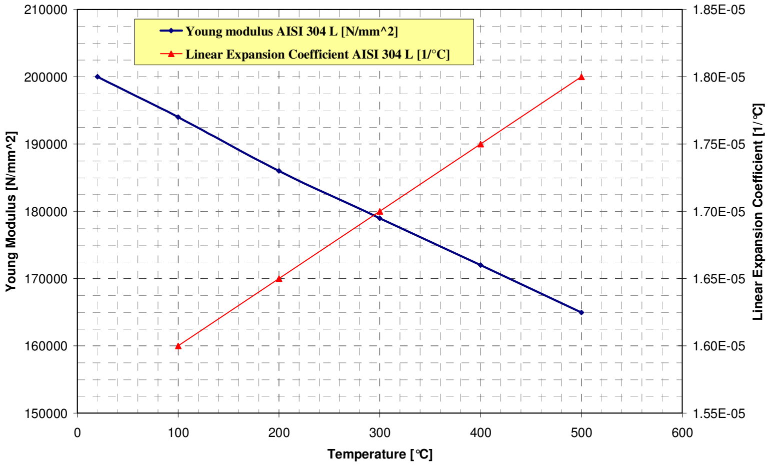

Fig. 31 – Mechanical properties of AISI 304 L.

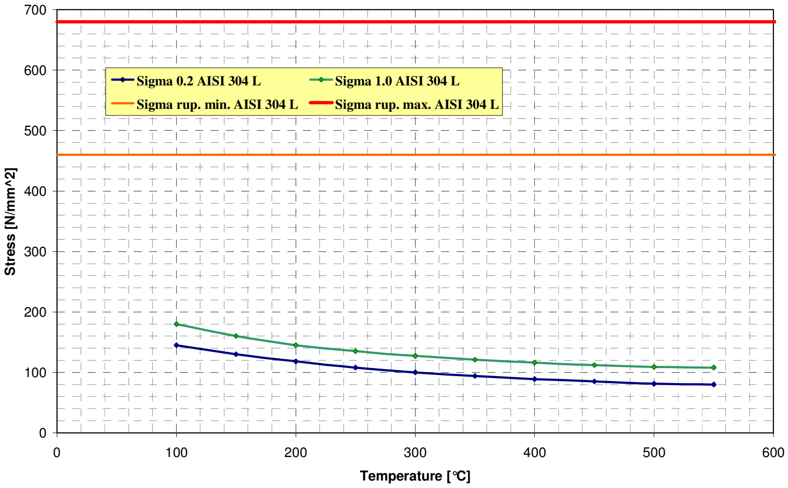

Fig. 32 – Mechanical properties of AISI 304 L.

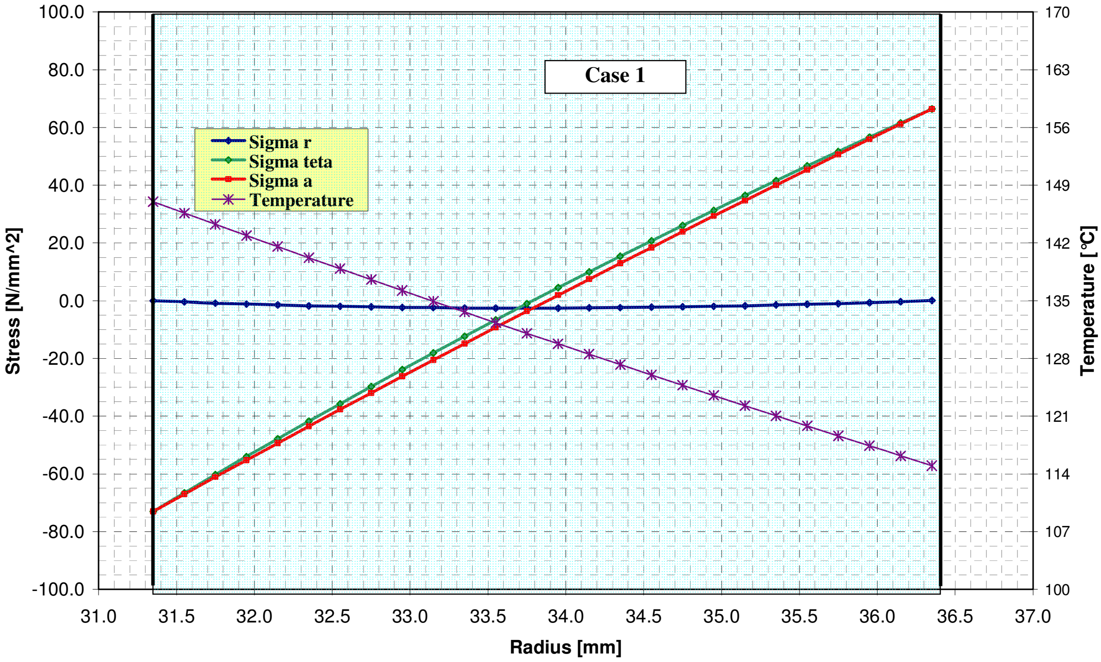

Fig. 33 – Thermo-Mechanical verification of IT: Diamond powder, porosity 0.5, case1, stresses distribution as function of radius.

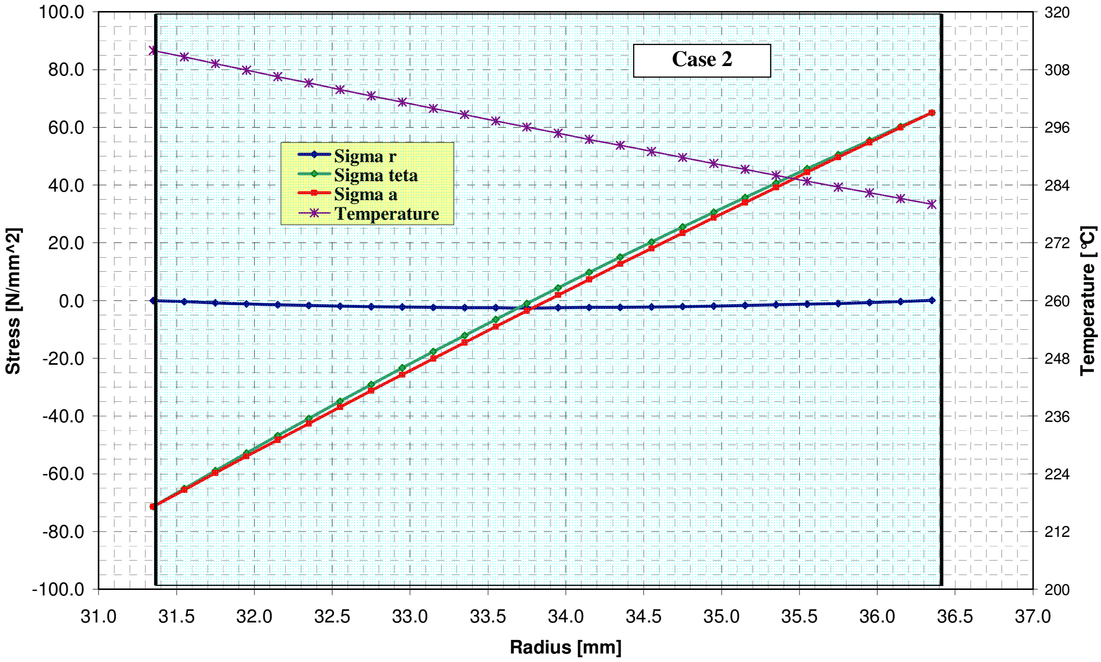

Fig. 34 – Thermo-Mechanical verification of IT: Diamond powder, porosity 0.5, case2, stresses distribution as function of radius.

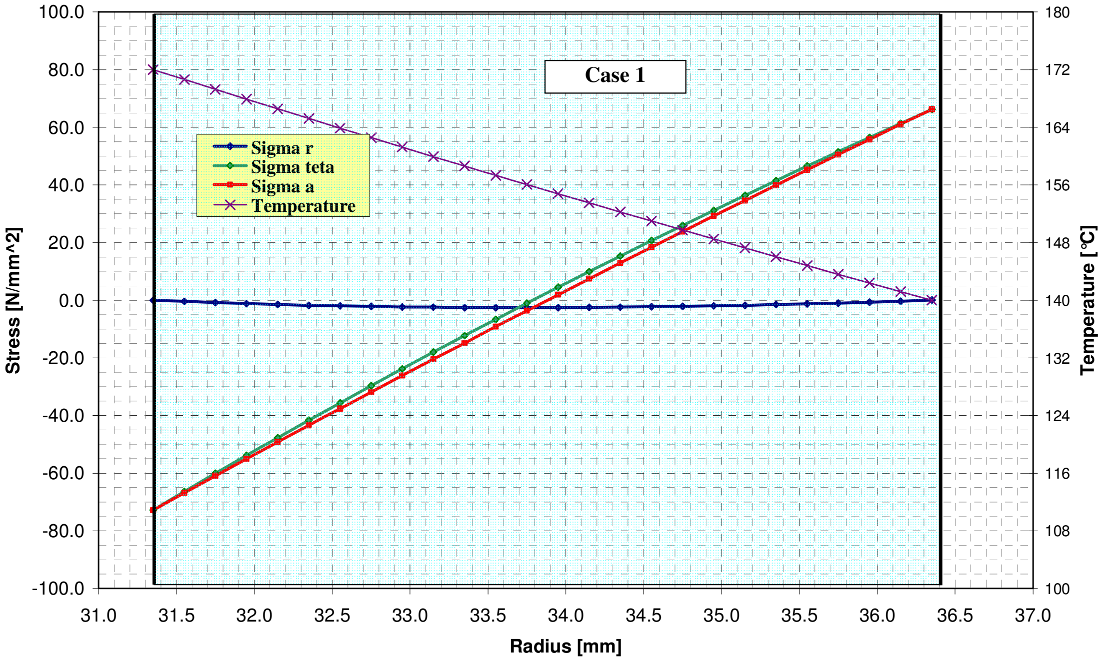

Fig. 35 – Thermo-Mechanical verification of IT: Copper powder, porosity 0.5, case1, stresses distribution as function of radius.

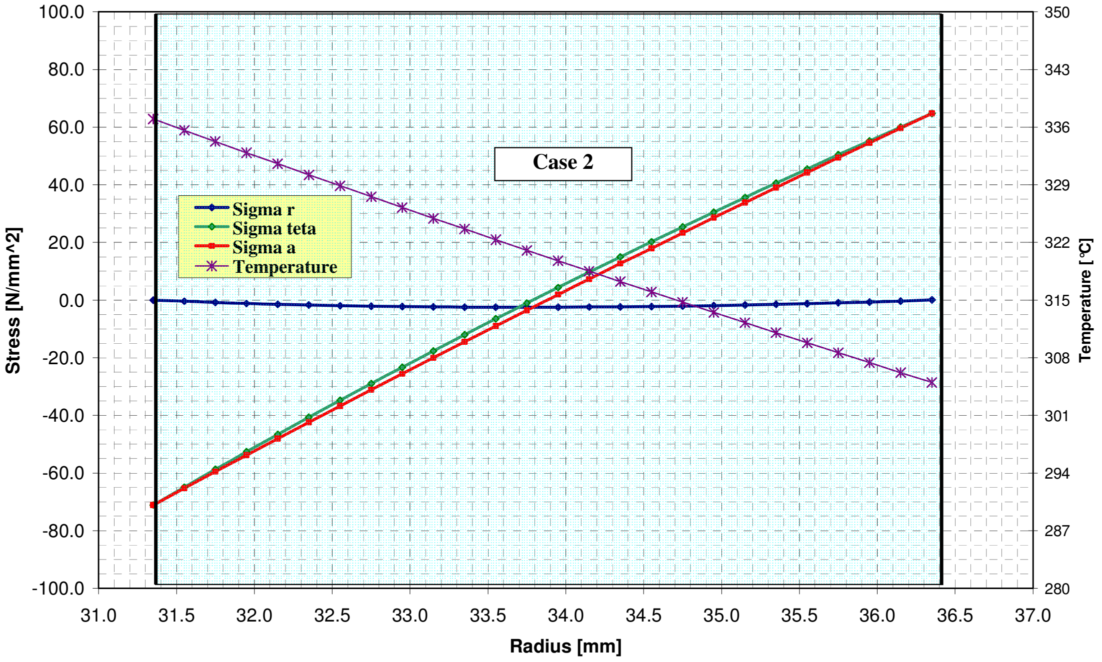

Fig. 36 – Thermo-Mechanical verification of IT: Copper powder, porosity 0.5, case2, stresses distribution as function of radius.

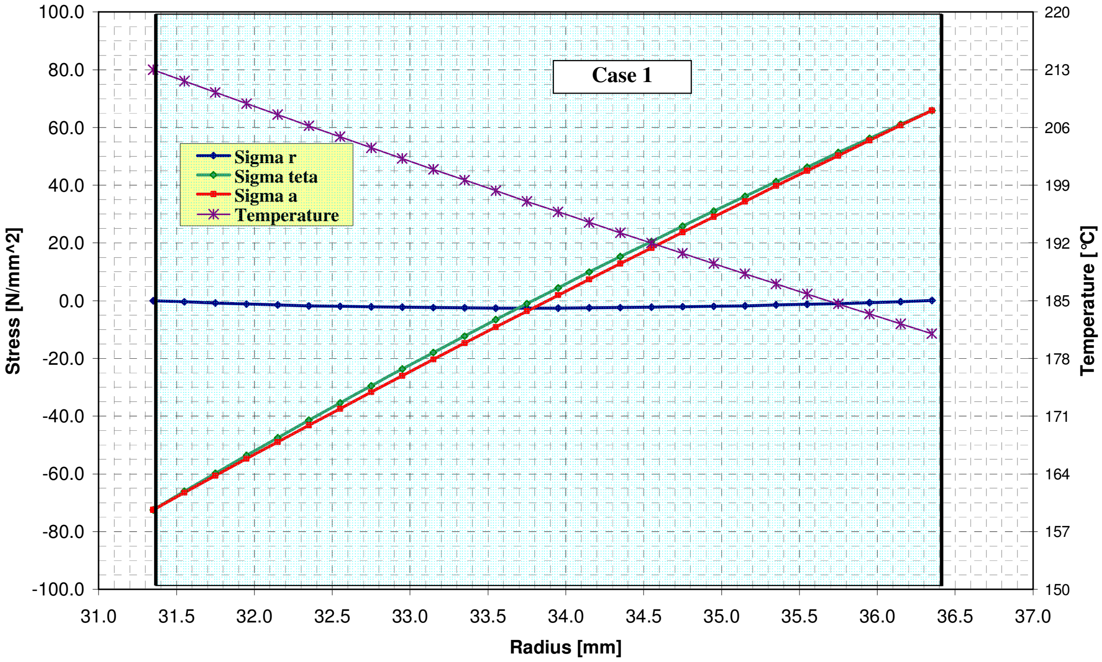

Fig. 37 – Thermo-Mechanical verification of IT: Brass powder, porosity 0.5, case1, stresses distribution as function of radius.

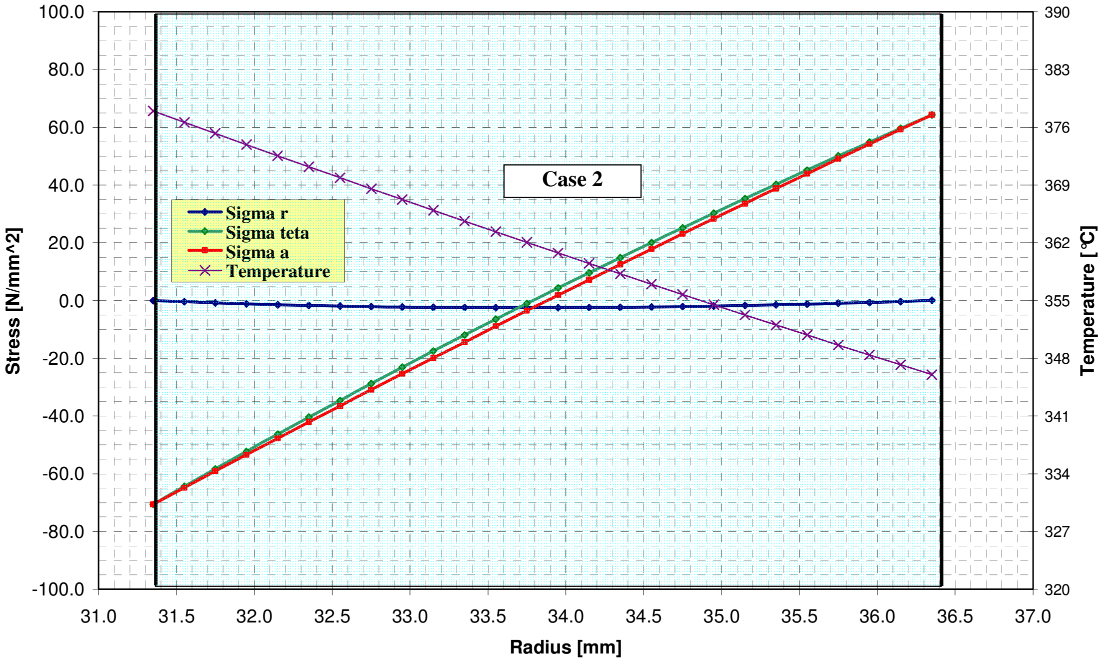

Fig. 38 – Thermo-Mechanical verification of IT: Brass powder, porosity 0.5, case2, stresses distribution as function of radius.

4 TxP Configuration and Auxiliary Components

4.1 Detailed design of TxP

The main objectives of the TxP Facility are connected to the evaluation of the thermal performance of several candidate powders for the application to the ALFRED SG. In particular it is focused on:

- Determine the thermal conductivity of the powders into a representative annular gap.
- Determine the influence of the powder compaction grade on the conductivity.
- Investigate the influence of the filling gas (Helium) pressure.
- Investigate the impact of selected thermal cycle.

The TxP facility consists of three concentric tubes; a conceptual scheme is reported in *Fig. 5*. The tube labeled as IT contains a heating rod HR that generates 25 kW (maximum). The free volume between the HR and the first tube (HP zone) is filled with high conductivity powders. In the first design diamond powder was selected for the HP zone. The intent of this zone (15 mm in width), was to obtain fruitful data on this material if the gap temperature drop resulted negligible. When the diamond solution was abandoned this objective was maintained in order to analyze high conductivity powders as copper. The gap between the IT and the PT tubes is designed to test several powders specimens, it is about 6 mm in width. In the outer tube, WT, a water flow removes the generated thermal power. The main data are given in *Tab. 8*.

The detailed design is reported from *Fig. 39* to *Fig. 52*. The TxP construction is un charge to the Li.Ma.inox srl.

4.2 Piping & Instrumentations Diagram (PID)

The PID is reported in *Fig. 53*. Power control purpose requires the instrumentation of two sides. In the heating rod side, it will be realized by mean of a wattmeter and in the water loop by mean of two thermocouples (at inlet-outlet) and a flow-meter. The power control will be operated with a temperature set point connected to the measure of the HR temperature: the signal will drive the electric source. The system will be capable to shutdown the HR if a maximum temperature is reached in the HR. The power will be checked with the value obtained from the waterside.

The water side does not require for pumps, the service water pressure is reduced from 8 to 6 bars by mean of a pressure reducer. In order to check the pressure, two manometers are required: the first one placed after the pressure reducer and the second in the pipeline at the facility outlet to check pressure drops. The water flow will be changed by mean of a control valve. Two safety components are inserted in the water line. The first is the safety valve located in the inlet-line (after the manometer). The second is located in the outlet-line line, it consists of a flux checker that reveal loss of water flux.

The design includes 48 + 1 + 1 thermocouples located in three azimuthal and four axial directions. Twelve are inserted at HR outer surface, 24 are located in IT (12 in the inner, 12 in the outer surfaces). The remaining 12 thermocouples are positioned in the inner surface of WT. One thermocouple is contained in the heating rod, at its center. One additional axially removable thermocouple will be inserted in HP. Its goal is to measure with great resolution the axial temperatures profile.

The He line is connected to a pressurized tank (200 bar). The pressure reducer (with an incorporated safety valve) brings the He pressure to 4 bar. The gas enters the TxP continuously from the top of IT, and then it enters from the bottom into the gap region. When it reaches the closure of the gap region, it flows into one dedicated channel. The system operates in variable pressure (1-4 bar). Two valves fulfil this purpose: the first one closes when He flow is detected in the outlet open tank, the second closes when the selected pressure is measured by the pressure transducers.

4.3 Description of the instrumentation

The HR is supplied by Rotfil S.r.l the main data are given in *Tab. 8* and *Fig. 54*.

The watt-meter is supplied by Yokogawa Italia S.r.l. the Digital Sampling Power Meters, con has the following features

- WT230 Digital Power meter - 3 input, 1 Pz
- 12 Chanel D/A output, 1 Pz
- External Input 2.5V/5V/10V, 1 Pz
- Transducer IT200-S (867-200l), 3 Pz
- 2M annullar (867-SC), 3 Pz
- Analog Input Module for MX (MX110-UNV-M10), 3 Pz

The 48 thermocouples are depicted in *Fig. 55*. They are supplied by ELSI S.r.l.

- 24 thermocouples type N, class 1, insulated hot junction, AISI 316 cladding, connector Mignon, code color ANSI, diameter 0.5 mm, length 2.5 m (placed in the powder gap).
- 24 thermocouples type N, class 1, insulated hot junction, AISI 316 cladding, connector Mignon, code color ANSI, diameter 0.8 mm, length 2.5 m (placed in the HP zone).

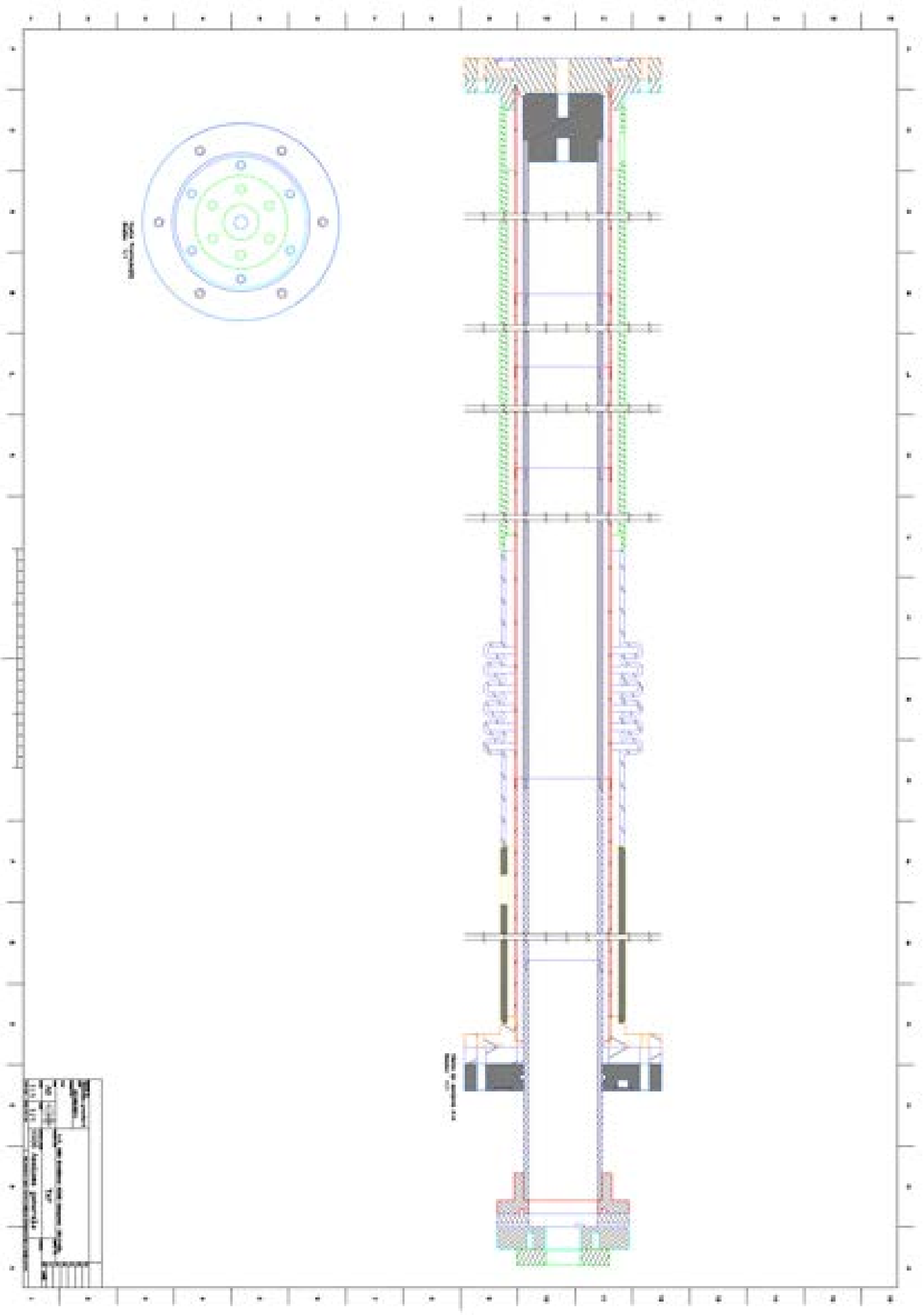

Fig. 39 – TxP arrangement.

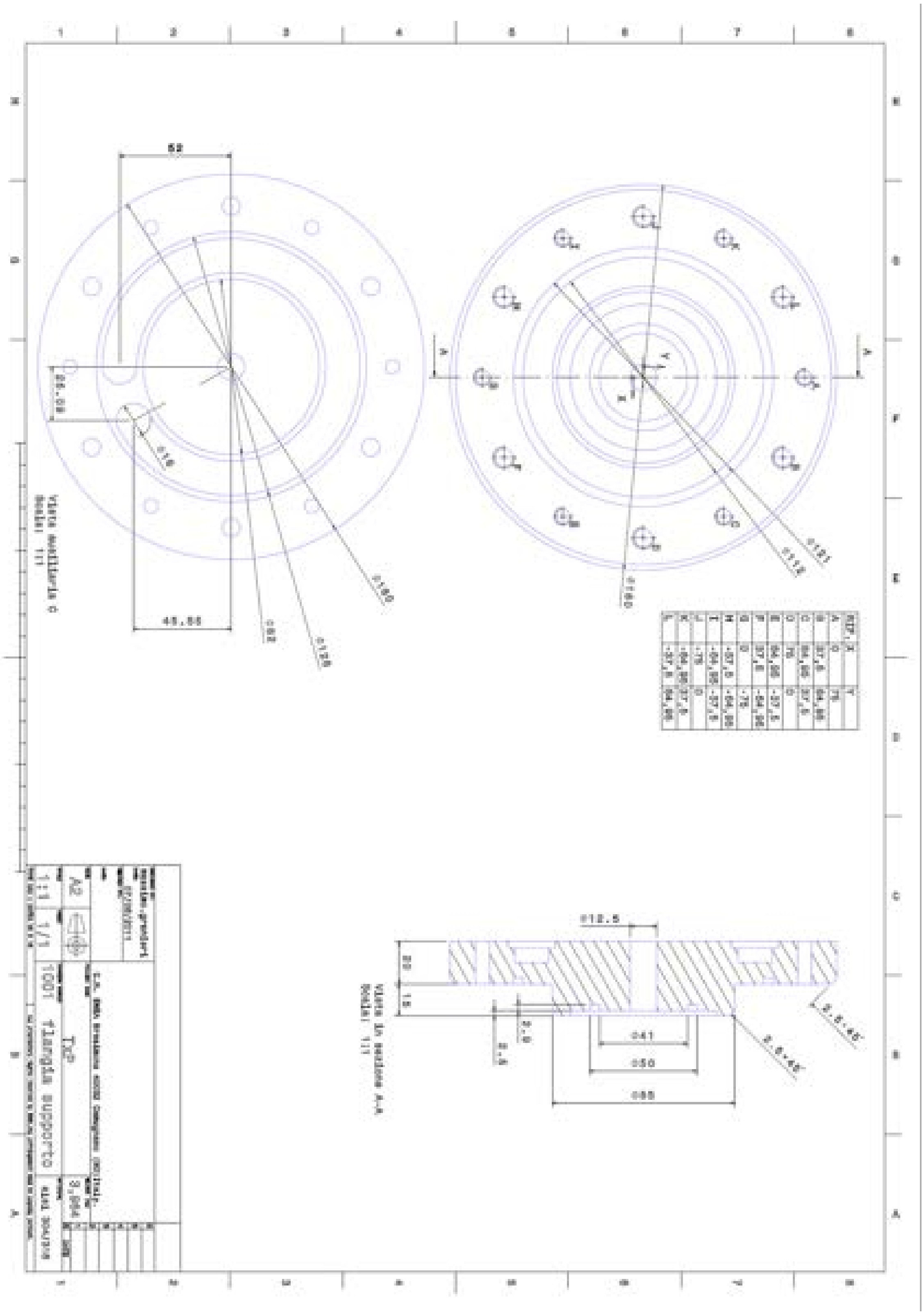

Fig. 40 – TxP design: bottom supporting flange.

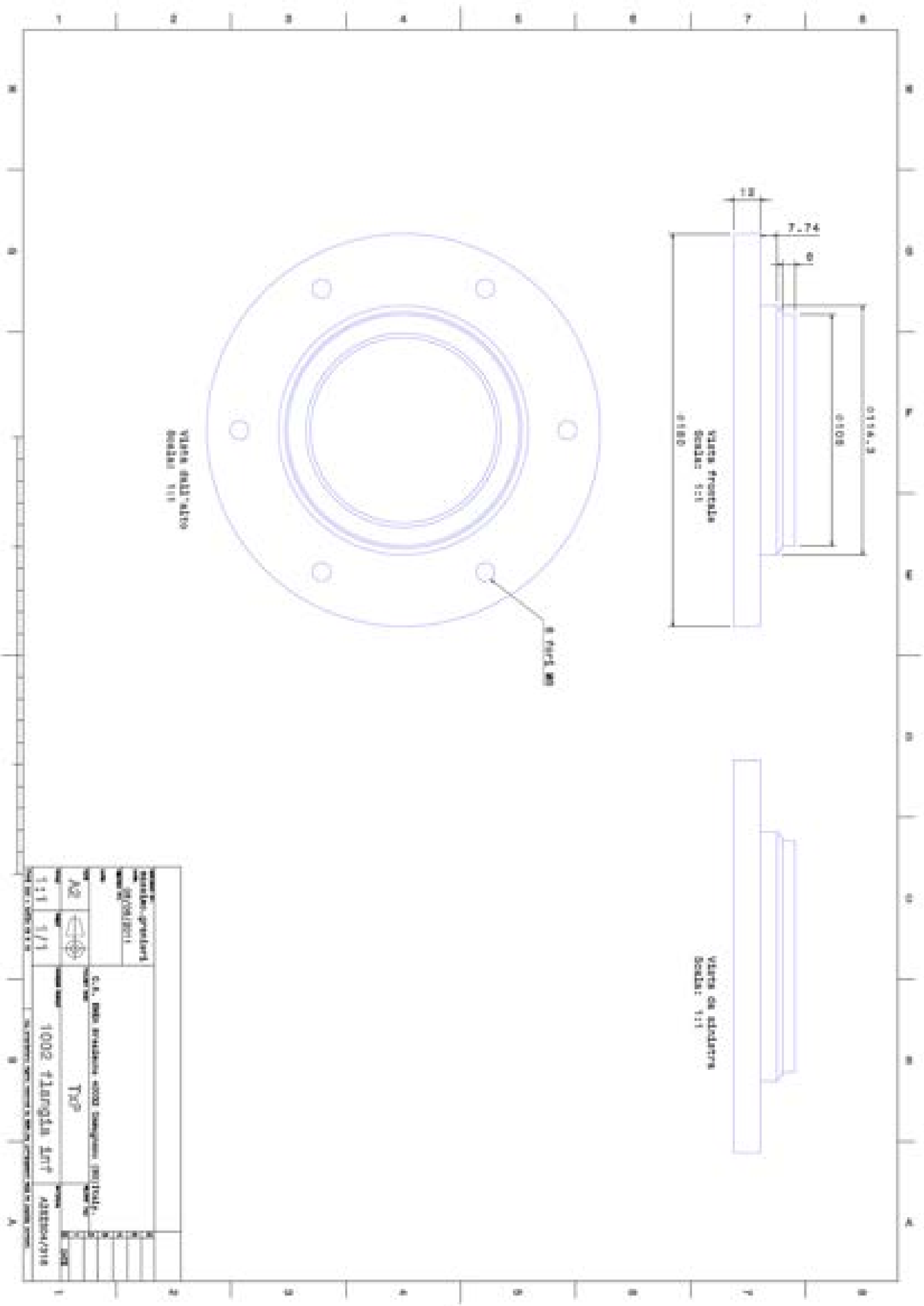

Fig. 41 – TxP design: PT bottom flange.

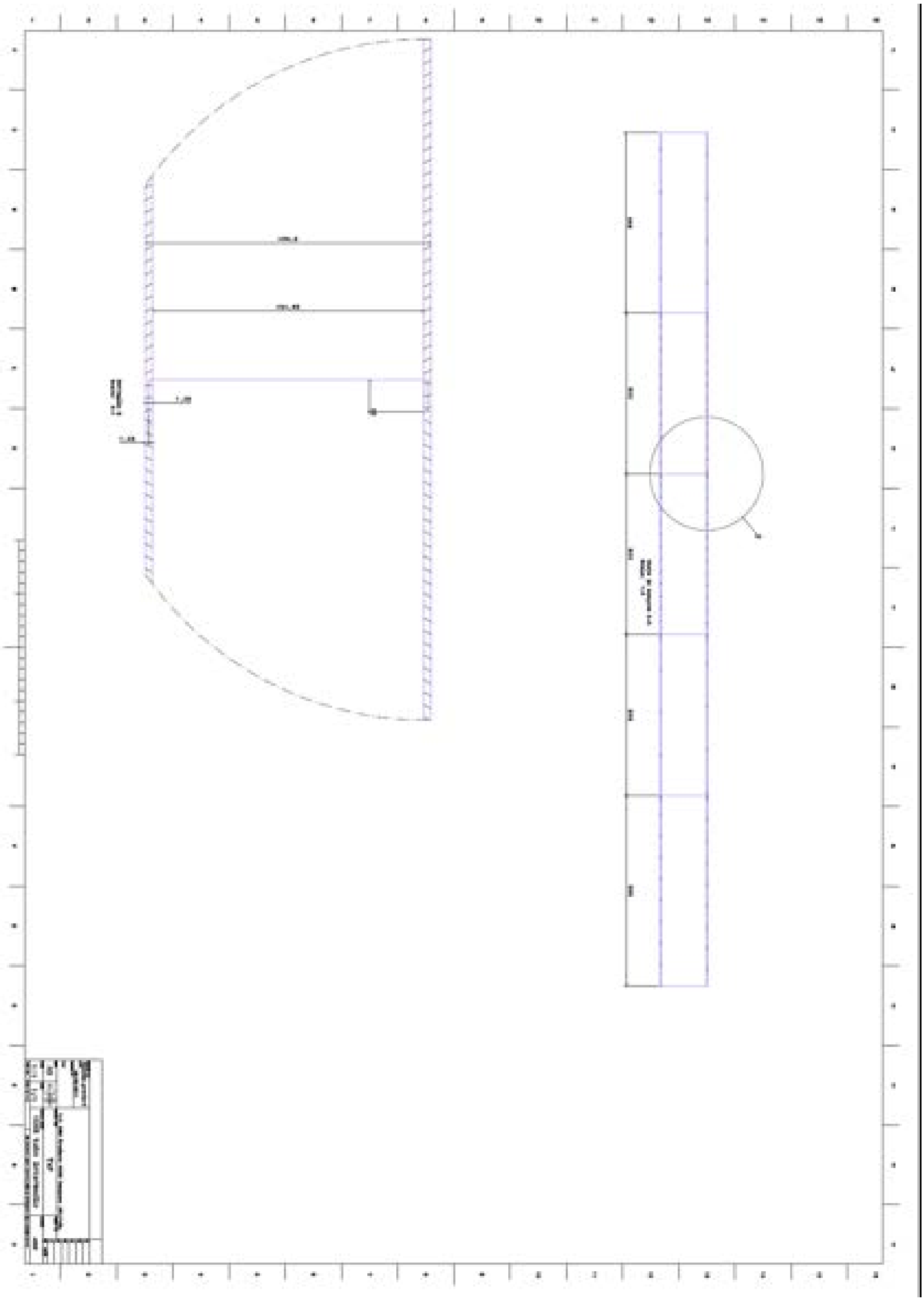

Fig. 42 – TxP design: PT tube.

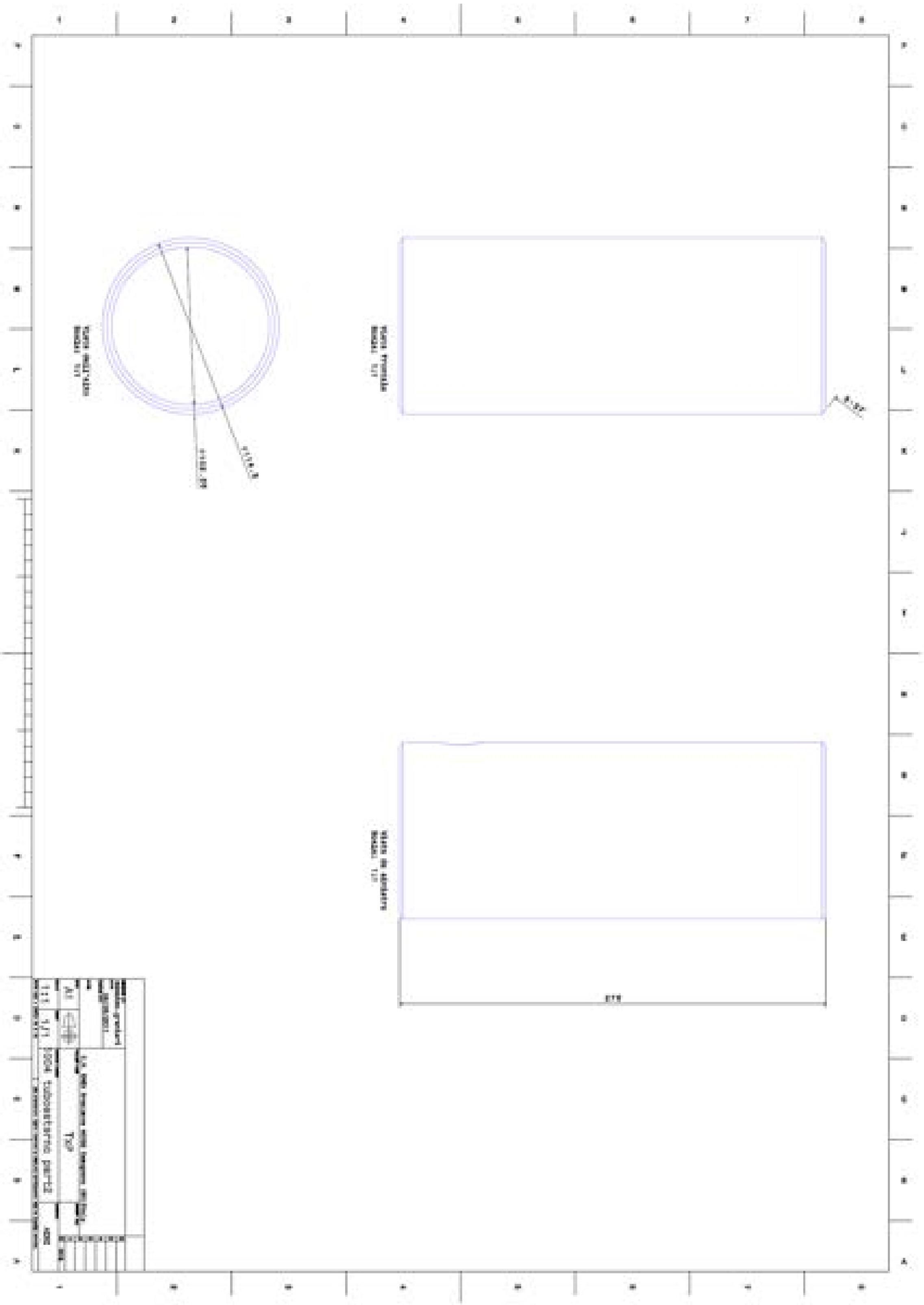

Fig. 43 – TxP design: WT tube part 1.

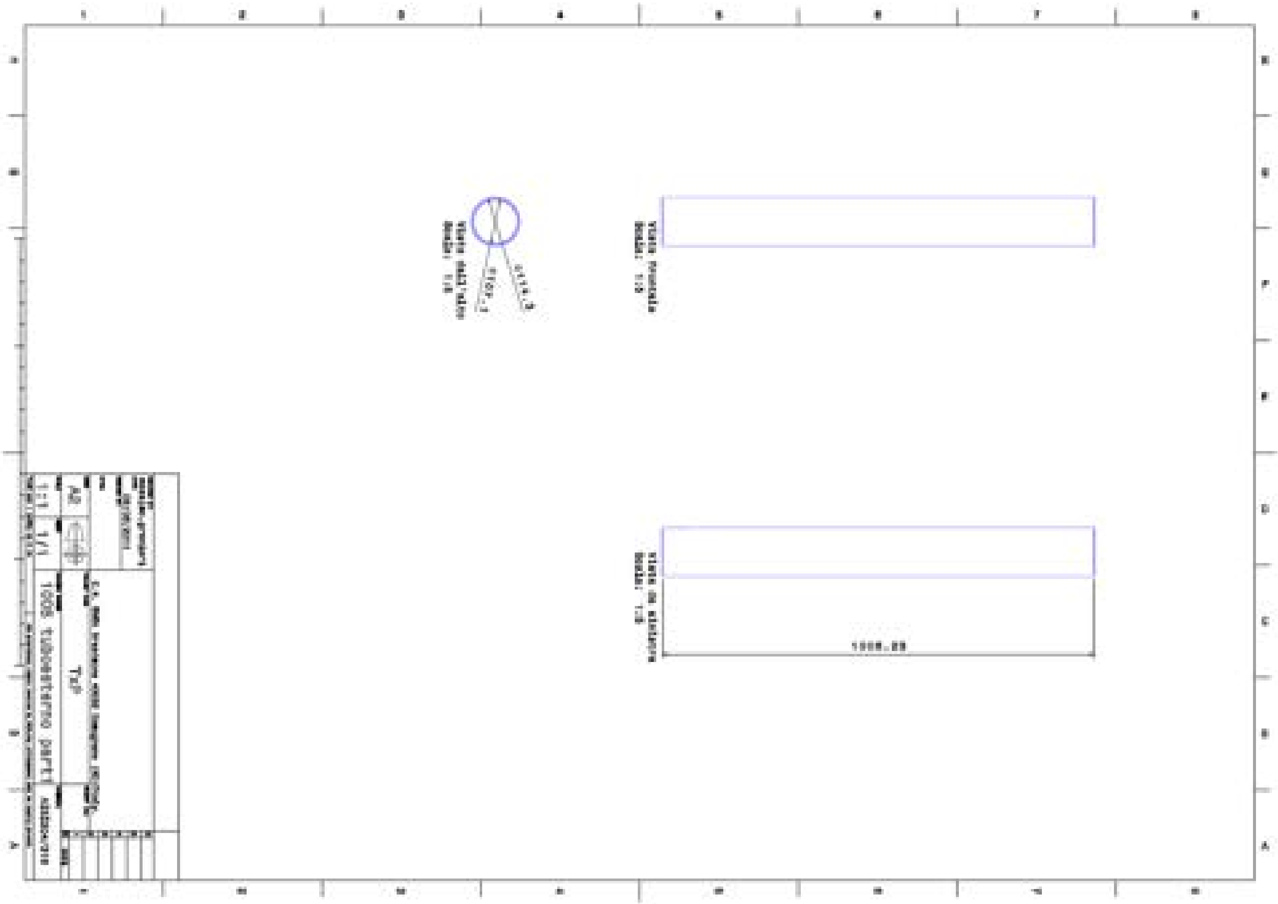

Fig. 44 – TxP design: WT tube part 2.

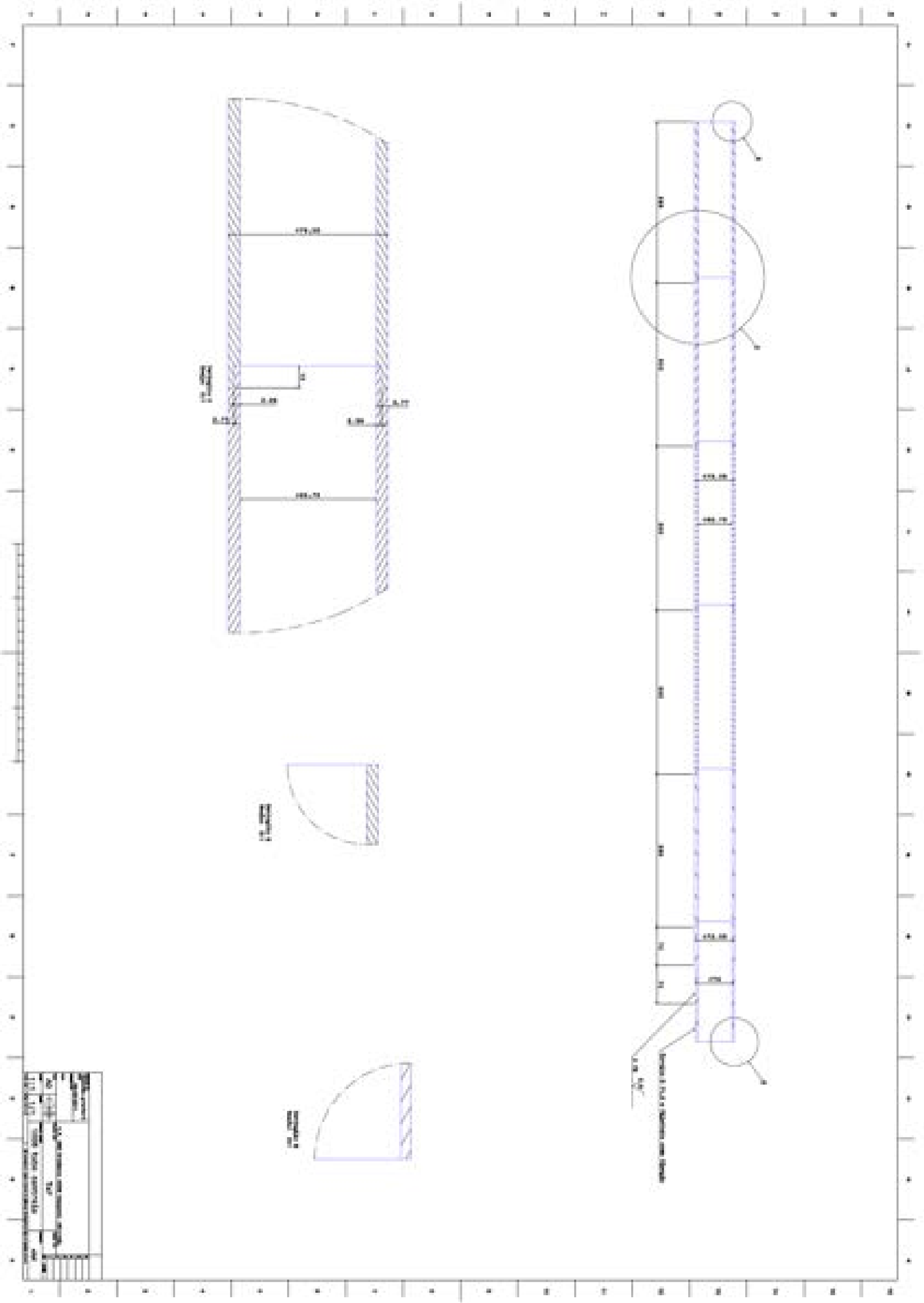

Fig. 45 – TxP design: IT tube.

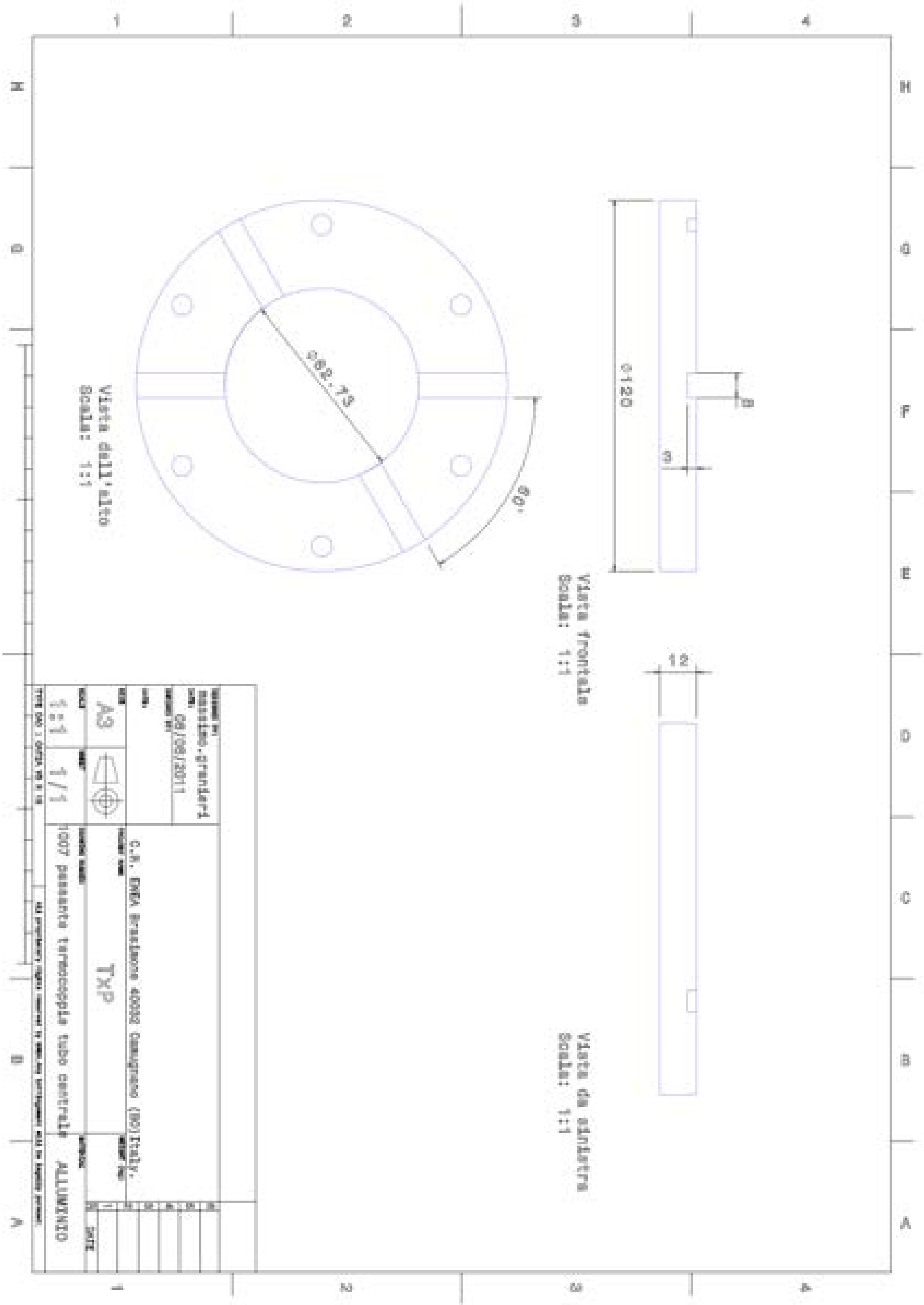

Fig. 46 – TxP design: IT thermocouples flange.

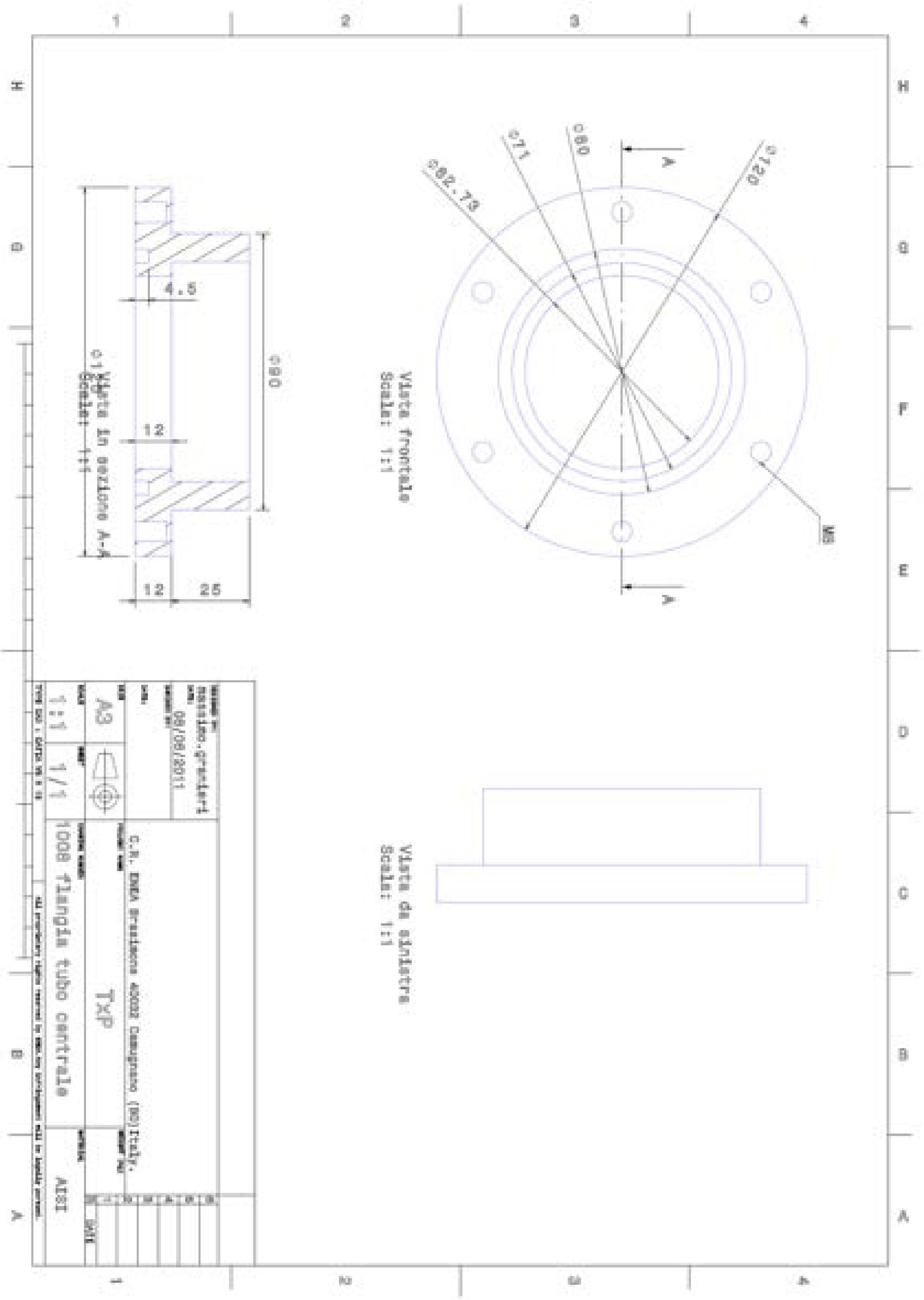

Fig. 47 – TxP design: IT flange.

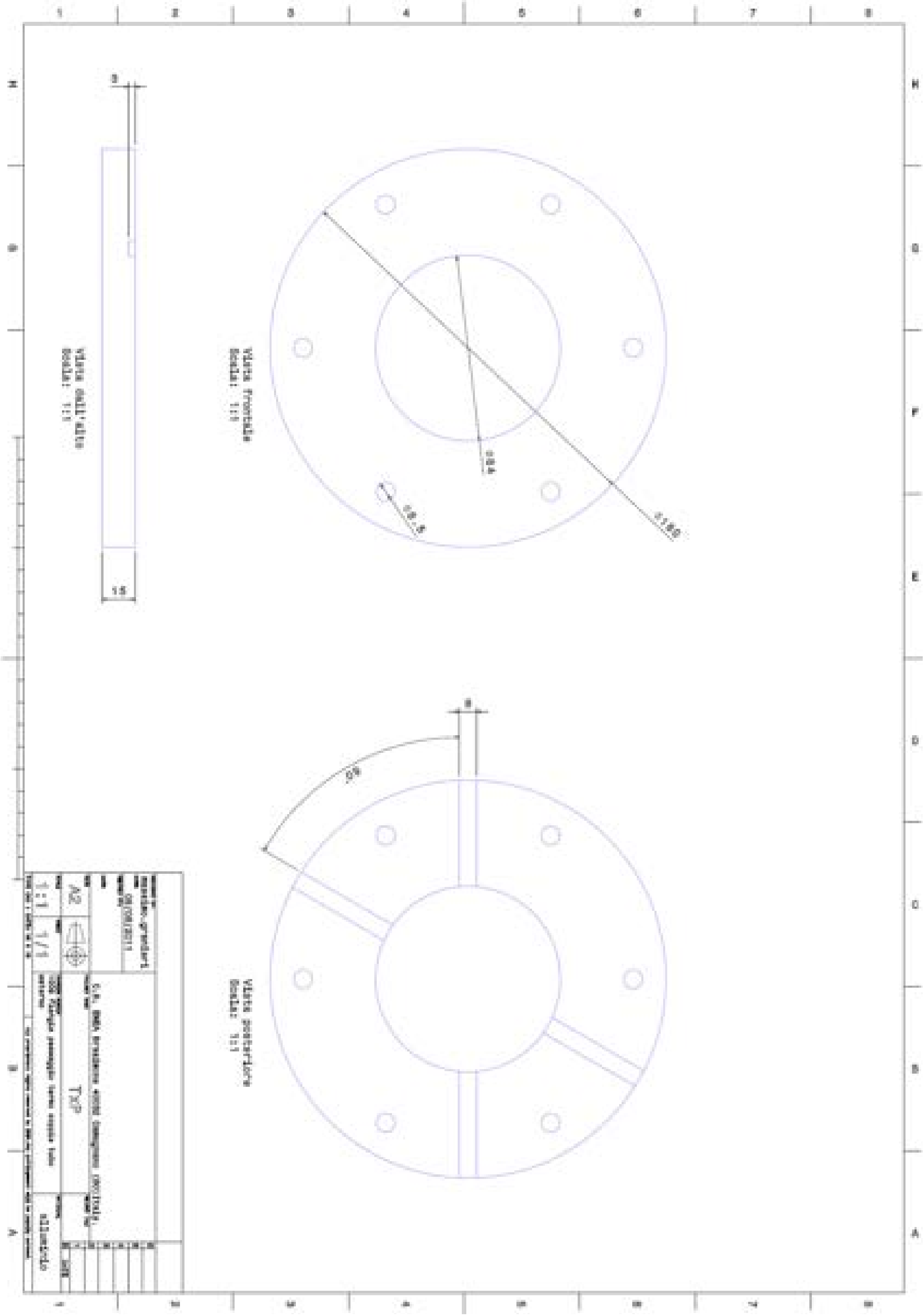

Fig. 48 – TxP design: PT thermocouples flange.

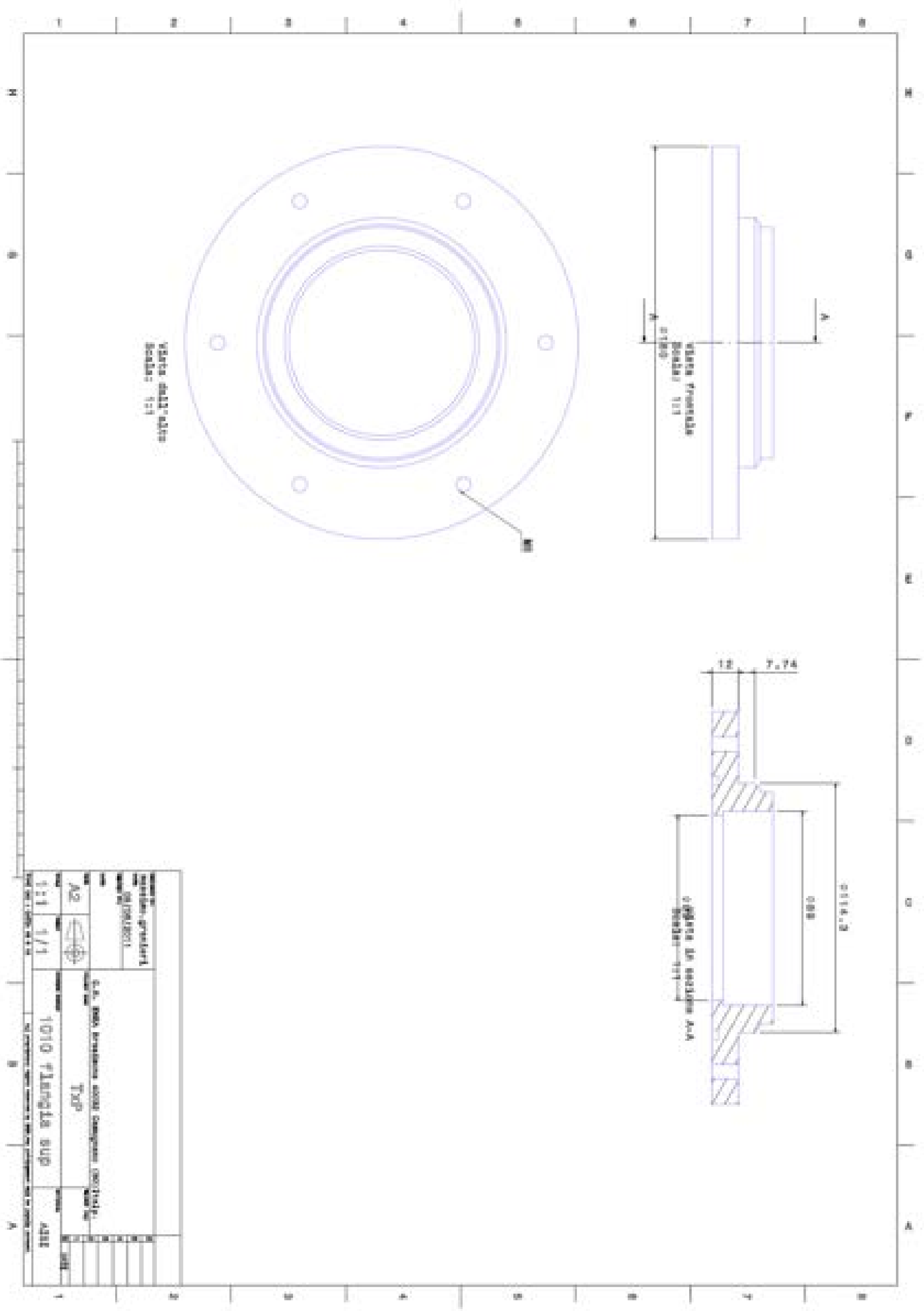

Fig. 49 – TxP design: top flange.

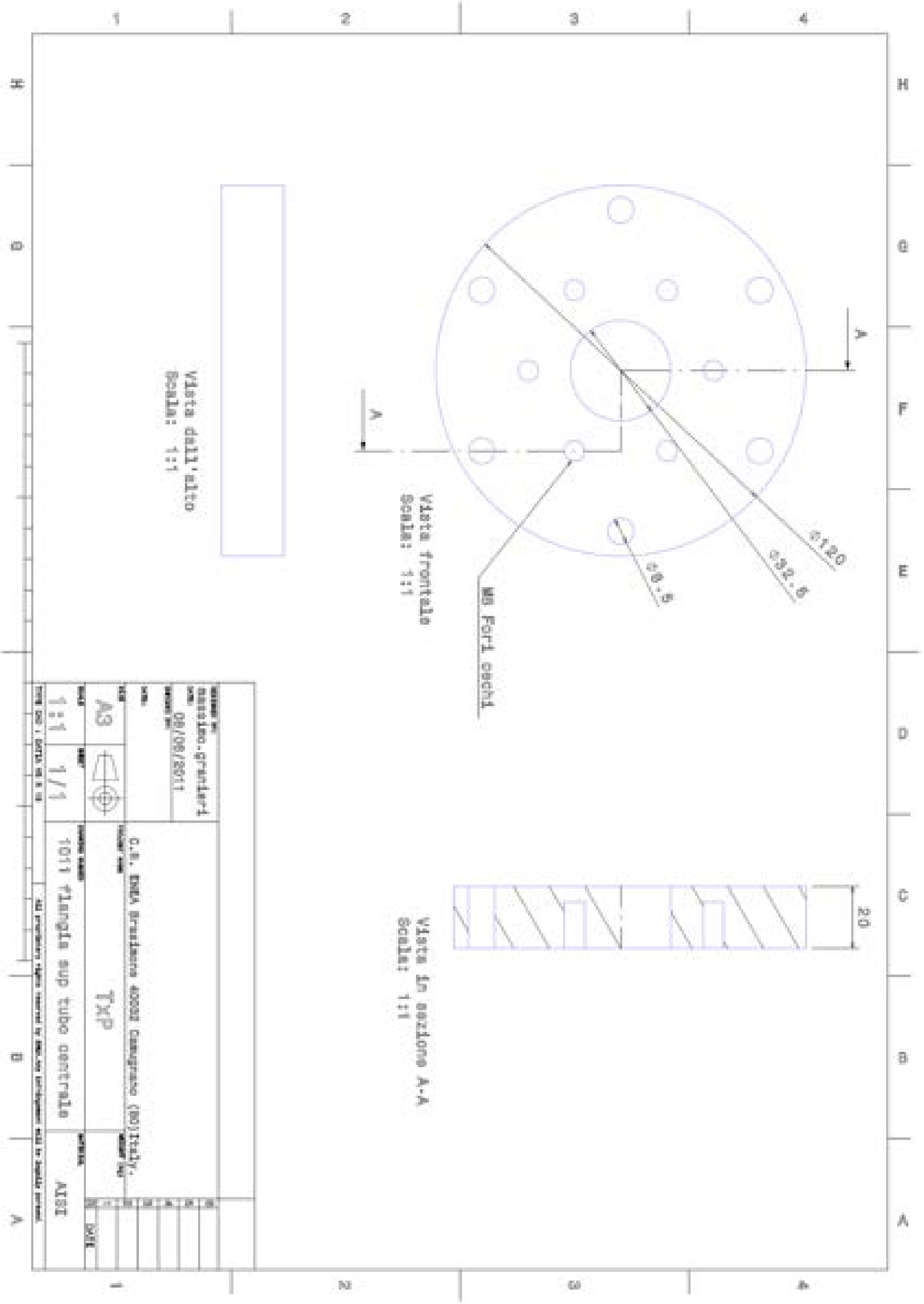

Fig. 50 – TxP design: upper sealing flange.

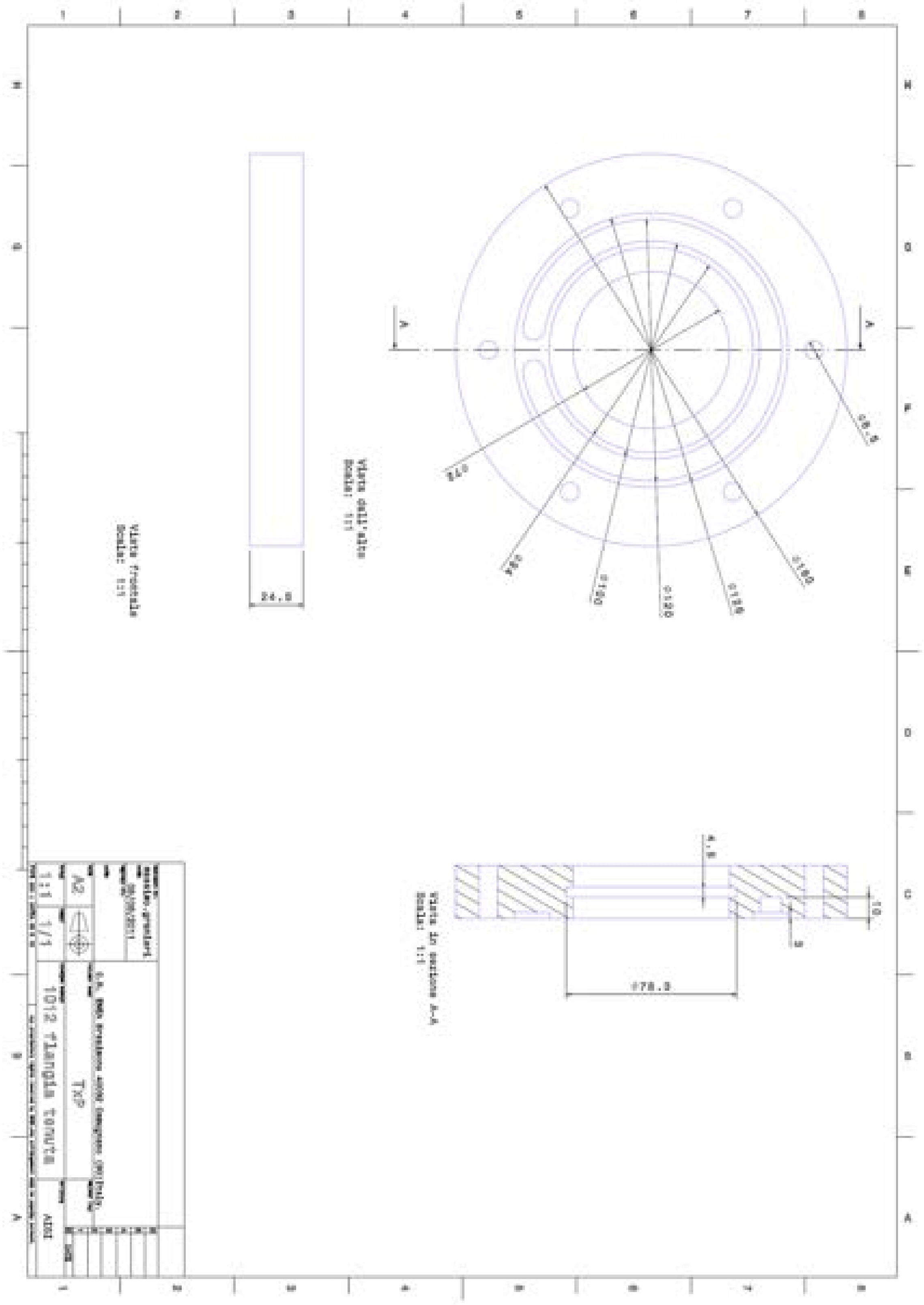

Fig. 51 – TxP design: intermidiate sealing flange.

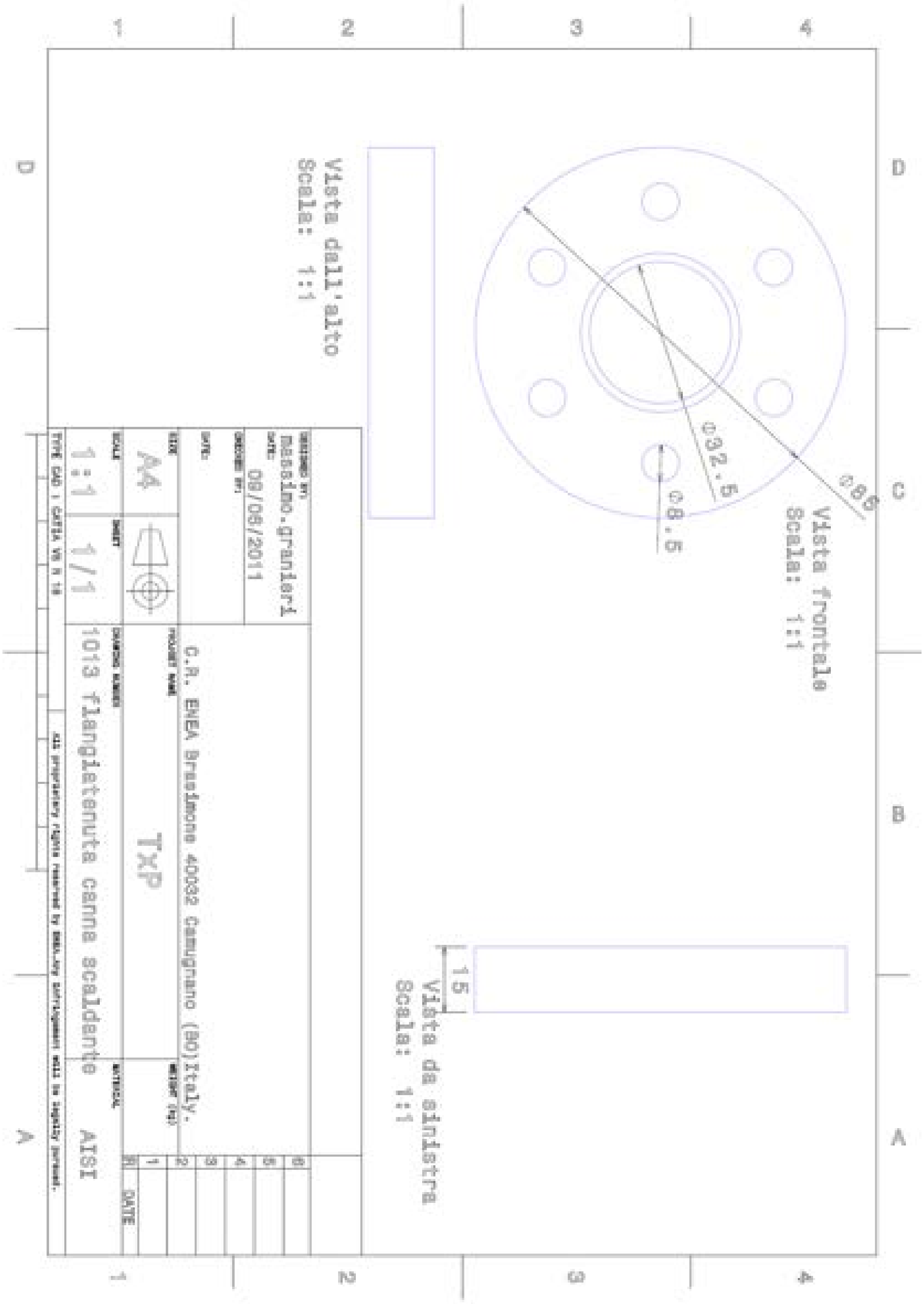

Fig. 52 – TxP design: HR sealing flange.

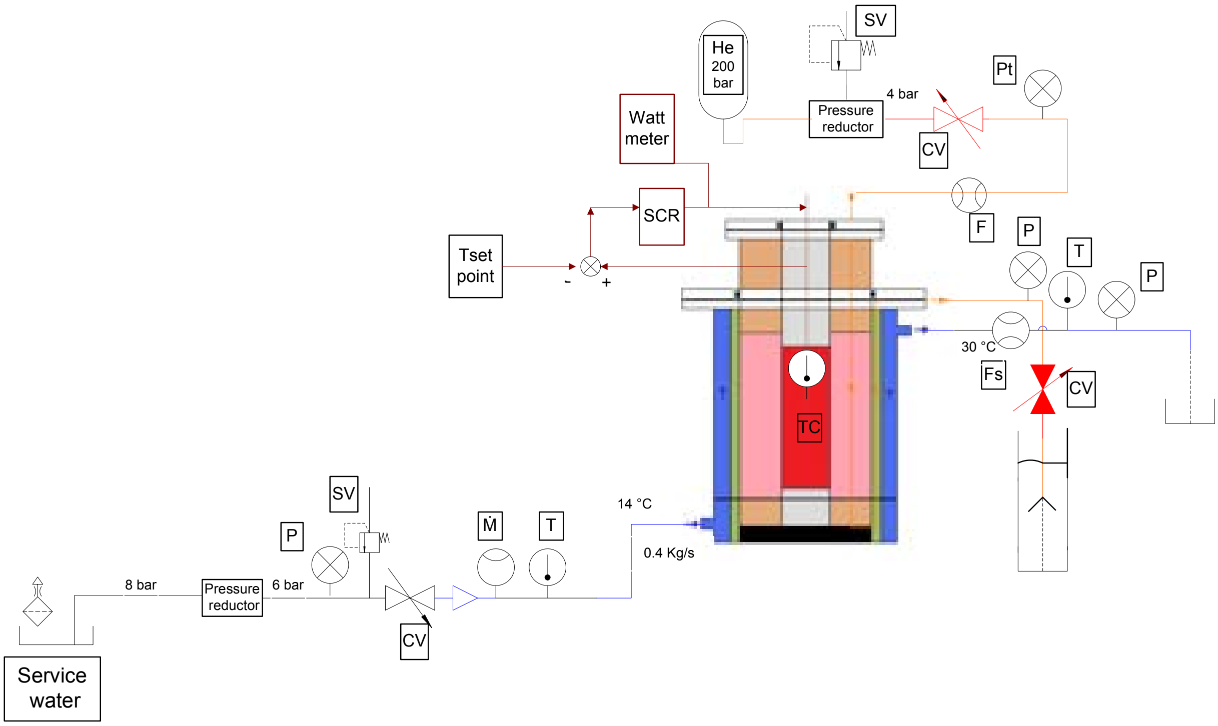

INSTRUMENTATION			
P	Manometer	Fs	Flux checker
T	Thermo-resistance	M	Flow meter
TC	Thermocouple	CV	Control valve
F	Flux meter	SV	Safety valve

Fig. 53 – TxP design: PID.

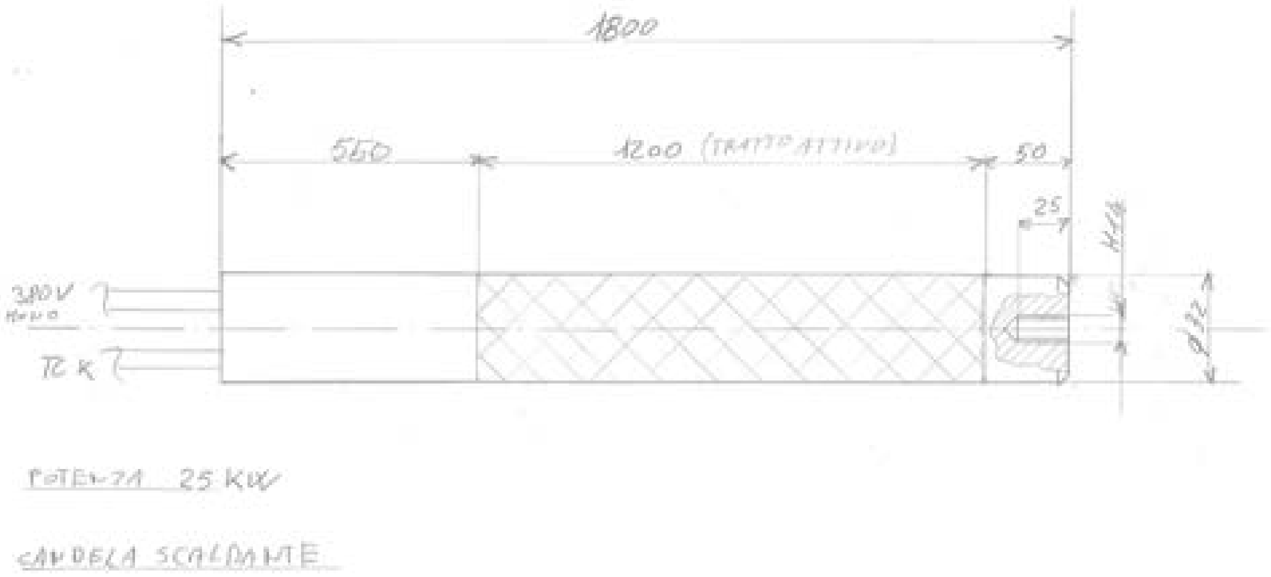

Fig. 54 – TxP design: HR scheme.

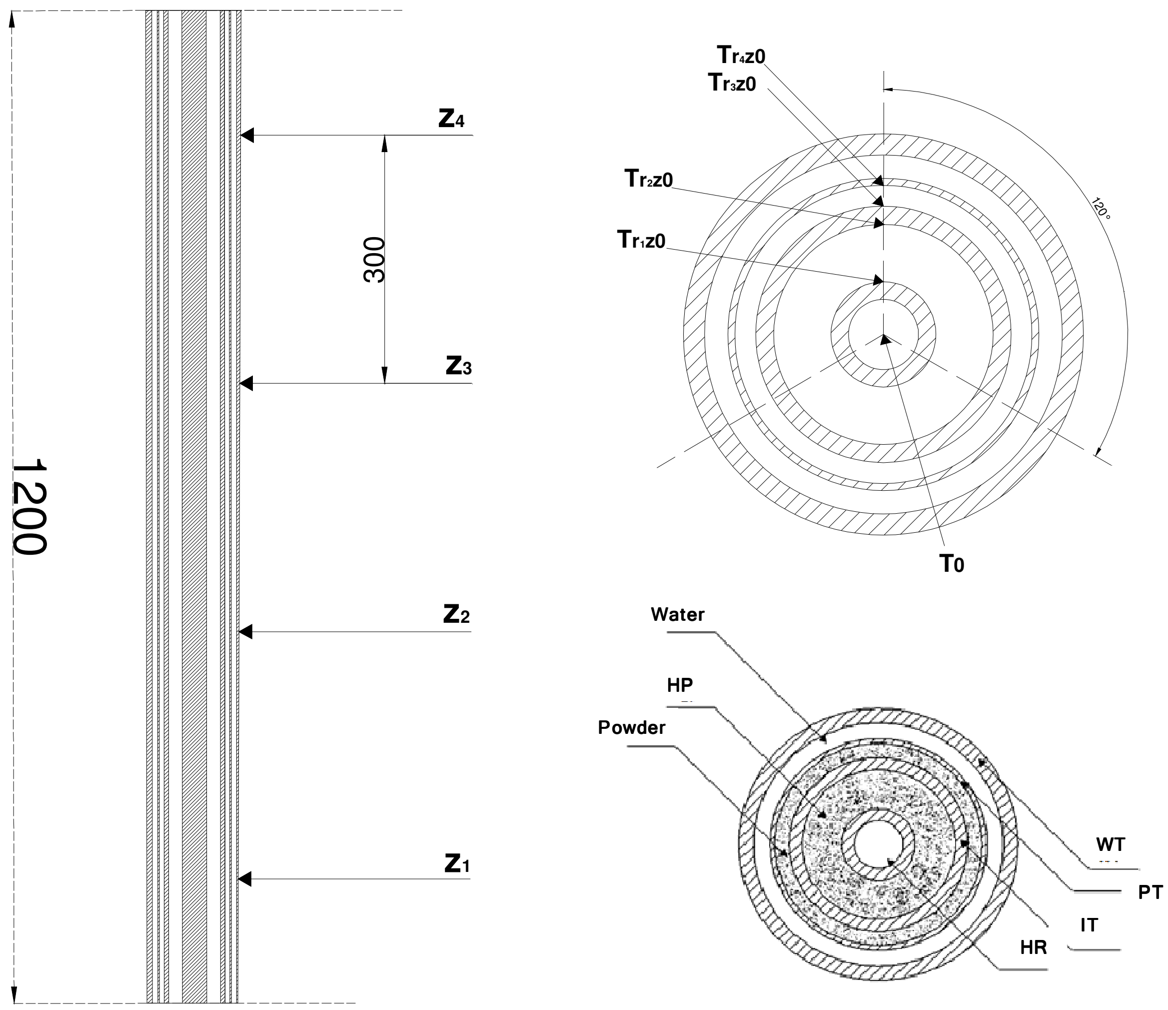

Fig. 55 – TxP design: thermocouples positions.

5 Modeling of the SG Bayonet Tube by mean of RELAP-5

5.1 Description of the input model

The single tube unit proposed by ANSALDO Nucleare for the ALFRED Reactor was modeled by RELAP 5 3.3[38] on the basis of the data reported in *Tab. 1*. The scheme adopted for the nodalization is showed in *Fig. 56*. Particular focus was devoted to model the annular gap thermal exchange:

- Synthetic Diamond powder was considered as ideal material,
- Copper, Brass and AISI – 1010 were analyzed,
- The powders were considered at 0.3 porosity and treated with the conductivity correlations adopted for the TxP design described in section 3.2.2.

Furthermore:

- The insulating paint contained in the slave-tube was modeled at the constant conductivity of 0.05 W/mK according to the ANSALDO nodalization.
- The heat exchange between the outer tube and the Argon chamber was neglected.
- The Heat Transfer Coefficient in the lead-side has been evaluated with Ushakov's correlation.

This nodalization will be updated on the basis of the results obtained by TxP in order to support the SG design with particular reference to the eventual investigation of turbulence promoters to be placed in the boiling and super-heated regions to reach steam temperatures close to 450 °C.

5.2 Assessment of the single tube performances

The steam temperature as function of tube length is reported in *Fig. 57*. Only the axial zone submerged in the Lead is depicted. The steam temperature outlet ranges from 420 to 450 °C if the conductivity of the powders is modeled according to case 1. Copper is very close to the ideal calculation performed with diamond. Case 2 produces steam outlet temperatures in the range 400 – 425 °C. The axial lead temperature drop is also given for diamond case1 and AISI-1010 case2. They embed all the investigations. The results suggest the analysis of design optimization such turbulence promoters in order to achieve 450°C at steam outlet.

The void fraction is depicted in *Fig. 58*. Super-heated steam is predicted in all the calculations. The water starts to boil in the first meter and the boiling process ends close to the fourth meter in the worst case (after 3 meters in the best case).

For sake of completeness, the results obtained by ANSALDO Nucleare are reported in *Fig. 59* and *Fig. 60*.

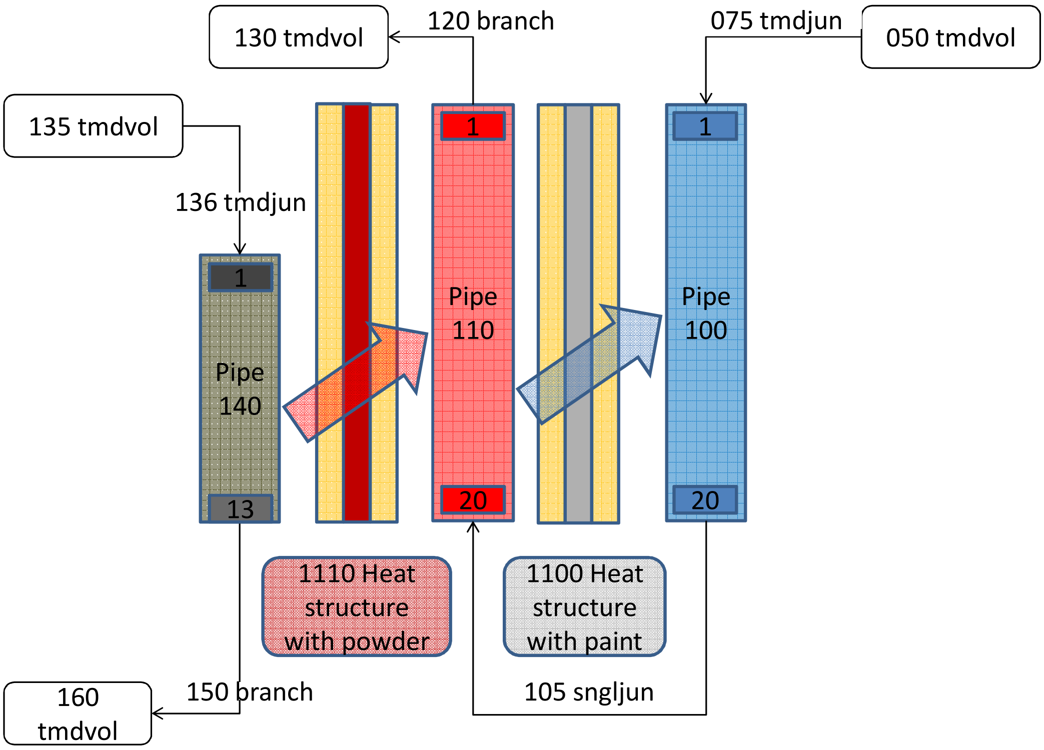

Fig. 56 – RELAP model scheme.

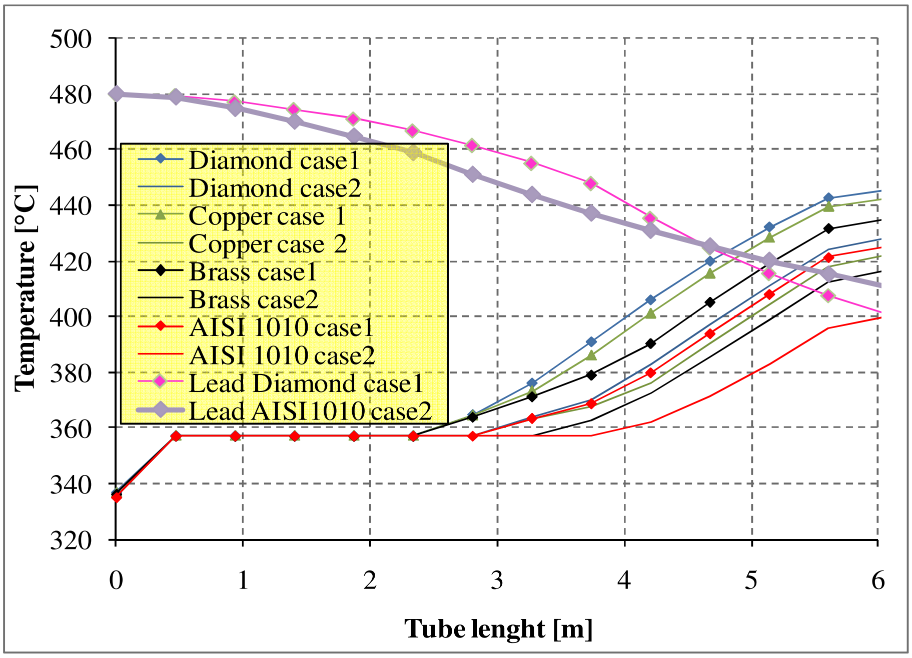

Fig. 57 – Single tube, RELAP 5-3.3, steam temperature.

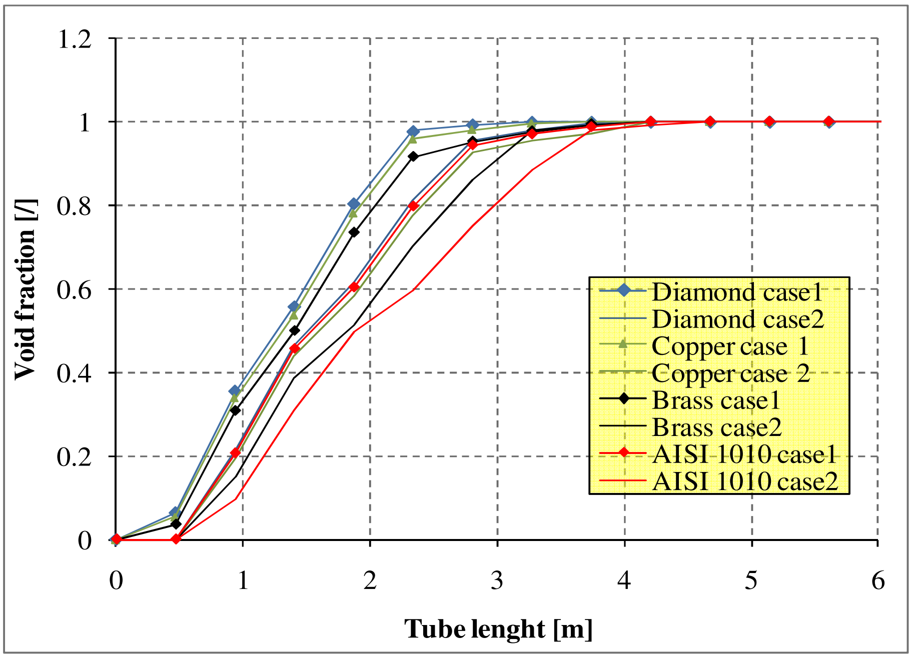

Fig. 58 – Single tube, RELAP 5-3.3, void fraction.

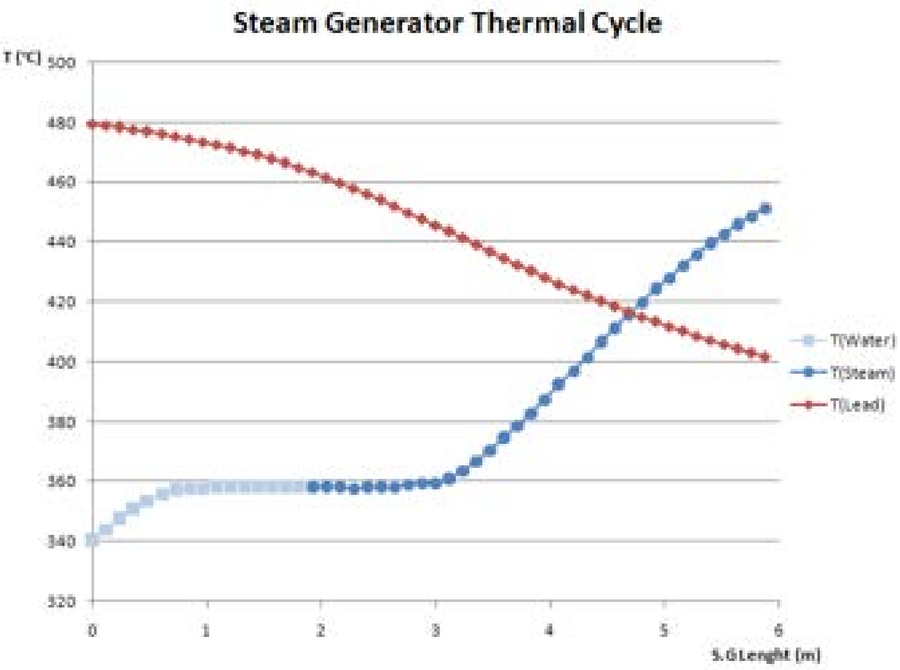

Fig. 59 – Single tube ANSALDO nodalization, RELAP 5-3.3, steam temperature.

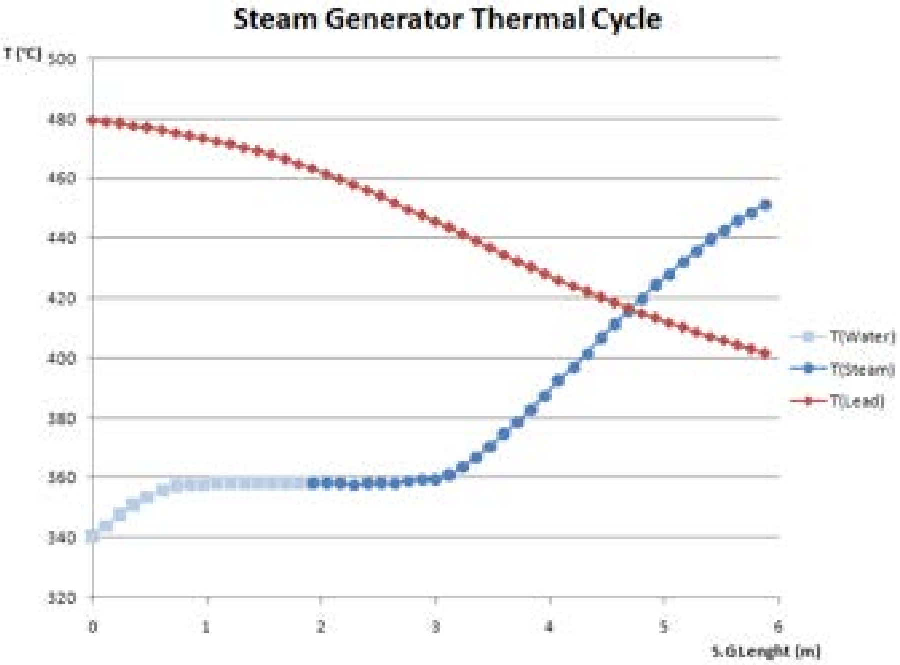

Fig. 60 – Single tube ANSALDO nodalization, RELAP 5-3.3, void fraction.

6 Preliminary Feasibility Analysis on Turbulence Promoters and Void Fraction Measurements

6.1 Heat Transfer Enhancement Techniques

The aim of this work is to perform a preliminary research on the heat enhancement devices that can be potentially used in the ALFRED SG. An enormous database of technical literature on this subject is available; in fact, a great number of heat enhancement devices have been experimentally tested in the last years for several kinds of fluids and flow configurations. In this document, particular emphasis is given to the works dealing with twisted tapes and wire coils. These devices are actually considered the most promising for the application to the double wall bayonet tube. *Fig. 61*, shows a possible insertion of enhancement devices in the single SG unit: in this case wire coil. Heat transfer enhancement techniques are classified in three broad categories:

1) Passive Techniques
Passive techniques do not require any direct input of external power[40]. They generally use surface or geometrical modifications of the flow channel by incorporating inserts or additional devices. They promote higher heat transfer coefficients by disturbing or altering the existing flow behavior, except for methodologies based on surfaces extension. Heat transfer augmentation by these techniques can be achieved by using treated surfaces, rough surfaces, extended surfaces, displaced enhancement devices, swirl flow devices, etc...

2) Active Techniques
Active techniques need for external power in order to achieve the desired flow modification and the concomitant improvement in the heat transfer rate[40]. Examples of these techniques are mechanical aids, surface vibration, electrostatic fields.

3) Compound Techniques
Compound enhancement refers to the use of two or more of these techniques simultaneously to obtain enhancement in heat transfer greater than that produced by each of them when used individually[40]. This technique involves complex design and hence has limited applications.

The effectiveness of any method is strongly dependent on the fluid dynamic configuration and the heat transfer mode (single-phase free or forced convection, pool boiling, forced convection, boiling or condensation, convective mass transfer). In this work, only passive techniques applicable in single-phase forced convection are investigated.

6.1.1 Passive heat transfer enhancement techniques

Several passive methods have been investigated in the last decades. A description of the most common passive methodologies has been given by Bergles [40] (1998):

- ***Treated surfaces*** are heat transfer surfaces that have a fine-scale alteration, which can be continuous or discontinuous. They are used primarily for boiling and condensing duties. Their working principle is based on the distortion of the laminar flow at the wall surfaces.
- ***Rough surfaces*** are generally surface modifications that promote turbulence in the flow field, primarily in single-phase flows. Generally, they do not increase the heat transfer

surface area. Their geometric features range from random sand-grain roughness to discrete three-dimensional surface protuberances.

- ***Extended surfaces*** provide an effective heat transfer surface area enlargement. Plain fins have been used routinely in many heat exchangers. However, the newest concept led to innovative surfaces that improve the heat transfer coefficients by disturbing the flow field in addition to the enlarged surface area.
- ***Displaced enhancement devices***, are used in confined forced convection, they are inserts that improve, indirectly, the energy transport at the heat exchange surface.
- ***Swirl flow devices*** produce secondary circulation or rotating flow (swirl flow) inside the flow channel. They include helical strip or cored screw-type tube inserts, twisted ducts, and various forms of altered (tangential to axial direction) flow arrangements. They can be used for single-phase as well as two-phase flows.
- ***Coiled tubes*** lead to relatively more compact heat exchangers. The tube curvature produces secondary flows or Dean vortices, which promote higher heat transfer coefficients in single-phase flows as well as in most regions of boiling.
- ***Surface tension devices*** consist of wicking or grooved surfaces, which improve the flow of liquid to boiling / condensing surfaces.
- ***Additives for liquids*** consist in the addition of solid particles, soluble trace additives, gas bubbles in single-phase flows, and trace additives, which usually depress the surface tension of the liquid, for boiling systems.
- ***Additives for gases*** include liquid droplets or solid particles which are introduced in single-phase gas flows.

These techniques are particularly attractive for gases or vapors since the convective coefficients are normally much lower than the liquid coefficients. This implies that a wide range of devices and geometrical configurations have been theoretically and experimentally tested. Only the rough surfaces (in particular wire coils), and the twisted tapes are here analyzed. Coiled tubes have been also investigated due to their analogies with twisted tapes, that impress helical circulation in the flow channel.

In general, the heat transfer enhancement is mainly due to flow blockage, partitioning of the flow and secondary flow generation. These flow modifications result in a higher fluid mixing and increased heat transfer coefficient. The flow modifications cause a pressure drops increase. In the fully developed turbulent flow, the thermal resistance is limited to the thin viscous sub-layer. Since the main purpose of wire coils insert is to mix the flow in this layer, they result more efficient comparatively with twisted tapes, that cannot properly mix the flow in the viscous sub-layer. In laminar flow, the thermal resistance involves a thicker region; therefore, twisted tapes insertion results more convenient. To conclude and summarize: in turbulent flow, wire coils performs better than any other insert (as found experimentally).

List of symbols

A	Heat exchange surface [m^2]	μ	fluid viscosity [Pa·s]
A_f	Cross sectional area [m^2]	μ_w	fluid viscosity evaluated at the wall temperature
c_p	Specific heat at constant pressure [kJ / kg k]	μ_b	fluid viscosity evaluated at the bulk temperature
d	Tube diameter [m]	η	Heat transfer enhancement efficiency [/]
D	Tube diameter [m]	Nu	Nusselt number [/]
D_h	hydraulic diameter [m]	p	pressure [Pa]
De	Dean number [/]	P_w	Wetted perimeter [m]
f	friction factor [/]	Pr	Prandtl number [/]
G	Specific mass flow rate [kg / s m^2]	R_c	Curvature radius of coiled tubes [m]
h	heat transfer coefficient [W / m^2 K]	Re	Reynold number [/]
He	Helical number [/]	ρ	fluid density [kg/ m^3]
j	Colburn factor [/]	S_w	Swirl parameter
k	thermal conductivity [W / m K]	T	Temperature [K]
L	Tube length [m]	V	fluid velocity [m/s]

6.1.2 Criteria for the assessment of heat transfer enhancement techniques

The main parameter used to evaluate the performance of an enhancement device is the *heat transfer efficiency* η, defined as the ratio of the heat transfer coefficient of an augmented configuration h_a, to that of a smooth surface h_0, at an equal pumping power PP:

$$\eta = \left(\frac{h_a}{h_0}\right)_{pp} = \left(\frac{Nu_a}{Nu_0}\right)_{pp} = \left(\frac{Nu_a}{Nu_0}\right)\left(\frac{f_a}{f_0}\right)^{-1/3} \qquad \text{Eq. 39}$$

where Nu, f, Nu_0 and f_0 are the Nusselt numbers and the friction factors for a duct configuration with and without inserts, respectively. This parameter is also used to compare the performance of different passive techniques.

The issue to quantify and evaluate the performance of enhancement devices, with an universal set of criteria, is rather complex. Besides the thermal–hydraulic behavior, there are many factors that have to be considered, as costs, manufacturability, reliability and safety. As said before, the main purpose of using enhancement methods is to increase heat exchange ratio. In forced convection, it is accompanied by an increase in the pressure drop along the tube. Therefore, the problem requires finding the optimum configuration considering heat transfer improvement from one hand, and pressure drop increase from the other hand. In most practical applications, the following *performance objectives*, along with a set of operating constraints and conditions, are usually considered for optimizing the use of a heat exchanger:

1. Increase the heat duty of an existing heat exchanger without altering the pumping power (or pressure drop) or flow rate requirements.
2. Reduce the approach temperature difference between the two heat-exchanging fluid streams for a specified heat load and size of exchanger.
3. Reduce the size or the heat transfer surface area required for a specified heat duty and pressure drop.
4. Reduce the process pumping power requirements for a given heat load and exchanger surface area.

These objectives functions have been described by many different *performance evaluation criteria* (PEC) (Bergles et al., 1974; Webb, 1981, 1994; Bergles, 1998)[40]. For the quantitative evaluation of these PEC, the main method is to relate the enhanced performance, given by parameters as Nu, j and *f, Re*, with that of the equivalent smooth duct. With reference to the simple tubes bundle geometry, the heat transfer coefficient *h* [W/m^2·K], and the pumping power *P* can be expressed as follow:

$$h = \frac{c_p j G}{Pr^{2/3}} \qquad \text{Eq. 40}$$

$$P = \frac{A j G^3}{2\rho^{2/3}} \qquad \text{Eq. 41}$$

where, c_p is the specific heat at constant pressure [kJ / kg k], *G* is the specific mass flow rate [kg / s m^2] *A* is the heat exchange surface [m^2], ρ is the fluid density [kg/ m^3] and the *Colburn factor j* is given by:

$$j = Nu\,Re^{-1}Pr^{-1/3} = \frac{h}{c_p G}\left(\frac{c_p \mu}{k}\right)^{2/3} \qquad \text{Eq. 42}$$

Where *k* is the thermal conductivity [W / m K] and μ is the fluid viscosity.

Thus, the performance of the enhanced tubes can be related to that of the equivalent smooth tubes (*N, L,* d_i same) as:

$$\frac{hA/h_0A_0}{(P/P_0)^{1/3}(A/A_0)^{1/3}} = \frac{j/j_0}{(f/f_0)^{1/3}} \qquad \text{Eq. 43}$$

Supposing as known *j* (or *Nu*) and *f* (data or correlations), for both the enhanced and the smooth ducts, the PEC assessment is rather straightforward. One of the groupings (hA/h_oA_o), (P/P_o), and (A/A_o) becomes the *objective function*, with the other two fixed equal to 1 for the corresponding operating constraints. This provides also the mass flux ratio (G/G_o) required to satisfy eq. *Eq. 43*.

For example, if the assumed criterion is to increase the thermal performance by using enhancement techniques, but without changing the pumping power and the approach temperature difference, the following expressions can be written as:

$$\frac{Q}{Q_0} = \left(\frac{Nu}{Nu_0}\right)_{N,l,di,\Delta T,P} \qquad \text{Eq. 44}$$

$$(f \cdot Re^3) = (f_0 \cdot {Re_0}^3) \qquad \text{Eq. 45}$$

The first term of Eq. 44 gives the enhancement of the thermal performance. The second one gives the constraint of the pumping power. The Eq. 45 establishes the relationship between the Reynolds numbers for the enhanced and the smooth flow passages. Because the enhanced duct geometry has higher friction factor *f* than those of the smooth passage, this constraint requires that for a given flow rate (*Re* or *G*), Re_o (or G_o) must be higher then *Re*. Another possible objective may deals with reducing the size of the heat exchanger (this criterion can be applied during the design phase). In this case the ratio (A/A_0) assumes the role of the objective function, and the constant pumping power constrain gives the ratio G/G_0.

6.1.3 General correlations

6.1.3.1 Nusselt number evaluation

In forced convective heat transfer inside a tube, the main parameters which have to be defined are the heat transfer coefficient *h*, expressed by the dimensionless Nusselt number *Nu*, and the friction factor *f*, which characterizes the pressure drop *ΔP* in the channel.

$$Nu = \frac{hD_h}{k} \qquad \text{Eq. 46}$$

$$f = \frac{\Delta P}{\left(\frac{L}{D}\right)\left(\rho\frac{v^2}{2}\right)} \qquad \text{Eq. 47}$$

Where D_h is the hydraulic diameter [m], *L* is the tube length and *v* is the fluid average velocity [m/s].There are several empirical relationships for the numerical evaluation of these parameters in fully developed flow. In the special case of a pipe with smooth internal surface, the following expressions are widely used:

Dittus – Boelter – Mc Adams:

$$Nu = 0.023\,Re^{4/5}\,Pr^{n} \qquad \text{Eq. 48}$$

Validity range:

$0.7 \le Pr \le 120$ $2500 \le Re \le 1.24 \times 10^5$, $L/D > 60$

The Prandtl number exponent is $n = 0.4$ when the fluid is being heated, and $n = 0.3$ when the fluid is being cooled. All the physical properties needed for the calculation of *Nu, Re*, and *Pr* have to be evaluated at the bulk temperature T_m.

Sieder and Tate (1936):

If the variations of the fluid properties with the temperature are relevant, a correction of the previous correlation has been proposed by *Sieder and Tate*:

$$Nu = 0.027Re^{4/5}Pr^{1/3}\left(\frac{\mu_b}{\mu_w}\right)^{0.14} \qquad \text{Eq. 49}$$

Validity range:

$0.7 \le Pr \le 16{,}700$ $Re > 10^4$

The effect of temperature-dependent properties is taken into account by evaluating all the properties, except for the viscosity μ_w, at the mean temperature of the stream, T_m (this apply also to the bulk viscosity μ_b). The viscosity μ_w is evaluated at the wall temperature T_w. In the case of gases, the ratio (μ_b/μ_w) can be replaced by (T_b/T_w).

Petukhov (1970):

$$Nu = \frac{f/8RePr}{1.07 + 12.7(f/8)^{1/2}(Pr^{2/3} - 1)} \qquad \text{Eq. 50}$$

Validity range:

$$4000 \le Re \le 5 \times 10^6 \qquad 0.5 \le Pr \le 10^6.$$

Gnielinski (1976):

$$Nu_D = \frac{(f/2)(Re_D - 10^3)Pr}{1 + 12.7(f/2)^{1/2}(Pr^{2/3} - 1)} \qquad \text{Eq. 51}$$

Validity range (accuracy +/-10%):

$$0.5 \le Pr \le 10^6 \qquad 2300 \le Re \le 5\times10^6.$$

6.1.3.2 *Friction factor evaluation:*

Correlation from Moody diagram (Moody, 1944):

$$f = 0.316\ \mathrm{Re}^{-1/4} \qquad \text{for Re} \le 2 \cdot 10^4 \qquad \text{Eq. 52}$$

$$f = 0.184\ \mathrm{Re}^{-1/5} \qquad \text{for Re} \ge 2 \cdot 10^4 \qquad \text{Eq. 53}$$

Petukhov (1970):

$$f = (0.790 \ln \mathrm{Re} - 1.64)^{-2} \qquad \text{for } 3000 \le \mathrm{Re} \le 5 \cdot 10^6 \qquad \text{Eq. 54}$$

Karman–Nikuradse correlation (Kays and Perkins, 1973)

$$\frac{1}{f^{1/2}} = 1.737\ ln\left(Re_D f^{1/2}\right) - 0.396 \qquad \text{Eq. 55}$$

which agrees with measurements for Re values up to $O(10^6)$.

6.1.3.3 *Extension to non cylindrical geometry*

The same relations valid for the case of the circular tube can be used for annuli and noncircular ducts by employing the concept of the hydraulic diameter D_h;

$$D_h = \frac{4\,A_f}{P_w} \qquad \textit{Eq. 56}$$

Where A_f is the transverse section and P_w is the wetted perimeter. Of course, the use of the previous equations is justified only if the sections do not vary appreciably from circular. Such channels are square, rectangular not too far from square, and probably equilateral or nearly equilateral triangles. For geometries far from circular, this method may not be satisfactory.

6.1.3.4 *Correlations comparison*

A comparison of the previous correlations has been performed, in particular for a super-heated steam forced convective flow. In this case, *Pr* varies with the temperature and the pressure.

Fig. 62 shows *Pr* number of superheated steam at *P*=180 bar in the range of temperature (360°C – 450°C), that represents the effective range expected in ALFRED SG (the saturation temperature of water at *P*=180 bar is T_{sat}=356°C). The *Pr* values have been evaluated by the mean of the software

"*Thermodynamic and Transport Properties of Water and Steam*", provided by Chemical Logic Corporation [41]. In this analysis, the value Pr = 1.4 has been chosen (value calculated at the mean temperature in the range (360°C – 450°C). For the implementation of the *Gnielinski* and *Petukhov* correlations, the friction factor has been evaluated by the mean of the *Petukhov* relationship. For the correlations of Sieder and Tate, that contain the corrective factor Φ (μ_b/μ_w), the Nusselt number has been plotted in terms of Nu/Φ, in order to remove this effect from the graph. In *Fig. 63* and *Fig. 64* are reported the achieved results, the term Φ is fixed to 1 for the other correlations. The correlations previously introduced can be applied to super-heated steam, and their predictions have been validated by experimental investigations.

Moreover, several specific correlations for super-heated steam have been developed. One example is the *Hadaller and Banerjee* (1969) correlation [42]:

$$Nu = 0.0101\, Re^{0.877} Pr^{0.611} (L/D)^{-0.33} \qquad \text{Eq. 57}$$

where all properties are evaluated at the temperature:

$$T = \frac{(T_w + T_b)}{2} \qquad \text{Eq. 58}$$

6.1.4 Assessment of Rough Surfaces

A simple way to enhance heat transfer coefficient in single-phase forced convection developed in tubes or in annular space is the utilization of surface roughness. The straightening points connected with the utilization of rough surfaces make them one of the most popular devices used in industrial heat exchangers:

- Low cost
- Easy installation and removal
- Preservation of original plain tube mechanical strength
- Possibility of installation in an existing smooth tube heat exchanger

In *Fig. 65* is depicted a scheme of the several rough surfaces used in industrial applications. Structured roughness can be integral part of the surface as well as protuberances that can be introduced in the form of wire-coil-type inserts. These last ones are taken as reference in this report. The main geometrical features of wire coils, as reported in *Fig. 66*, are the pitch p, the wire thickness e and the pitch ratio y, defined as the ratio of the pitch p to the tube diameter d. Important parameters are also the ratio (e/d) and the corrugation inclination α with respect to the flow direction. Over the last five decades, an extensive set of experimental data for the heat transfer coefficients and the friction factors in rough tubes has been created (Ravigururajan and Bergles, 1986; Esen et al., 1994; Bergles, 1998) [40].

Adopting an empirical approach, Ravigururajan and Bergles (1996) proposed a set of correlations, that have been validated by mean of a large experimental database. Their model is actually considered the most general and accurate method for predicting the heat transfer and friction factor improvement for rough surfaces devices. Ravigururajan and Bergles correlations are applicable to the following range of parameters:

$0.1 < e/d < 0.2$, $0.1 < p/d < 7.0$, $0.3 < \alpha/90 < 1.0$, $5000 < Re < 250000$ and $0.66 < Pr < 37.60$

The parameter β represents the profile contact angle of the rib to the internal surface of the tube and *n* is the number of sharp corners of the rib facing to the flow (two for triangular or rectangular cross section and infinity for smoother profiles). The parameter β, is taken as 90° for circular profiles.

$$Nu = Nu_0 \left\{ 1 + \left[2.64 Re^{0.036} \left(\frac{e}{d}\right)^{0.212} \left(\frac{p}{d}\right)^{-0.21} \left(\frac{\alpha}{90}\right)^{0.29} Pr^{-0.024} \right]^7 \right\}^{1/7} \qquad \text{Eq. 59}$$

$$f = f_0 \left\{ 1 + \left[29.1 Re^{a_1} \left(\frac{e}{d}\right)^{a_2} \left(\frac{p}{d}\right)^{a_3} \left(\frac{\alpha}{90}\right)^{a_3} \left(1 + 2.94 \sin\frac{\beta}{n}\right) \right]^{15/16} \right\}^{16/15} \qquad \text{Eq. 60}$$

where:

$$a_1 = 0.67 - 0.06\left(\frac{p}{d}\right) - 0.49\left(\frac{\alpha}{90}\right) \qquad a_2 = 1.37 - 0.157\left(\frac{p}{d}\right)$$

$$a_3 = -1.6 \cdot 10^{-6} Re - 0.33\left(\frac{\alpha}{90}\right) \qquad a_4 = 4.59 + 4.11 \cdot 10^{-6} Re - 0.15\left(\frac{p}{d}\right)$$

The parameters Nu_0 and f_0, referred to the equivalent smooth tube, are evaluated by the mean of the *Petukhov* correlations:

$$Nu_0 = \frac{Re \cdot Pr\,(f_0/2)}{1 + 12.7\sqrt{f_0/2}\,(Pr^{2/3} - 1)} \qquad \text{Eq. 61}$$

$$f_0 = (1.58\,lnRe - 3.28)^{-2} \qquad \text{Eq. 62}$$

In *Fig. 67* and *Fig. 68*, are plotted the Ravigururajan and Bergles correlations for superheated steam (Pr=1.4) as function of Reynolds number. The numerical values assumed for the geometrical parameters (e/d), ($\alpha/90$) and (p/d) are summarized in *Tab. 23*. The ratio (e/d) is fixed at 0.1. It is considered a reasonable value for a standard wire coils application. The pitch ratio p/d is set as 2, higher values are often assumed. For continuous wire coils, the pitch ratio p/d determines the inclination angle α: in the configuration here investigated, α = 45°. *Fig. 69* shows various geometrical features investigated in a large set of experimental works found in the literature research[43].

The achieved results agree with the experimental investigations: the enhanced Nusselt number ranges from 160% to 180% higher than that of the equivalent smooth tube. The smaller is the value assumed by the pitch ratio *p/d,* the grater is the heat transfer improvement. As expected, the decrease of this parameter leads to the increase of the friction factor; this can be attributed to dissipation of the dynamic pressure of the fluid due to higher surface area and the action caused by the reverse flow.

6.1.5 Assessment of Swirl flow devices

Swirl flow devices generally consist of a large variety of tube inserts that produce secondary flows [40]. Typical examples of these techniques are twisted-tape inserts, periodic tangential fluid injection and helically twisted tubes. In last decades, these devices have been intensely studied.

The swirl flow devices can be classified into two categories: the first is the *continuous swirl flow* and the second is the *decaying swirl flow*. For the continuous swirl flow, the swirling motion persists over the whole length of the tube, while in the decaying swirl flow, the swirl is generated at the tube inlet and decays along the flow path. For the decaying swirl flow, the heat transfer coefficient and pressure drop decrease with the axial distance, while for the continuous swirl flow, the heat transfer coefficient and pressure drop are keep as constant. In this report, only *twisted-tape* inserts are taken into account. As shown in *Fig. 70*, they can be placed in a cylindrical duct or into an annular space. The main geometrical features of twisted tapes are the twist pitch H and the tape thickness δ. The performance of tape twist is described by the dimensionless twist ratio y (H/d). For discontinuous twisted tapes elements, a significant parameter is the regularly spaced twisted tape ratio S, defined as the ratio of the distance between two swirl elements to the tube diameter d. The introduction of twisted tapes in a circular tube involves several modifications of the flow pattern:

- increased flow velocity
- increased wetted perimeter
- longer effective flow length in the helically twisting partitioned duct
- helical secondary fluid circulation or swirl
- radial pressure gradient

Among these topics, the dominant mechanism is the swirl generation. It creates a centrifugal force that improves the convective heat transfer. As expected, the pressure drops result increased; this is due to the higher contact surface between the fluid and the wall and to the longer effective flow length. The laminar swirl flow has been investigated with both experimental and numerical approach[40]. On the basis of the experimental results, several correlations for laminar flows have been developed (Manglik and Bergles, 1993)[40]. These correlations are not discussed in this report since only high turbulent flows are investigated.

For fully developed turbulent flows, the following correlations have been developed by Manglik and Bergles, (1993):

$$f = \frac{0.0791}{Re^{0.25}}\left(1 + \frac{2.752}{y^{1.29}}\right)\left[\frac{\pi}{\pi - (4\delta/d)}\right]^{1.75}\left[\frac{\pi + 2 - (2\delta/d)}{\pi - (4\delta/d)}\right]^{1.25} \qquad \textit{Eq. 63}$$

valid for turbulent flow heat transfer with $Re \geq 10^4$.

$$Nu = 0.023 Re^{0.8} Pr^{0.4}\left(1 + \frac{0.769}{y}\right)\left[\frac{\pi + 2 - (2\delta/d)}{\pi - (4\delta/d)}\right]^{0.2}\left[\frac{\pi}{\pi - (4\delta/d)}\right]^{0.8}\Phi \qquad \text{Eq. 64}$$

where the parameter Φ is given by:

$$\Phi = \left(\frac{\mu_b}{\mu_w}\right)^n \quad or \quad \left(\frac{T_b}{T_w}\right)^m \qquad \text{Eq. 65}$$

with:
Where the indexes b, w refer to bulk or wall respectively.

$$\text{n} = \begin{cases} 0.18 & \text{liquid heating} \\ 0.30 & \text{liquid cooling} \end{cases} \quad \text{and} \quad m = \begin{cases} 0.45 & \text{gas heating} \\ 0.15 & \text{gas cooling} \end{cases}$$

Twisted tapes have been also studied by Keppler [44] for applications in gas-cooled nuclear reactors. It was found a proportional relationship between the twist ratio y and the heat-transfer enhancement; the tape with the tightest twist ($y = 2.38$) showed the greatest heat transfer improvement. In this experimental campaign, the following correlation, that consists in a modification of the *Sieder and Tate* relationship, has been proposed:

$$Nu = 0.023\, Re^{0.8}\, Pr^{0.4} \left(1.105 + \frac{0.59\, Re^{0.05}}{y^{0.6}}\right)\Phi \qquad \text{Eq. 66}$$

Where Φ, is the wall – to –bulk viscosity or temperature ratio. The correlation developed by Keppler remains valid only for the fully developed flow.

A comparison of the correlations here discussed is shown in *Fig. 71* and *Fig. 72*. For the calculations, the value $y = 2$ is assumed, typical values are in the range (1 - 10) [45]. With regard to the tape thickness, the value δ/d=0.05 has been considered as reasonable. Pr=1.4 has been assumed. Keppler and Manglik - Bergles correlations give similar results across the range of Reynolds number.

The main geometrical parameter that characterizes a twisted tape insert is the twist ratio $y = H/d$. The smaller is the twist ratio y the greater is the heat transfer improvement. This is due to the higher turbulent intensity and, therefore, to the higher flow mixing generated. On the other hand, the experimental results, reveal that the use of a small twist ratio leads to higher friction factor due to the increased tangential contact between the swirling flow and the tube surface. The predicted effect of the parameter y is shown in *Fig. 73*, that reports the Manglkik and Bergles correlation for different value of the twist ratio y. For the calculations, the same configuration of the previous analysis is considered, and the parameter keep as variable is y.

In discontinuous twisted tapes elements (*Fig. 74*), the influence of the regularly spaced twisted tape ratios S may be evaluated. The use of small value of S yields a higher heat transfer rate. If the value of the S is too high, in fact, the swirl effect is not sufficient to maintain the swirl intensity to the next twisted tape. Therefore , it was experimentally found that the optimum value of the space ratio S/d should be less than unity to get benefit of a better heat transfer rate and reduction of pressure loss in comparison with the plain tube.

6.1.6 Assessment of Coiled tubes

Coiled tubes are used in several applications, including hot water heaters, chemical process reactors, industrial and marine boilers… (Bergles et al., 1991; Nandakumar and Masliyah, 1986)[40]. They have been intensely investigated also for applications in nuclear reactors. In coiled or curved tubes, the secondary fluid motion is generated essentially by the continuous change in direction of the tangential vector to the bounding curved surface of the duct, which results in the local deflection of the bulk flow velocity vector. The complex flow patterns obtained, characterized by multiple helical vortices superimposed over the main axial flow, leads to an increase of the fluid mixing and, therefore, of the heat and mass transfer. Pressure drop result also increased because of two different factors: the increase of the turbulence intensity and the increase of the tubes length.

For coiled tubes, *Fig. 75,* the main geometrical parameters are the duct diameter *d* and the pitch *H*. The following dimensionless parameter are introduced:

Dean number:

$$\mathrm{De} = Re\sqrt{\frac{d}{2R}} \qquad \text{Eq. 67}$$

Radius of curvature:

$$R_c = R\left[1+\left(\frac{H}{2\pi R}\right)^2\right] \qquad \text{Eq. 68}$$

Helical number:

$$\mathrm{He} = Re\sqrt{\frac{d}{2R_c}} = De\left[1+\left(\frac{H}{2\pi R}\right)^2\right]^{1/2} \qquad \text{Eq. 69}$$

The main purpose of the ducts curvature is to impose a centrifugal force on the fluid motion, thereby generating a secondary circulation which is often referred in the literature as *Dean flow*. Several investigations have been performed for laminar flow heat transfer. As in the case of swirl flows generated by twisted-tape inserts, it has been widely observed that the transition from laminar flow to turbulent flow in delayed, and occurs at higher Reynolds number. However, laminar heat transfer is not discussed in this report.

For fully developed turbulent flows in curved or coiled circular tubes, the following correlation for the evaluation of the friction factor is available (Mishra and Gupta, 1979)[40]:

$$f = \frac{0.079}{Re^{0.25}} + \left(0.0075\sqrt{\frac{d}{2R_c}}\right) \qquad \text{Eq. 70}$$

valid for:

$Re_{tr} < Re < 10^5$ $\quad 6.7 < 2\,R/d < 346.0$ $\quad 0 < H/\,2R < 25.4$

For the evaluation of the Nusselt number, a common correlation valid for Pr~1 is given by *Mori and Nakayama* (1967).

$$Nu_g = \frac{1}{26.2}\left(\frac{Pr}{Pr^{2/3}-0.075}\right)\cdot Re^{4/5}\left(\frac{d}{D}\right)^{1/10}\cdot\left\{1+\frac{0.098}{[Re(d/D)^2]^{1/5}}\right\} \qquad \text{Eq. 71}$$

Fig. 76 and *Fig. 77* show the Nusselt number and friction factor enhancement, evaluated for superheated steam ($Pr = 1.4$), as function of the Reynolds number. In the analysis, the values of the geometrical parameters are chosen in order to investigate an helical duct generated by a helical tape insertion in a cylindrical tube. These assumptions are summarized in *Tab. 24*. The ratio *d/D* assumes, for standard applications of coiled tubes, very low values that can be considered in the range (0.1 – 10^{-2}). In this analysis, in order to simulate an helical flow generated by a twisted tape insert in a circular duct, the value d/D=0.5 is assumed. The pitch ratio H/D is set as 2, as for the calculation performed for twisted tapes. The validity of these assumptions is visible in *Fig. 78*, where the Nusselt number enhancements for twisted tapes and coiled tubes with similar geometrical configuration are compared.

6.1.7 Conclusive remarks on turbulence promoters

The wire coils analysis reveals that a significant improvement of the convective heat transfer can be reached; this analysis, based on the correlations developed by Ravigururajan and Bergles, reveals an improvement of the Nusselt number from 160% to 187%, depending on the Reynolds number. The increase of the turbulence intensity leads also to an increase of the pressure drops. Therefore, the utilization of these devices requires finding the optimum configuration considering heat transfer improvement from one hand and pressure drop increase from the other hand.

Twisted and helical tapes represent the alternative candidate technology. For them, the same methodology used for wire coils analysis has been adopted. The correlations found in the literature have been implemented in order to assess the heat transfer improvement and the friction factor increase for superheated steam. A considerable enhancement of the Nusselt number is available. Nevertheless it is lower than that achieved with wire coils. This result is confirmed by a large set of experimental works, in which has been observed that for fully developed flow, wire coils performs better than any other insert.

6.2 Steam Quality Measurement techniques

The main aim of this section is to investigate devices and procedures for the experimental measurement of the steam quality. Such instrumentation will support the assessment of the single tube testing (planned in the next two years). The measurement of the steam quality pursuits the objective to characterize the state of the substance in the two-phase region while is transforming to the single-phase or superheated region. This process can be performed by the mean of *calorimeters*. The following types of calorimeters are commonly used [47][47][48][49]:

- Barrel Calorimeter
- Separating Calorimeter
- Throttling Calorimeter
- Combined Separating and Throttling calorimeter
- Electrical Calorimeter

6.2.1 Barrel Calorimeter

Dryness fraction of steam can be pointed out very conveniently by mean of the barrel calorimeter. A scheme of this instrument is shown in *Fig. 79*.

A given mass of steam at pressure p_1 is extracted from the main pipe. This steam is then condensed by mean of a known quantity of water contained into an insulated vessel. The steam condensation causes an increase of the mass and the temperature of the water. The amount of heat lost by the steam condensation and the amount of heat received by the water (equal quantities), are used to obtain the dryness fraction.

$$Q = m_s\left[(xr_1) + c_{pw}(T_{sat} - T_2)\right] \quad \text{Eq. 72}$$

$$Q = \left(m_c c_{pc} + m_w c_{pw}\right)(T_2 - T_1) \quad \text{Eq. 73}$$

$$x = \frac{\left(m_c c_{pc} + m_w c_{pw}\right)(T_2 - T_1) - m_s c_{pw}(T_{sat} - T_2)}{m_s r_1} \quad \text{Eq. 74}$$

where:
Q: heat received by the water, [kJ]
m_s mass of steam condensed, [kg]
x: steam quality, [/]
r_1: latent heat of vaporization of water at the pressure p_1, [kJ/kg]
T_{sat}: saturation temperature at the pressure p_1,[K]
T_2: final temperature of water, [K]
T_1: initial temperature of water, [K]
m_c: mass of calorimeter, [kg]
c_{pc}: specific heat of the barrel calorimeter, [kJ/kg K]
m_w: mass of water contained in the calorimeter, [kg]
c_{pw}: specific heat of water, [kJ/kg K]

The value of the dryness fraction obtained with these methods generally involves a considerable error, since the heat losses due to convection and radiant effect are not taken into account. Furthermore, this method can apply only to low-pressure steam.

6.2.2 Separating Calorimeter

When steam is in very wet (low values of the dryness fraction) conditions, a separating calorimeter can be use to estimate the steam quality. A scheme of this device is given in *Fig. 80*. The steam is collected out of the main pipe and enters the separator from the top. A vortex flow is generated in the calorimeter that promotes water droplets separation from the steam by mean of the centrifugal action. The condensate thus is collected in the collector tank while the dry steam moves upwards to the condenser. For the described system, a simple mass balance, referred to the steam mass, allows the evaluation of the dryness fraction:

$$x_1 = \frac{m_s}{m_s + m_l} \quad \text{Eq. 75}$$

where:
x_1: dryness fraction
m_s: mass of steam read from gauge of condenser
m_l: mass of water separated

The main advantage of the separating calorimeter is that it allows a quick and easy determination of dryness fraction of very wet steam. Nevertheless, it may leads to inaccuracy due to incomplete separation of water.

6.2.3 Throttling Calorimeter

In a throttling calorimeter, whose scheme is shown in *Fig. 81*, a sample of steam of mass m_s at pressure p_1 is taken from the Main Steam pipe through a perforated sampling tube .Then, it is throttled by the partially-opened valve to a pressure p_2 (generally atmospheric pressure), measured by a manometer, and a temperature T_2. After throttling, the steam reaches the superheated region. The process is shown in the *h – S* diagram depicted in *Fig. 82*. The enthalpy before throttling can be considered equal to the enthalpy after the process (isenthalpic process called lamination). The initial state is given by p_1 and x_1, and the final state is given by p_2 and T_2 (superheated).

$$h_1 = h_2 \qquad \text{Eq. 76}$$

$$h_1 = h_{L1} + x_1 r_1 = h_{L2} + r_2 + \bar{c}_{p(2-2')}(T_2 - T_{2'}) \qquad \text{Eq. 77}$$

$$x_1 = \frac{h_{L2} - h_{L1} + r_2 + \bar{c}_{p(2-2')}(T_2 - T_{2'})}{r_1} \qquad \textit{Eq. 78}$$

where:

h_1: specific enthalpy before throttling, [kJ/kg]
h_2: final specific enthalpy after throttling, [kJ/kg]
h_{L1}: specific enthalpy of the liquid phase at pressure p_1, [kJ/kg]
h_{L2}: specific enthalpy of the liquid phase at pressure p_2, [kJ/kg]
r_1: latent heat of vaporization of water at the pressure p_1, [kJ/kg]
r_2: latent heat of vaporization of water at the pressure p_2, [kJ/kg]
$c_{p(2-2')}$:average specific heat of water in the temperature range (T_2 - $T_{2'}$)
T_2: final temperature of superheated steam
$T_{2'}$: saturation temperature of at pressure $p_{2'}$

In order to have sufficient confidence that the steam after throttling is in the superheated region, at least 5°C superheating is necessary. As shown in *Fig. 83*, this means that exists a minimum value of steam quality (at pressure p_1), which can be measured by using a throttling calorimeter alone. The applicability of the throttling calorimeter is thus limited to high value of the steam quality. Nevertheless, for wetted steam applications, a separating calorimeter can be inserted upstream to the throttling calorimeter.

6.2.4 Combined Throttling and Separating Calorimeter

To achieve an accurate determination of low value of steam quality, the combination of a separating calorimeter and a throttling calorimeter should be used. A scheme of this configuration is reported in *Fig. 84*, while the thermodynamic transformations are shown in the *–h - S* diagram depicted in *Fig. 85*. In the combined calorimeter, the steam is first passed through a separator where some part of the moisture separates due to the sudden change in direction and falls by gravity (process *1 – 2* in the *h - S* diagram of *Fig. 85*). The partially dry vapor is then throttled up to the superheated region. A simple steam mass balance of the separator is enough to determine the relation between the steam quality before and after the separation:

$$x_1(m_1 + m_2) = x_2 m_1 \qquad \text{Eq. 79}$$

After the steam separation, the steam passes from pressure p_2 to the superheated region, at atmospheric pressure p_3 (process *2 – 3* in the *S –h* diagram of *Fig. 85*), through an isenthalpic process (lamination):

$$h_2 = h_3 \qquad \text{Eq. 80}$$

$$x_2 = \frac{h_{L3} - h_{L2} + r_3 + \bar{c}_{p(3-3')}(T_3 - T_{3'})}{r_2} \qquad \textit{Eq. 81}$$

where:

x_1: steam quality before separation in the separating calorimeter
x_2: steam quality after separation in the separating calorimeter
h_2: specific enthalpy before throttling, [kJ/kg]
h_3: final specific enthalpy after throttling, [kJ/kg]
h_{L2}: specific enthalpy of the liquid phase at pressure p_2, [kJ/kg]
h_{L3}: specific enthalpy of the liquid phase at pressure p_3, [kJ/kg]
r_2: latent heat of vaporization of water at the pressure p_2, [kJ/kg]
r_3: latent heat of vaporization of water at the pressure p_3, [kJ/kg]
$c_{p(3-3')}$:average specific heat of water in the temperature range ($T_3 - T_{3'}$)
T_3: final temperature of superheated steam
$T_{3'}$: saturation temperature at pressure $p_{3'}$

6.2.5 Electrical Calorimeter

The electrical calorimeter operating principle is similar to that of throttling calorimeter; a scheme of this device is shown in *Fig. 86*. Wet mixture is brought to the superheated state in this case by heating (and not by throttling). The knowledge of the amount of heat added and the final enthalpy of the superheated steam allows the determination of the initial enthalpy, and so of the initial dryness fraction x_1. If m is the mass of steam taken in t seconds, the energy equation for the heater gives:

$$w_1 h_1 + Q = w_1 h_2 \qquad \text{Eq. 82}$$

where:

w_1: steam mass flow rate, [kg/s]
Q: thermal power of the electrical heater, [kW]
h_1: initial enthalpy of the moisture, [kJ/kg]
h_2: final enthalpy of the moisture, [kJ/kg]

The initial enthalpy is given by:

$$h_1 = w_1 h_2 - \frac{Q}{w_1} = h_{L1} + x_1 r_1 \qquad \text{Eq. 83}$$

which allows the determination of the initial dryness fraction x_1.

6.2.6 Conclusive remarks on steam quality measurement

Steam calorimeters are widely used in industrial applications. They are commonly used in process industries, power plants, etc., for determining the steam quality. The standard solution provides a separating calorimeter combined to a throttling calorimeter. This configuration allows an accurate determination of the steam quality into a large range of values.

For the direct determination of high water contents, $x \leq 0.5$, the separating calorimeter is required and can be used alone. On the other hand, in the high steam quality region ($x > 0.95$), the throttling calorimeter can be used alone. In case of intermediate values, the combination of the two systems is necessary to obtain fruitful measurements.

Parameter	Value
e/d	0.1
p/d	2
α/90	1/2

Tab. 23 – Values of the geometrical parameters assumed for the implementation of the wire – coils correlations.

Parameter	Value
d/D	0.5
H/D	2
R_c	0.70
d/R_c	0.71

Tab. 24 – Geometrical parameters assumed for the implementation of the coiled tubes correlations.

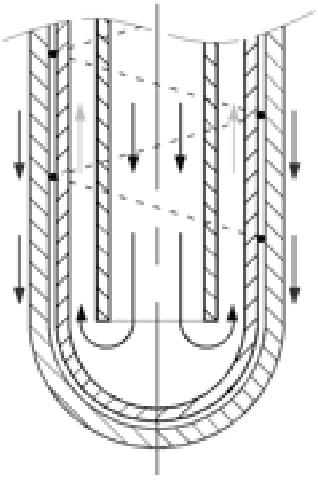

Fig. 61 – Scheme of the SG double wall bayonet tube with wire coil inserts.

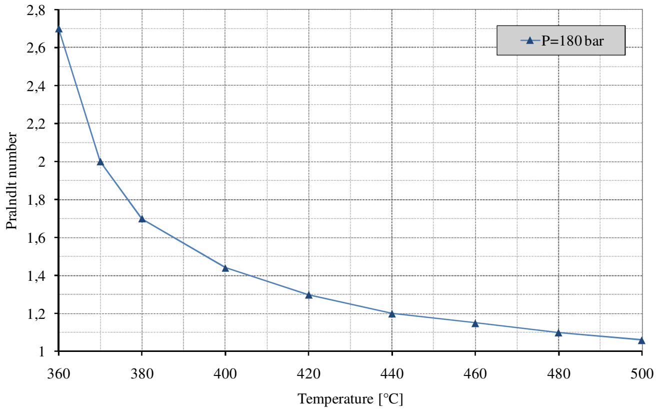

Fig. 62 – Prandlt number of superheated steam as function of temperature at different pressure.

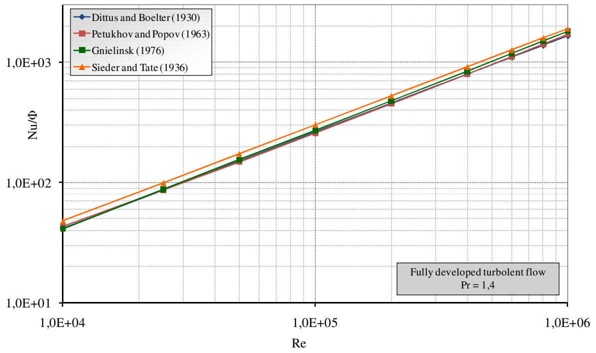

Fig. 63 – Nusselt number as function of Reynolds number.

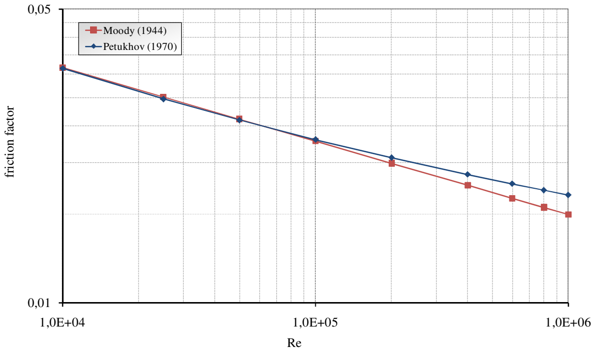

Fig. 64 – Friction factor as function of Reynolds.

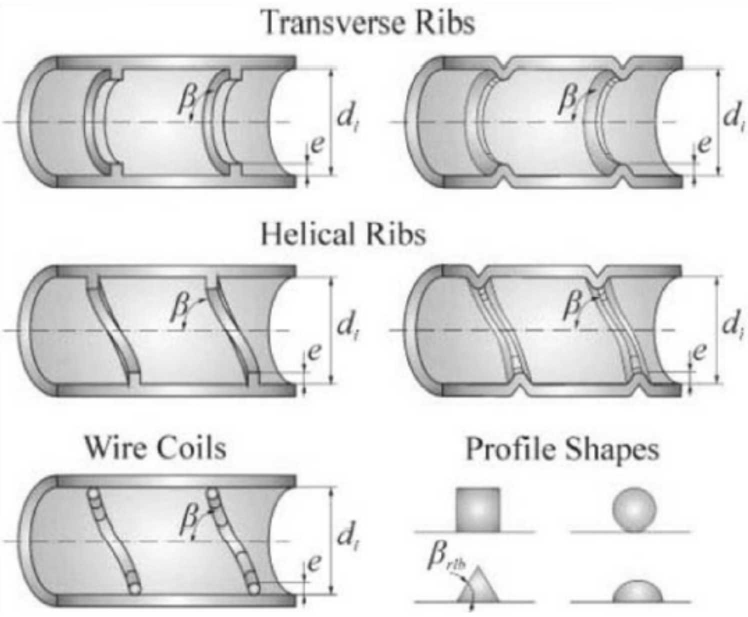

Fig. 65 – Several types of structured roughness with the main geometrical parameters.

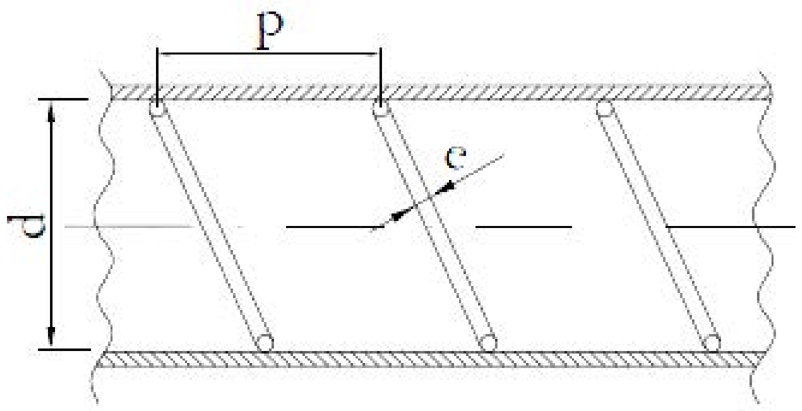

Fig. 66 – Main geometrical parameters of wire coils.

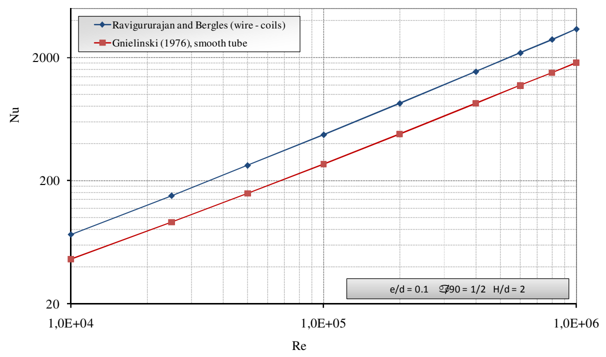

Fig. 67 – Wire coils, enhancement of the Nusselt number.

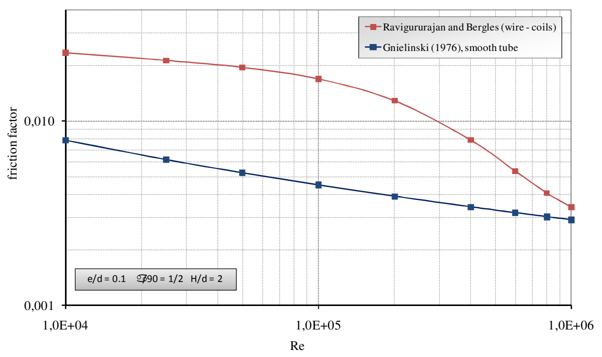

Fig. 68 – Wire coils, enhancement of the friction number.

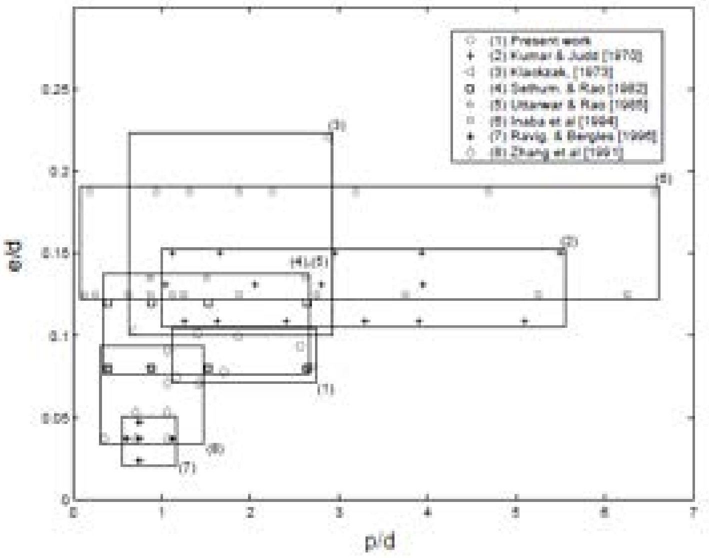

Fig. 69 – Geometrical configurations of wire coils in several experimental work.

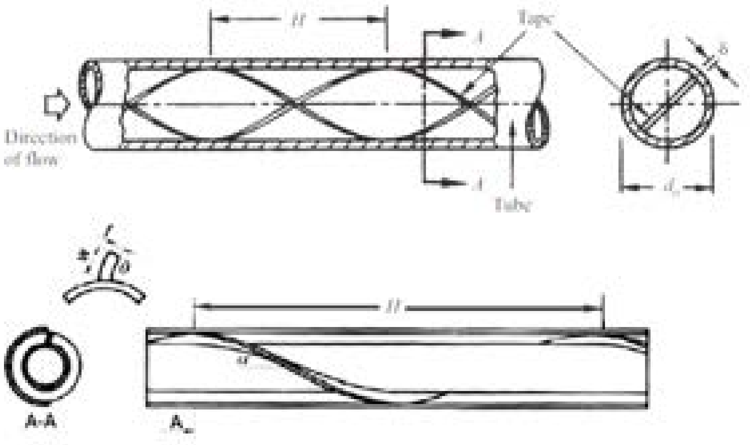

Fig. 70 – Scheme of twisted tape in circular tube and in a annular space.

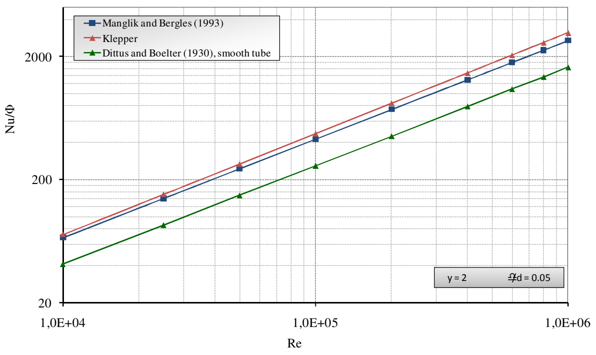

Fig. 71 – Twisted tapes insert, enhancement of Nussel number.

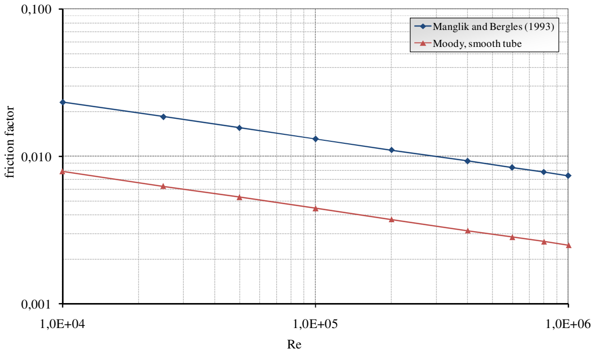

Fig. 72 – Twisted tapes insert, enhancement of the friction factor.

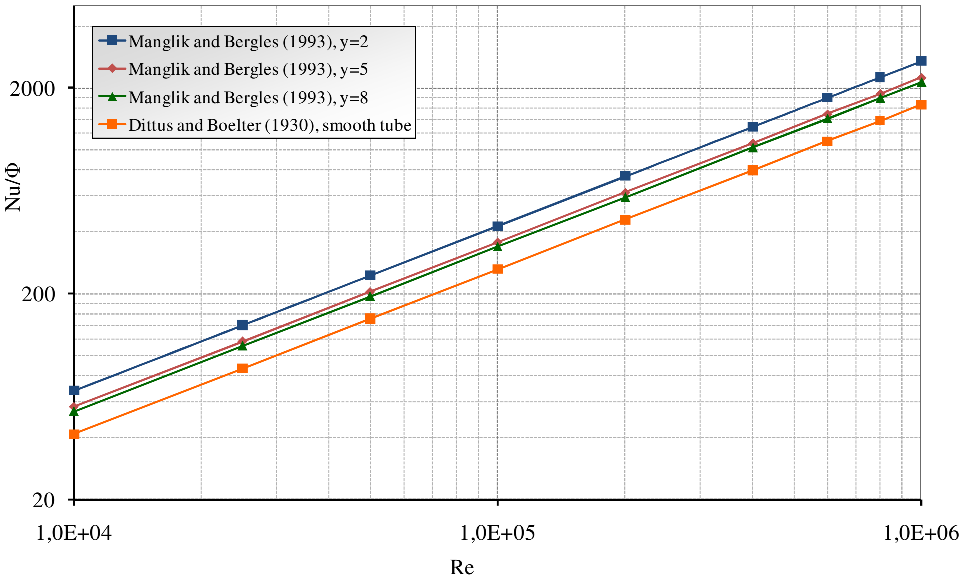

Fig. 73 – Twisted tapes insert, influence of the twist ratio y.

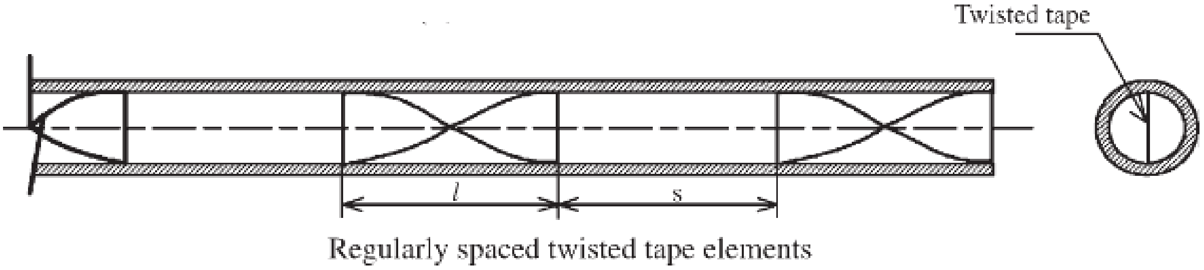

Fig. 74 – Regularly spaced twisted tape elements.

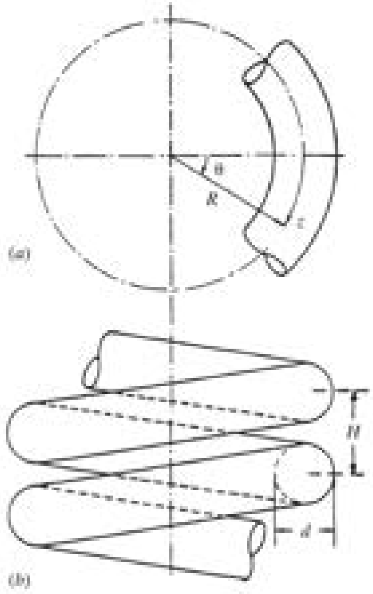

Fig. 75 – Scheme of coiled tube with the main geometrical parameters.

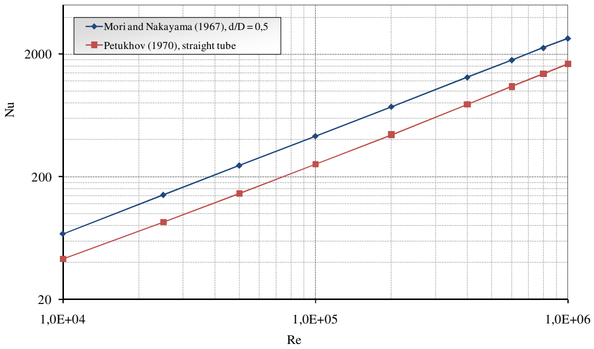

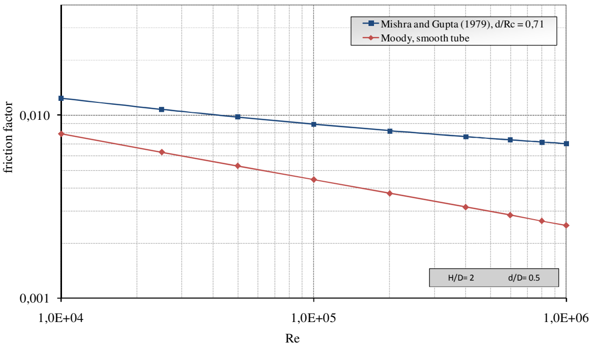

Fig. 76 – Coiled tube: enhancement on the Nusselt number.

Fig. 77 – Coiled tube, enhancement of the friction factor.

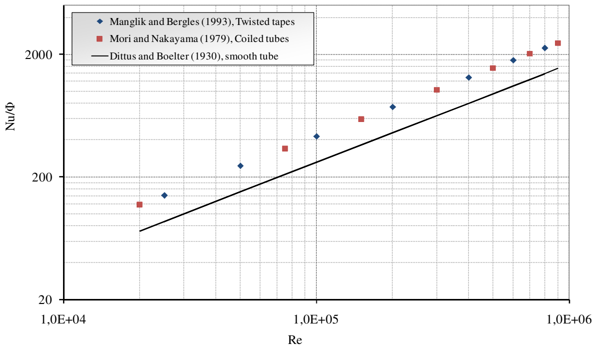

Fig. 78 – Comparison of Nusselt number improvement for coiled tubes and twisted tape with the same geometrical configuration.

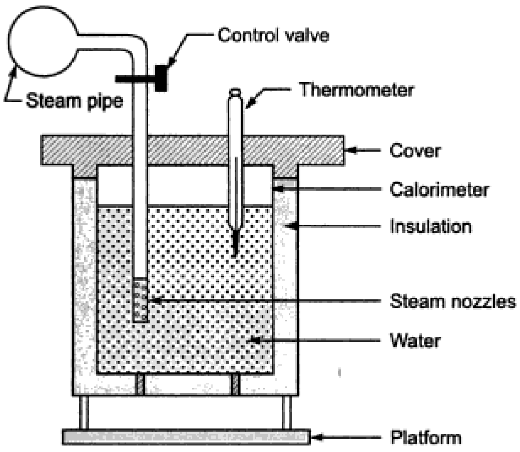

Fig. 79 – Barrel calorimeter scheme.

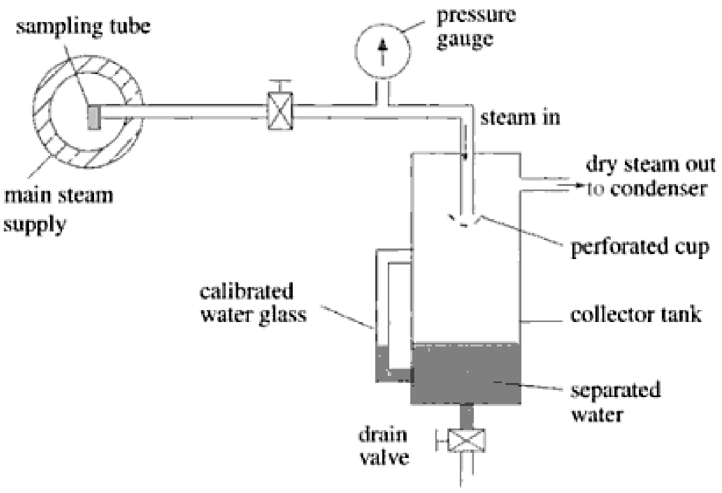

Fig. 80 – Separating calorimeter scheme.

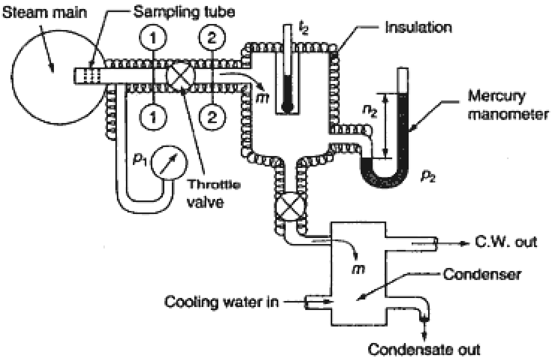

Fig. 81 – Throttling calorimeter scheme.

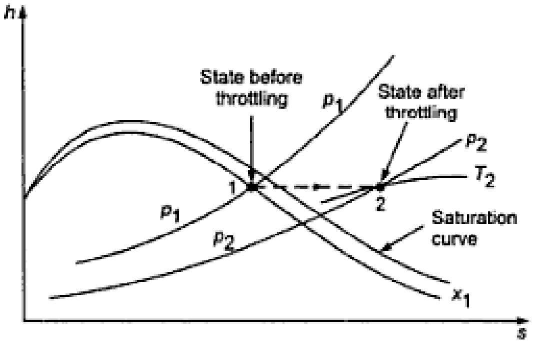

Fig. 82 – Throttling calorimeter: thermodynamic process h - S diagram.

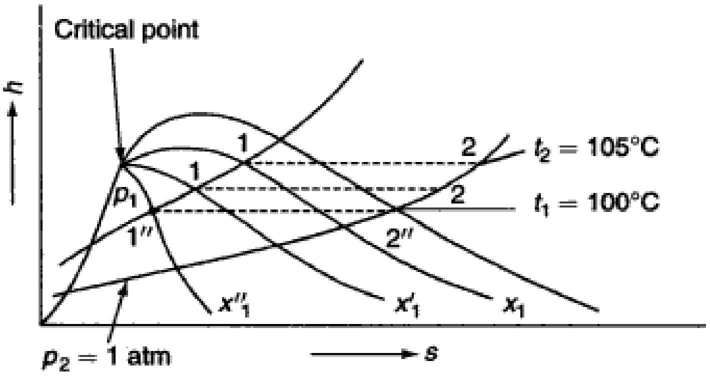

Fig. 83 – Minimum value of steam quality, at pressure p_1, which can be measured by only a throttling calorimeter.

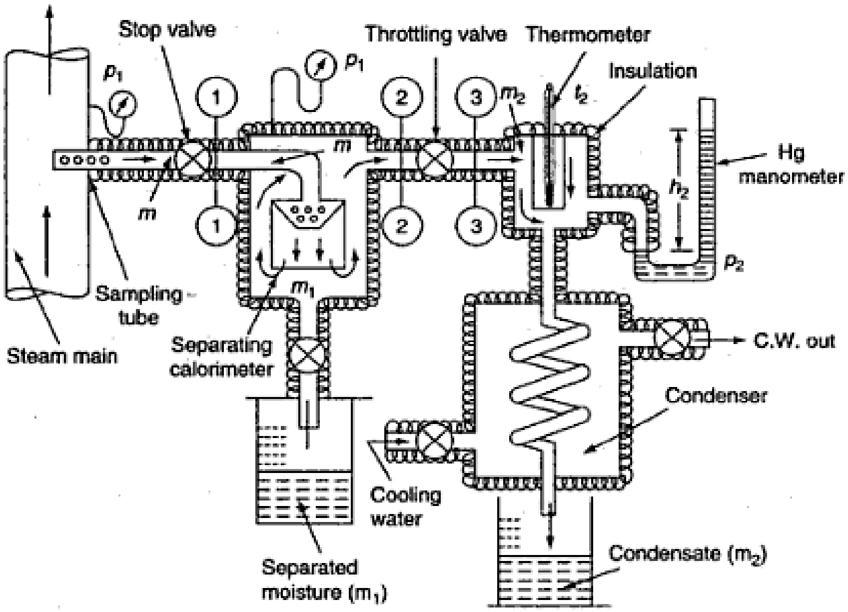

Fig. 84 – Throttling and separating calorimeter scheme.

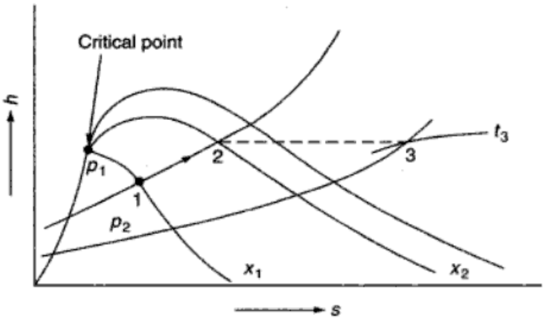

Fig. 85 – Throttling and separating calorimeter: thermodynamic process in h - S diagram.

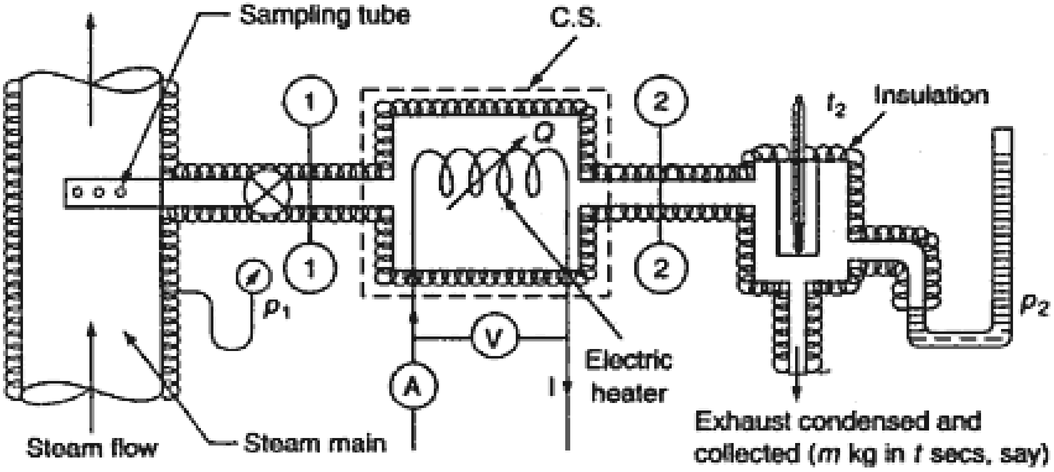

Fig. 86 – Electrical calorimeter scheme.

7 Conclusions

ALFRED is a pool type conceptual LFR. The SG design deals with the double wall once-trough bayonet type. The aim of this concept is to improve the reactor safety by physical separation of lead and water with an annular gap easily monitored by He pressurization. High temperature superheated steam is a design requirement that imposes the use of an high conductivity powder coupled with the pressurized He. The TxP Facility aims to characterize the thermal conductivity and the behavior of several candidate powders. The TxP operation and design have been presented in the current report. The SG single tube has been modeled by RELAP in connection to the analyses conducted during the TxP design. The first experimental campaign will address Copper, Brass and AISI-1010 powders. Further materials will be considered. The startup is planned for September-October 2011. The experimental characterization of high conductivity powders will support the refinement of the SG design.

The basis for the future work have been presented in the last section. The analysis of the turbulence promoters techniques will be the intermediate step for the experimental qualification of the single bayonet tube planned in the next three years.

REFERENCES

[1] www.gen-4.org **GEN-IV technology website**

[2] ***DOE NERAC, GIF*, A Technology Roadmap for Generation IV Nuclear Energy Systems, GIF-002-00, December 2002.**

[3] *OECD*, **Generation IV International Forum Annual Report**, 2007.

[4] www.ist-world.org/ProjectDetails.aspx?ProjectId=511f2e5a509041c5be90a0df653e425f ELSY Project website.

[5] *R Garcia Rodriguez, A. Orden,* **Description of Preliminary Overall Plant Layout and Preliminary Arrangement Drawings; D 22,** 092-159-F-M-00002, February 2009.

[6] *European Community*, **Lead-cooled European Advanced DEmonstration Reactor**, LEADER FP7 – 249668, May 3, 2010.

[7] www.leader-fp7.eu. LEADER Project website

[8] *D. A. Nield, A. Bejan*, **Convection in Porous Media, Third Edition**, Springer Science Business Media, Inc., 233 Spring Street, New York, NY 10013, USA.

[9] *M. Kandula*, **On the Effective Thermal Conductivity of Porous Packed Beds with Uniform Spherical Particles,** ASRC Aerospace, John F. Kennedy Space Center, FL, USA.

[10] *Y. Feng, B. Yu, M. Zou, D. Zhang,* **A generalized model for the effective thermal conductivity of porous media based on self-similarity,** J. Phys. D: Appl. Phys. **37** (2004) pp 3030–3040.

[11] *J. H. Lienhard IV, J. H. Lienhard V*, **A Heat Transfer Textbox third edition**, Published by Phlogstone Press, Cambridge Massachusetts, USA 2003.

[12] *D. Rozzia, A. Toti, G. Venturi, N. Forgione, M. Tarantino, A. Alemberti* **Experimental Investigation on Powders Thermal Performance to Support the Design of Innovative SG for LFR**- DR_/PhD/01(11)-IIR-Rev1a, ENEA CR Brasimone 2011.

[13] *J. R. Olson, et. Al.*, **Thermal conductivity of diamond between 170 and 1200 K and isotope effect**, The American Physical Society vol. 47, number 22, pp 850-856 1993.

[14] http://periodictable.com/Elements/005/data.html Material properties website.

[15] http://en.wikipedia.org/wiki/Allotropy#Metals Allotrope materials website.

[16] http://en.wikipedia.org/wiki/Aluminium Aluminium properties website.

[17] http://en.wikipedia.org/wiki/Silver#Characteristics Silver properties website.

[18] http://en.wikipedia.org/wiki/Chromium Chromium properties website.

[19] http://en.wikipedia.org/wiki/Copper Copper properties website.

[20] http://en.wikipedia.org/wiki/Iron Iron properties website.

[21] http://en.wikipedia.org/wiki/Magnesium#As_metal Magnesium properties website.

[22] http://en.wikipedia.org/wiki/Molybdenum Molybdenum properties website.

[23] http://en.wikipedia.org/wiki/Nickel Nickel properties website.

[24] http://en.wikipedia.org/wiki/Silicon Silicon properties website.

[25] http://en.wikipedia.org/wiki/Tungsten Tungsten properties website.

[26] http://www.substech.com/dokuwiki/doku.php?id=iron-carbon_phase_diagram Fe-C website.

[27] *CDA,* **Selected copper alloy diagrams illustrating the major types of phase transformation,** Copper Development Association, Publication No 94, 1992.

[28] http://www.chemguide.co.uk/inorganic/period3/elementsreact.html periodic element website

[29] *P. Miller, A. Navarro,* **Hazardous reaction of Aluminum powders**, Unclassified Report August 1996.

[30] http://www.webelements.com/tungsten/chemistry.html Tungsten properties website.

[31] http://www.webelements.com/molybdenum/chemistry.html Mo properties website.

[32] *M. Kilpatrick, S. K. Lott*, **Reaction of Flowing Steam with Refractory Metals**, Argonne National Laboratory, November 20, 1964.

[33] http://www.webelements.com/nickel/chemistry.html Nickel properties website.

[34] http://www.webelements.com/tungsten/chemistry.html Tungsten properties website.

[35] *Guerrini, Paci S.* **Appunti di Impianti Nucleari Parte I: aspetti generali**, UNIPI DIMNP dispensa universitaria RL810(99).

[36] *IMS s.p.a.*, **Acciai speciali**, 1.4306 Reference standard EN10088.

[37] *A. Pasta*, **Appunti delle lezioni di costruzioni di macchine**, Università di Palermo 1999.

[38] *NSAD*, **RELAP5/Mod3.3 Code Manual volume II, Input Requirements** Washington, DC 20555 June 2004.

[39] *A. Toti, D. Rozzia M. Tarantino*. **Heat Transfer Enhancement techniques in forced convection**-HEE-BRR-01(11)- Rev0c, ENEA CR Brasimone 2011.

[40] *Adrian Bejan, Allan D. Kraus*, **Heat transfer handbook**, John Wiley & Sons, 2003.

[41] http://www.chemicalogic.com thermal hydraulic properties website.

[42] *Eugene Saltanov,* **Steam reheat option for supercritical water cooled reactor**, Master Thesis in Nuclear Engineering, University of Ontario, Institute of Technology, December 2010.

[43] *A. Garcia, P.G. Vicente, A. Viedma*, **Experimental investigation on heat transfer and frictional characteristics of wire coils inserts in transition flow at different Prandls number.** Unclassified report.

[44] *O.H. Klepper*, **Heat transfer performance of short twisted tapes**, Oak Ridge National Laboratory, Oak Ridge, Tennessee 37830.

[45] *A Dewan, P Mahanta, K Sumithra Raju and P Suresh Kumar*, **Review of passive heat transfer augmentation techniques,** Proceedings of the Institution of Mechanical Engineers, Part A: Journal of Power and Energy 2004.

[46] *A. Toti, D. Rozzia M. Tarantino*. **Steam Quality Measurements, basic principles and methods**. 18-05-11-SQ-BRR-02(11), ENEA CR Brasimone 2011.

[47] *P.K. Nag*, **Basic and Applied Thermodynamics, Second Edition,** McGrw Hill, 2009.

[48] *J.A. Leach,* **Engineering Thermodynamics**, Juta & Co., 2007.

[49] *Onkar Singh,* **Applied Thermodynamics**, New Age International Publisher, 2003.

[50] *M. M. Rathore,* **Thermal Engineering**, Tata Mc Graw Hill Education Private Limited, 2010.

[51] *Rozzia D., et al* **Experimental evaluation of thermal performance of powders for GEN-IV technology applications**. Proc. of UIT Nat. Conf., June, 2011, Torino, Italy.

[52] *Rozzia D., et al.* **Basis for the Experimental Evaluation of Powders Conductivity in the TxP Facility for Generation IV Technology Application**. Proceeding of NENE-2011 Int. Conf. Bovec, Slovenia 12-15 September 2011.